NUREG/CR-3505
EPRI NP-3547
ANL-83-66

NUREG/CR-3505
EPRI NP-3547
ANL-83-66

# A VOLUME-WEIGHTED SKEW-UPWIND DIFFERENCE SCHEME IN COMMIX

by

C. C. Miao, R. W. Lyczkowski, G. K. Leaf,
F. F. Chen, B. K. Cha, B. C-J. Chen,
H. M. Domanus, W. T. Sha, and V. L. Shah




ARGONNE NATIONAL LABORATORY, ARGONNE, ILLINOIS
Operated by THE UNIVERSITY OF CHICAGO

Prepared for the Office of Nuclear Regulatory Research
U. S. NUCLEAR REGULATORY COMMISSION
under Interagency Agreement DOE 40-550-75

Available from

GPO Sales Program
Division of Technical Information and Document Control
U. S. Nuclear Regulatory Commission
Washington, D.C. 20555

and

National Technical Information Service
Springfield, Virginia 22161

NUREG/CR-3505
EPRI NP-3547
ANL-83-66

Distribution
Category: R7

ARGONNE NATIONAL LABORATORY
9700 South Cass Avenue
Argonne, Illinois 60439

# A VOLUME-WEIGHTED SKEW-UPWIND DIFFERENCE SCHEME IN COMMIX

by

C. C. Miao, R. W. Lyczkowski, G. K. Leaf, F. F. Chen,
B. K. Cha, B. C-J. Chen, H. M. Domanus, W. T. Sha, and V. L. Shah

Prepared by

Analytical Thermal Hydraulic Research Program
Components Technology Division

May 1984

Prepared for

Office of Nuclear Regulatory Research
U.S. Nuclear Regulatory Commission
Washington, D.C. 20555
under Interagency Agreement DOE 40-550-75

NRC FIN No. A2045

# A VOLUME-WEIGHTED SKEW-UPWIND DIFFERENCE SCHEME IN COMMIX

by

C. C. Miao, R. W. Lyczkowski, G. K. Leaf, F. F. Chen
B. C. Cha, B. C-J. Chen, H. M. Domanus, W. T. Sha, and V. L. Shah

## ABSTRACT

Several of the numerous techniques proposed in the literature as remedies to reduce numerical diffusion were examined for implementation in the COMMIX-1B[1-3] computer program. Raithby's[4-5] two-dimensional skew-upwind difference (SUD) scheme, compatible with the current numerical procedure in COMMIX, has been extended to three dimensions. In addition, a scheme called the volume-weighted skew-upwind difference (VWSUD) scheme has been developed. Both schemes, SUD and VWSUD, have been implemented in the energy equation of the COMMIX-1B computer program. The VWSUD scheme has the following major features:

- It has the same order of accuracy as the SUD scheme, but eliminates all of the undershoots and overshoots (computational values over and above the limits of physically allowable values) observed in the SUD scheme in this study.
- It retains the simplicity of the SUD scheme without resorting to the artificial cut-offs needed in the SUD scheme. This advantage is crucial in many thermal-hydraulic applications.
- It significantly reduces numerical diffusion for steady-state and transient thermal mixing with flow oblique to computational grids.
- A two-dimensional Von Neumann linear stability analysis shows that the VWSUD scheme is numerically stable.
- A coarser mesh than for the pure-upwind difference scheme can be used while obtaining results that are of the same order of accuracy. Hence, computer running time is significantly decreased.

We have quantitatively assessed the ability of the SUD and VWSUD schemes to reduce numerical diffusion for flow oblique to the computational grids. The assessments were accomplished by comparing several multidimensional steady-state and transient thermal mixing benchmark computations with analytical solutions. Analysis of two thermal mixing experiments shows that use of the VWSUD scheme substantially improves agreement with thermocouple response data in regions with highly angled flows. Validation of the VWSUD scheme will require many more applications.

| FIN No. | Title |
|---|---|
| A2045 | 3-D Time-Dependent Code Development |

CONTENTS

FIGURES

FIGURES (Contd.)

FIGURES (Contd.)



TABLES

# A VOLUME-WEIGHTED SKEW-UPWIND DIFFERENCE SCHEME IN COMMIX

by

C. C. Miao, R. W. Lyczkowski, G. K Leaf, F. F. Chen,
B. K. Cha, B. C-J. Chen, H. M. Domanus, W. T. Sha, and V. L. Shah

## EXECUTIVE SUMMARY

Several methods for reducing numerical diffusion have been examined for their suitability to be implemented in the COMMIX-1B code. The skew-upwind differencing scheme as proposed by Raithby was most compatible with the current COMMIX scheme. However, two drawbacks of Raithby's scheme needed to be corrected. To address these drawbacks, a volume-weighted skew-upwind difference VWSUD scheme has been developed and implemented in the energy equation of COMMIX. The importance of numerical diffusion in the momentum equation was found to be significantly smaller by many investigators.

The VWSUD scheme takes advantage of the simplicity of Raithby's skew-upwind differencing scheme and yet does not have Raithby's drawbacks. It reduces the bulk of numerical diffusion without the problems of overshooting and undershooting (computational values over and under the limits of the physically allowable values), and without the need for artificial cut-off as an upper bound. The scheme is proven to be numerically stable by the Von Neumann stability (Appendix A) analysis.

Several analyses were performed with this newly implemented scheme to compare computational results with analytical solutions or experimental data. Cases studied include (1) two-dimensional corner-to-corner flow; (2) two-dimensional highly angled flow; (3) three-dimensional corner-to-corner flow; (4) transient simulation of an SAI experiment; and, (5) transient simulation of a CREARE experiment. These validation efforts were motivated by a need to resolve the numerical diffusion issue brought up during earlier COMMIX calculations for thermal mixing related to the so-called pressurized thermal shock problem. In all cases studied so far, agreement between the computational results and the analytical solution or experimental data was improved significantly by using the volume-weighted skew-upwind difference scheme. Furthermore, the experience from various analyses shows that VWSUD permits use of coarser mesh, thus saving significant computer running time, than corresponding upwind scheme while maintaining same order of accuracy. However, much more validation and applications of this new scheme are needed in the future.

# 1. INTRODUCTION

## 1.1 COMMIX-1B

COMMIX-1B, the advanced version of COMMIX-1A, is a computer program designed and developed for thermal-hydraulic analysis of reactor component/multicomponent systems under normal and off-normal operation conditions. It uses a finite-difference numerical procedure to solve three-dimensional, steady-state/transient partial differential conservation equations of mass, momentum, and energy.

Recently, we have added three major features to the code. They are:

- Implicit solution procedure,
- Turbulence models, and
- Skew-upwind difference (SUD) and volume-weighted skew-upwind difference (VWSUD) schemes.

These three features have augmented the capabilities of the COMMIX code. In this report we describe only the third feature, the SUD and VWSUD schemes, implemented using only the implicit solution procedure. The other two features are described in other reports[6,7]. The reason for implementing the SUD and VWSUD schemes is to reduce numerical diffusion. The following sections give some background and an explanation as to why we have implemented the SUD and VWSUD difference schemes in COMMIX-1B.

## 1.2 Definition of Numerical Diffusion

In fluid-dynamic calculations, pure-upwind differencing instead of central differencing is generally used to discretize the convective terms. The reason is that for high Peclet-number flows, pure-upwind differencing prevents instability, although it produces what is known as numerical diffusion.

The concept of numerical diffusion can be described as follows. We first make the consistency check between the finite difference equation and the original differential equation by using Taylor series expansions (both in space and time). In the case of pure-upwind differencing, the second-order derivative terms do not get cancelled as they do in the case of central differencing. The contributions that result from these additional second-order derivative terms are known as numerical diffusion. The coefficient of the additional second-order derivative term is interpreted as a false or numerical diffusion coefficient.

The apparent ways to reduce numerical diffusion are

- To use very fine mesh and
- to use higher-order finite-difference approximations.

But these procedures are not possible in practice when one is trying to analyze a large, complex, real engineering situation. In addition, it may be very uneconomical to do so. What is needed is a scheme that is simple to implement, permits the use of coarser mesh for given accuracy, and has acceptable numerical diffusion.

When flow is aligned parallel to one of the coordinate grid lines, the magnitude of numerical diffusion is generally very small and can be considered negligible. However, the magnitude of numerical diffusion does increase with the increase in the angle between flow direction and coordinate grid lines. This report describes the modifications that are implemented to minimize numerical diffusion when flow is inclined to coordinate grid lines.

### 1.3 Review of Alternative Schemes to Reduce Numerical Diffusion in COMMIX

Numerous methods for reducing numerical diffusion have been proposed in the open literature. We are presenting here our brief review of several of these procedures that are applicable to the finite-difference formulation (COMMIX employs the finite-difference formulation). The review is only from the points of view of accuracy and ease of implementation in the existing COMMIX-1B code, which uses the pure-upwind scheme in its numerical formulation.

The method of Truncation Error Cancellation (TEC), used by LASL[8], involves adding diffusive terms to make sure that the coefficients of all second-order terms are positive. In the upwind scheme, the coefficients are already positive. The procedure, therefore, requires use of negative diffusion coefficients. We tried this procedure and found that it decreases the stability of a solution.

The Flux-Corrected Transport (FCT) theory is developed by Boris and Book[9] and extended by Zalesak[10]. As described by Zalesak, the method requires the governing equations to be in conservation law form and computes the net transportive flux as a weighted average of a flux computed by a low-order scheme (e.g., upwind) and a flux computed by a higher-order scheme (e.g., a leapfrog-trapezoidal algorithm with fourth-order spatial differences). Some filtering is required to suppress over- and undershoots ("wiggles"). The procedure is a very high-order scheme, requires major modifications to COMMIX, and is computationally more expensive.

The use of the Asymmetric Weighted Residual method, as propounded by Romstedt and Werner[11], was not considered for two reasons:

- It would require substantial modifications of COMMIX, and
- It is an untried technique for multidimensional fluid-flow problems, and is inappropriate for a COMMIX-type code.

R. G. Steinke[12] describes the use of a step function rather than a flat shape in the pure-upwind scheme. This approach does not address numerical diffusion due to cross-flow; instead, it is concerned only with numerical diffusion due to pure-upwind differencing.

A nonlinear fitting technique (FRAM), presented by Chapman[13], is for multidimensional homogeneous equations in conservative form. The basic idea is to use a higher-order scheme and then locally introduce artificial diffusion when spurious oscillations appear. The technique seems to offer several advantages over FCT. In particular, the high-order scheme can be like Crowley's[14,15], which is akin to central differences. Thus, the basic scheme would be a nine-point scheme in two dimensions and a 27-point scheme in three dimensions. Also, artificial diffusion is introduced locally rather than globally, as in FCT. The modification can be moderate in scope. We wanted to see if we could find a simpler alternative.

A skew-upwind difference (SUD) scheme is described by G. D. Raithby[5] and J. N. Lillington[16]. In this approach, one applies upwind difference in the stream direction and uses a linear variation differencing in the cross-stream direction. This technique addresses the problem of numerical diffusion due to cross-flow gradients in the pure-upwind scheme. In two dimensions, this scheme leads to, at most, a nine-point formula.

### 1.4 Selection of a Scheme to Reduce Numerical Diffusion

After reviewing the alternatives described, we decided to (1) extend Raithby's two-dimensional SUD scheme to three dimensions, (2) develop the VWSUD scheme, and (3) implement both of these schemes (SUD and VWSUD) into the energy equation in COMMIX-1B. The following are our considerations.

- As mentioned earlier, our objective was to develop a scheme that is simple to implement, computationally efficient, and displays acceptable numerical diffusion for flows oblique to the computational grids.

- The pure-upwind scheme is simple. It is based on the assumption that for a steady-state convection-dominated flow, the variation of property value in the streamwise direction is very small. This is a very valid assumption. A major deficiency of the pure-upwind scheme is that it produces numerical diffusion when a flow is inclined to the computational grid lines.

- The skew-upwind scheme, an extension of the pure-upwind scheme, reduces the deficiency of the pure-upwind scheme. But SUD has two other problems: it predicts results that may overshoot or undershoot, and it requires an arbitrary cutoff value during linear interpolation.

We therefore developed a scheme called the volume-weighted skew-upwind difference (VWSUD) scheme, which is an extension of the SUD scheme. It eliminates the two problems of the SUD scheme, but still retains the simplicity of the SUD scheme. It approximates the property value at the surface of a computational cell using the volumes of two upstream cells as weighting factors.

We have implemented the VWSUD scheme in COMMIX-1B only in the energy equation and not in the momentum equation for the following reasons:

- All our analyses have shown that the numerical diffusion due to pure-upwind approximation is mainly through the energy equation and not through the momentum equation.

- The analysis of Hassan et al.[17] has shown that increasing the order of approximation (from pure-upwind to central difference) in the momentum equation does not make any appreciable difference in the velocity field.

### 1.5 Numerical Simulations

To assess the ability of the SUD and VWSUD schemes to reduce numerical diffusion for flow oblique to computational grids, we have analyzed several problems. Comparisons have been made between the multidimensional steady-state and transient thermal mixing benchmark problems and the analytical solutions. Also, the analysis of two thermal mixing experiments is compared with experimental data. In this report, we present the results of five problems:

- 2-D corner-to-corner flow,
- 2-D highly-angled flow,
- 3-D corner-to-corner flow,
- SAI thermal and fluid mixing experiment[21], and
- CREARE thermal and fluid mixing experiment[23].

It can be seen from the results presented here that the VWSUD scheme is simple to implement, removes some of the deficiencies of the SUD and pure-upwind schemes, and reduces numerical diffusion.

### 1.6 Outline of the Report

So that a reader can clearly understand our scheme, we have included Raithby's skew-upwind difference (SUD) scheme as background information in Sec. 2. Our extension, the volume-weighted skew-upwind difference (VWSUD) scheme, is described in Sec. 3. The results along with comparisons of five numerical problems are given in Sec. 4. Section 5 contains our concluding remarks. For those who are interested in knowing the stability of the scheme, we have presented in Appendix A the stability analysis of the VWSUD scheme.

## 2. EXTENDED RAITHBY SKEW-UPWIND DIFFERENCE (SUD) SCHEME

### 2.1 Background

Because of its stabilizing effect, the pure-upwind difference scheme is used extensively in one-dimensional hydrodynamic computer programs[18]. The basic concept is briefly discussed here in reference to Fig. 1.

It is easy to difference the model equation

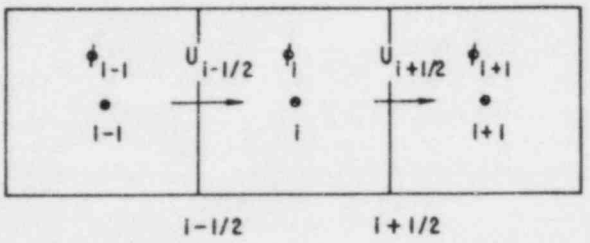


Fig. 1. One-Dimensional Upwind or Donor Cell

$$\frac{\partial}{\partial x}(u\phi) = 0 \tag{1}$$

at node i, where $\phi$ is some scalar and u is the velocity. Equation 1 may be differenced at center node i as

$$\frac{(u\phi)_{i+1/2} - (u\phi)_{i-1/2}}{\Delta x} = 0 , \tag{2}$$

where subscripts i±1/2 refer to the values of $(u\phi)$ at the cell edges. In a staggered mesh system, $\phi$ and u are not known at the same points. If it is assumed that $\phi$ is continuous, Eq. 2 may be approximated as

$$\frac{(u\phi)_{i+1/2} - (u\phi)_{i-1/2}}{\Delta x} \simeq \frac{u_{i+1/2}\,\phi_i - u_{i-1/2}\,\phi_{i-1}}{\Delta x} \tag{3}$$

for the case $u_{i\pm1/2} > 0$. That is, the values of $\phi_{i\pm1/2}$ are considered "donated" (or upwinded) to the cell edge, depending on the signs of $u_{i\pm1/2}$. In the case considered, both velocities are assumed positive.

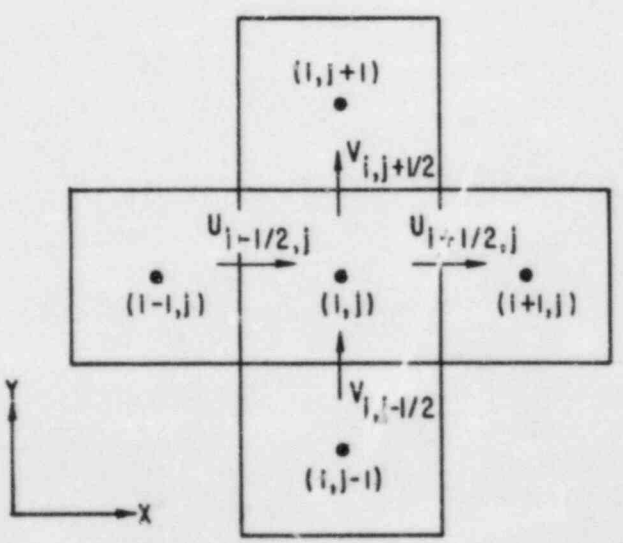


Fig. 2. Two-Dimensional Upwind or Donor Cell

Now consider the two-dimensional situation, as shown in Fig. 2. The application of the one-dimensional pure-upwind difference scheme to the two-dimensional model equation

$$\frac{\partial}{\partial x}(u\phi) + \frac{\partial}{\partial y}(v\phi) = 0 \tag{4}$$

produces

$$\frac{\partial(u\phi)}{\partial x} = \frac{(u\phi)_{i+1/2,j} - (u\phi)_{i-1/2,j}}{\Delta x}$$

$$\simeq \frac{u_{i+1/2,j}\,\phi_{i,j} - u_{i-1/2,j}\,\phi_{i-1,j}}{\Delta x}\,, \tag{5}$$

and

$$\frac{\partial(v\phi)}{\partial y} = \frac{(v\phi)_{i,j+1/2} - (v\phi)_{i,j-1/2}}{\Delta y}$$

$$\simeq \frac{\left(v_{i,j+1/2}\,\phi_{i,j}\right) - \left(v_{i,j-1/2}\,\phi_{i,j-1}\right)}{\Delta y}\,, \tag{6}$$

assuming u and v are both positive. This extension assumes that the velocities are locally one-dimensional, i.e., each cell face is associated with one velocity component only, as shown in Fig. 2.

This apparently straightforward application of the one-dimensional pure-upwind concept to two and three dimensions is incorrect and has been identified as one of the main sources of numerical diffusion [5,19,20]. It has been shown that for a steady-state two-dimensional flow with constant velocity components u and v and equal grid sizes $\Delta x = \Delta y = \Delta$, the numerical diffusion coefficient $\Gamma_f$, resulting from using Eqs. 5 and 6 in Eq. 4 is given approximately by

$$\Gamma_F = \frac{\sqrt{2}}{4}\sin\left(\frac{\pi}{4} + \theta\right)\left|\vec{V}\right|\,\Delta\,\sin(2\theta)\,, \tag{7}$$

where

$$\theta = \tan^{-1}\left(\frac{u}{v}\right)\,. \tag{7a}$$

The maximum value of the numerical diffusion coefficient occurs for $\theta = \pi/4$, i.e., $u = v$.

## 2.2 Raithby's Two-Dimensional Skew-Upwind Difference (SUD) Scheme

Raithby[5] developed what is called the skew-upwind difference (SUD) scheme applicable to a two-dimensional flow field. His motivations were based on the assumption that in a small domain surrounding the center of a cell surface, a scalar property function $\phi$ (e.g., density, temperature, etc.) is continuous, linearly varying and constant along a streamline. He then proceeded to derive the SUD scheme, but his extremely compact and elegant notation obscures the true interpretation of the essence of the method and perhaps accounts for its relative lack of development[16].

We have been able to strip the interpretation of the method to its barest essence. This was absolutely necessary to properly extend it to three dimensions and to modify it to correct some of its defects. We assume

$$\frac{d\phi}{d\psi} = 0 \ , \tag{8}$$

where $d/d\psi$ is the directive derivative along the stream direction $\psi$. Consider the west face of node (i,j) (Fig. 3).

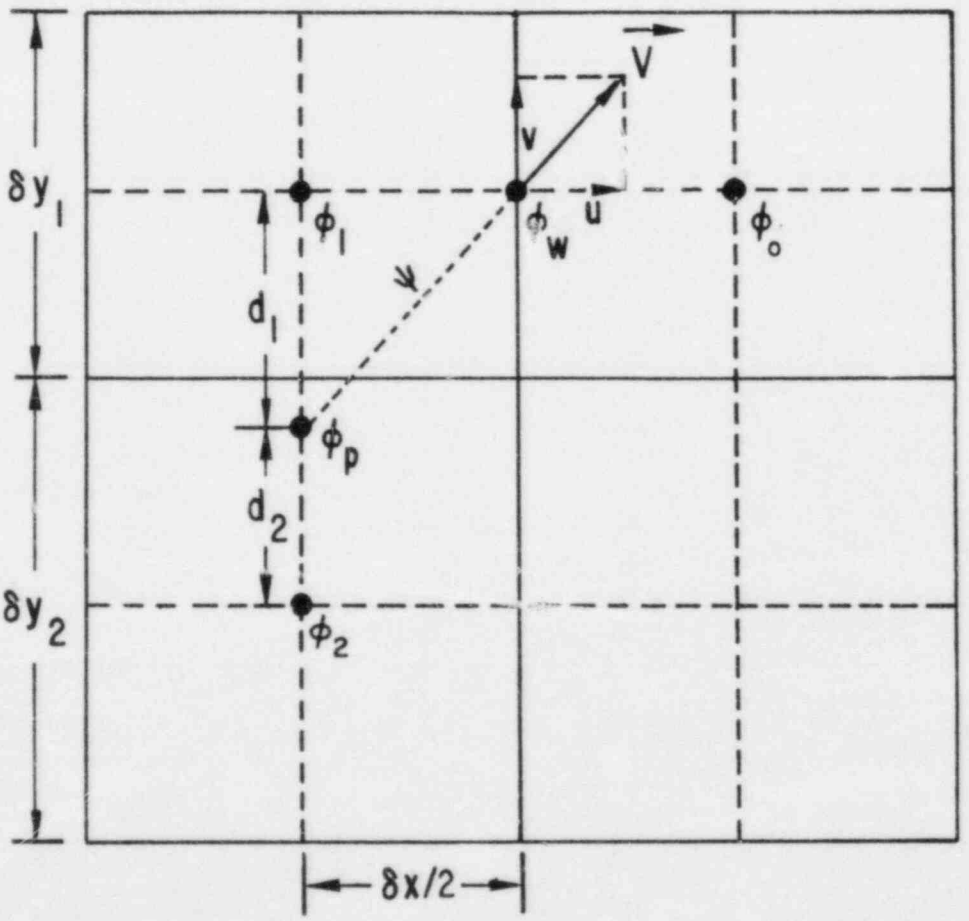


Fig. 3. Two-Dimensional Skew-Upwind Difference Scheme

We denote for clarity

$$\phi_o = \phi_{i,j}$$

$$\phi_w = \phi_{i-1/2,j}$$

$$\phi_1 = \phi_{i-1,j}$$

$$\phi_2 = \phi_{i-1,j-1} \cdot \tag{9}$$

Equation 8 implies that

$$\phi_w = \phi_p \, , \tag{10}$$

where $\phi_p$ is the value of $\phi$ at the point of intersection between the projection of the velocity vector $\vec{V}$ and the vertical line connecting $\phi_1$ and $\phi_2$. The property value $\phi_p$ in turn can be evaluated from the values $\phi_1$ and $\phi_2$ using simple linear interpolation as

$$\phi_w = \phi_p = \left(\frac{\delta y - d_1}{\delta y}\right)\phi_1 + \left(\frac{\delta y - d_2}{\delta y}\right)\phi_2 \, , \tag{11}$$

where

$$\delta y = (\delta y_1 + \delta y_2)/2 \tag{11a}$$

and $\delta y_1$ and $\delta y_2$ are the cell heights. The lengths $d_1$ and $d_2$ are determined from

$$d_1 = \left|\frac{v}{u}\right| (\delta x/2) \tag{12}$$

and

$$d_2 = \delta y - d_1 \, . \tag{12a}$$

Here u and v are the components of the velocity vector $\vec{V}$, considered centered at the middle of the west face, and $\delta x$ is the grid width for the cell containing $\phi_1$ (or $\phi_2$). When $d_1$ is greater than $\delta_y$, then $d_1$ is set equal to $\delta_y$ and $d_2$ is set equal to zero, and vice versa for the case of $d_2$ greater than $\delta_y$. These are Raithby's artificial cutoffs to prevent the possibility of negative coefficients in the interpolation formula given by Eq. 11. Equation 11 may be rewritten as

$$\phi_w = \phi_p = \left(1 - \frac{1}{2}\frac{\delta x}{\delta y}\left|\frac{v}{u}\right|\right)\phi_1 + \left(\frac{1}{2}\frac{\delta x}{\delta y}\left|\frac{v}{u}\right|\right)\phi_2 \, . \tag{13}$$

This is the same as Raithby's results for both u and v positive. Thus, Raithby's SUD scheme is nothing more than a method to replace $\phi_w$ by a linear interpolation between $\phi_1$ and $\phi_2$ using velocity components u and v. The flux on the west face is then computed in the usual manner as

$$F_w = \phi_w \, \delta y_1 \, u \, . \tag{14}$$

One benefit of the method is some reduction in the numerical diffusion in the direction normal to the stream direction introduced by the indiscriminate extension of the one-dimensional pure-upwind difference scheme to three-dimensions. The method does not address the problem of numerical diffusion that persists in that direction; neither does it address numerical diffusion resulting from time-dependent terms.

The interpretation of the method as merely an interpolation procedure for $\phi_w$ allows easy implementation in an existing computer code, such as COMMIX-1A, without major reprogramming.

In the following section, we explain the extension of the method to the three-dimensional situation.

## 2.3 Extension of Raithby's Two-Dimensional Skew-Upwind Difference (SUD)

The approach employed in Sec. 2.2 to derive the skew-upwind difference (SUD) scheme in a two-dimensional flow field is simple and straightforward. All the terms involved in Eq. 11 may be interpreted with physical and geometrical meanings. The same approach is used to derive the three-dimensional skew-upwind difference scheme shown in Fig. 4. To illustrate the configuration easily and without losing generality, we will assume that the velocity components u, v, and w of $\vec{V}$, passing through the center of the north face (+y) of the cell containing $\phi_o$ (Fig. 4) are all positive.

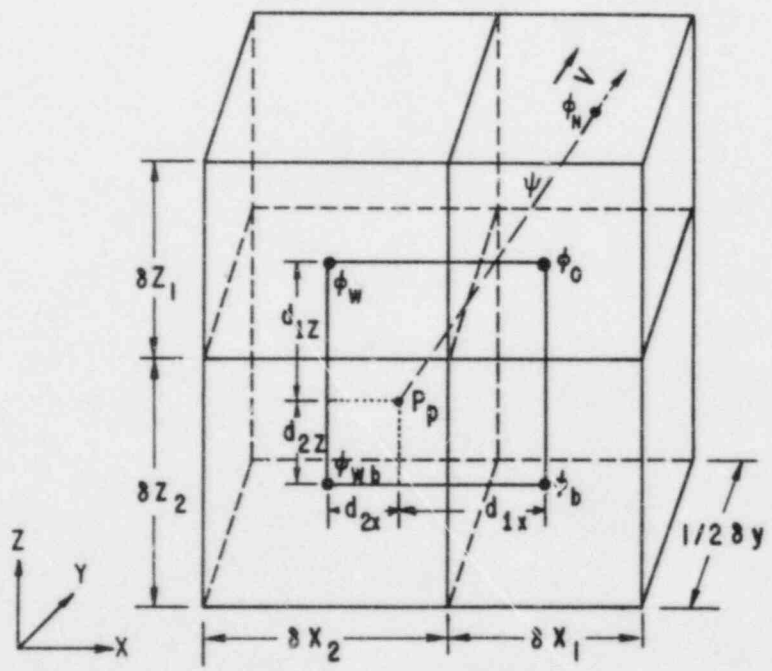


Fig. 4. Three-Dimensional Skew-upwind Difference Scheme

The three-dimensional model equation under consideration is given by

$$\frac{\partial}{\partial x}(u\phi) + \frac{\partial}{\partial y}(v\phi) + \frac{\partial}{\partial z}(w\phi) = 0 \ . \tag{15}$$

Equation 15 may also be written as Eq. 8 and the same considerations described in Sec. 2.2 are now directly extended to three dimensions.

The location of point $P_p$ is the intersection of the projection of velocity $\vec{V}$ with the plane containing the scalar values $\phi_o$, $\phi_w$, $\phi_{wb}$, and $\phi_b$. The length of $d_{lz}$ and $d_{lx}$ can be derived easily from Fig. 4. as

$$d_{lz} = \frac{w}{v}(\delta y/2) \tag{16}$$

and

$$d_{lx} = \frac{u}{v}(\delta y/2) \ . \tag{17}$$

If the center of the north face (+y) of the cell containing $\phi_o$ is considered to be the origin of the local coordinate system, then the coordinates of point $P_p$ may be written as

$$(P_p)_{local} = P_p\,(-d_{lx}, -\delta y/2, -d_{lz}) \ .$$

We define the interpolation coefficients as

$$\alpha_z = \left(\frac{\delta z - |d_{lz}|}{\delta z}\right) \qquad \text{if } \delta z > |d_{lz}| \ , \tag{19}$$

$$\alpha_z = 0 \qquad \text{otherwise}$$

and

$$\alpha_x = \left(\frac{\delta x - |d_{lx}|}{\delta x}\right) \qquad \text{if } \delta x > |d_{lx}| \ , \tag{20}$$

$$\alpha_x = 0 \qquad \text{otherwise,}$$

where

$$\delta z = \frac{1}{2}(\delta z_1 + \delta z_2) \tag{20a}$$

and

$$\delta x = \frac{1}{2}(\delta x_1 + \delta x_2) \ . \tag{20b}$$

Therefore, the intensive property $\phi_N$ defined on the north face of the cell containing $\phi_o$ can be simply written, analogous to the two-dimensional case given by Eq. 11, as

$$\phi_N = \phi_p = (\alpha_z\,\alpha_x)\,\phi_o + [(1-\alpha_z)\alpha_x]\,\phi_w + [\alpha_z(1-\alpha_x)]\,\phi_b + [(1-\alpha_z)\,(1-\alpha_x)]\,\phi_{wb} \ . \tag{21}$$

## 3. VOLUME-WEIGHTED SKEW-UPWIND DIFFERENCE (VWSUD) SCHEME

In this section, we describe the volume-weighted skew-upwind difference (VWSUD) scheme, which overcomes some of the deficiencies of the skew-upwind difference (SUD) scheme.

### 3.1 Two-Dimensional Volume-Weighted Skew-Upwind Difference (VWSUD) Scheme

As discussed in preceding sections, the only assumption made to derive the SUD scheme is

$$\frac{d\phi}{d\psi} = 0 \tag{22}$$

and the only conclusive implication from this assumption in two or three dimensions (shown in Figs. 3 and 4) is that

$$\phi_w \sim \phi_p \,. \tag{23}$$

Nevertheless, the expression of $\phi_p$ in terms of $\phi_1$ and $\phi_2$ in Eq. 2, or $\phi_o$, $\phi_w$, $\phi_b$, and $\phi_{wb}$ in Eq. 21, is straightforward but not necessarily unique.

In some cases, the interpolation may result in significant under- or overshoots. For the case of highly angled flow, shown in Fig. 5, the projected point $P_p$ falls outside of the line connecting $\phi_1$ and $\phi_2$.

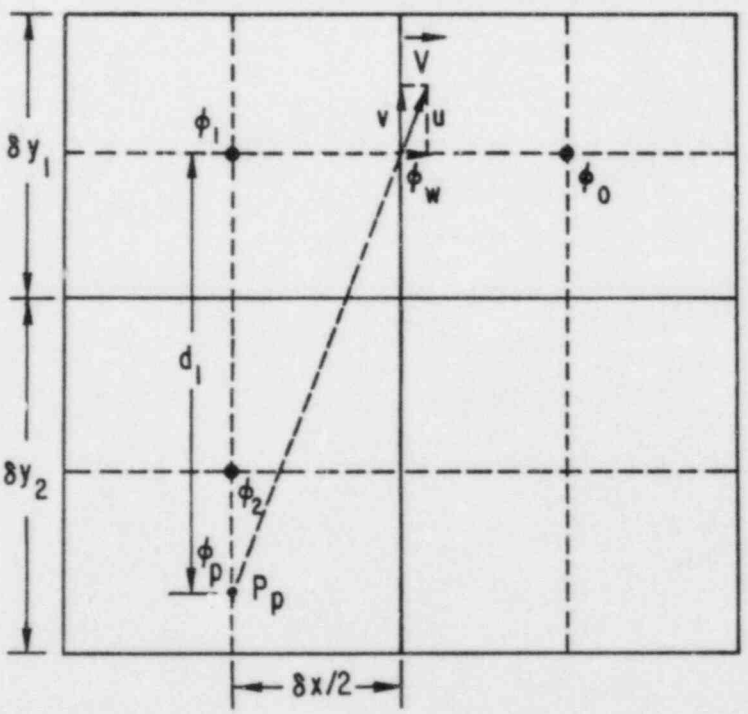


Fig. 5. Deficiency of Skew-Upwind Difference Scheme

To avoid the extrapolation, which may result in gross errors,[5] we may simplify Eq. 11 using the cutoff

$$\phi_w = \phi_p = \phi_2 \cdot \tag{24}$$

However, based on physical intuition, the intensive property of the flow passing the west face of the cell containing $\phi_o$ should involve both $\phi_2$ and $\phi_1$.

To correct this situation, we consider the volume of the flow passing through the west face of the cell containing $\phi_o$, shown in Fig. 6. The volume of flow passing through the west face originating from the portion of the control volume containing $\phi_1$ is $A_1 h$, where h is the unit depth of the flow. The remainder of the flow that passes through the west face originating from the control volume containing $\phi_2$ is given by $A_2$ h.

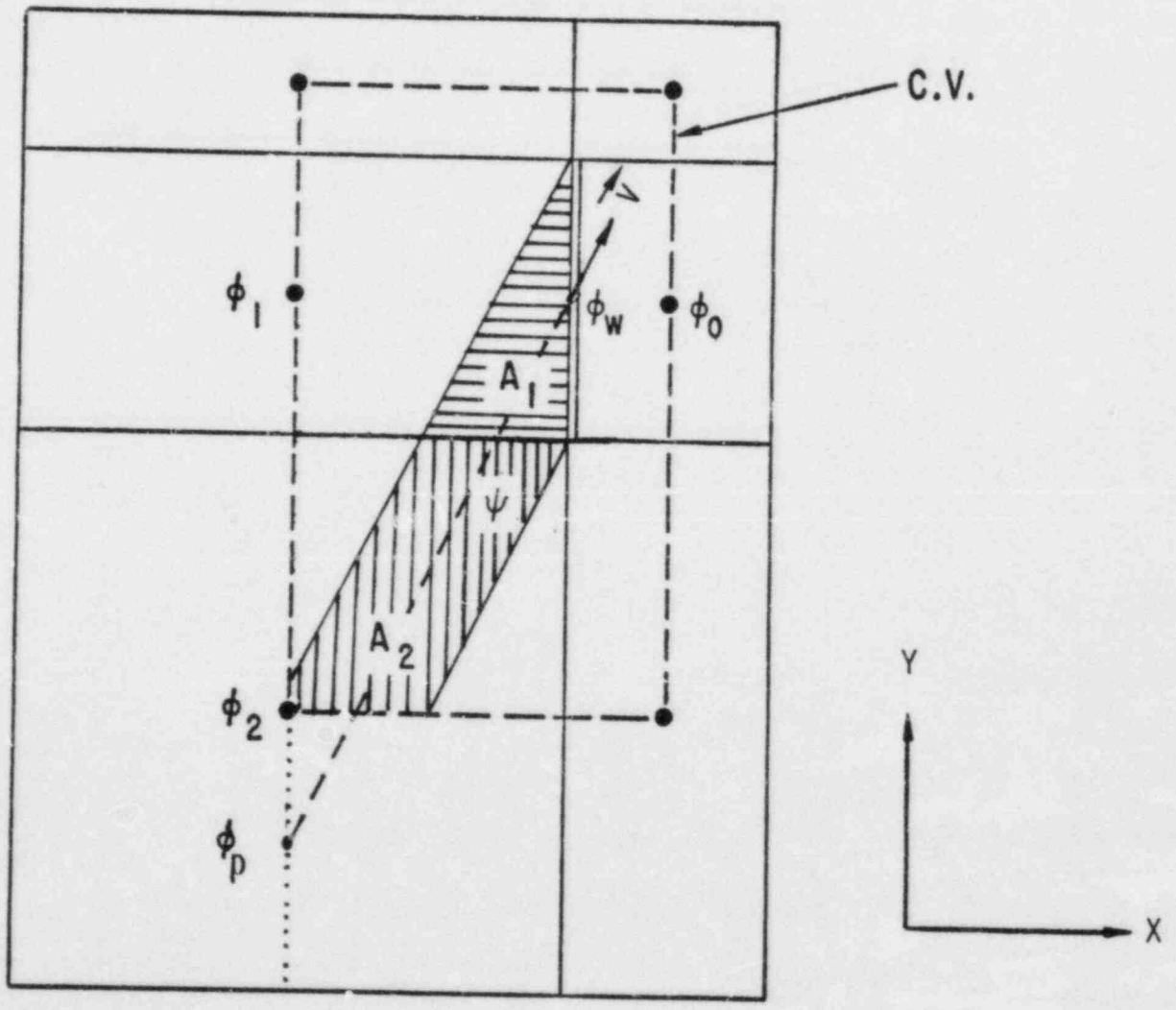


Fig. 6. Concept of Volume-Weighted Skew-Upwind Scheme

Therefore, the average of the intensive property associated with the volume of the flow can be expressed as

$$\phi_w = \phi_p = \left(\frac{A_1}{A_1 + A_2}\right)\phi_1 + \left(\frac{A_2}{A_1 + A_2}\right)\phi_2 \ . \tag{25}$$

Since the coefficients in Eq. 25 are always between 0 and 1, there is no need for any artificial cutoffs in the VWSUD.

### 3.2 Three-Dimensional Volume-Weighted Skew-Upwind Difference (VWSUD) Scheme

The extension of the two-dimensional VWSUD scheme to three dimensions is quite straightforward but difficult to visualize. As shown in Fig. 7, the projection line $\tau$ of the vector $\vec{V}$ that passes through the north face (+y) of the cell containing $\phi_o$ may result in the formation of subvolumes inside the surrounding cells. To simplify the representation, we number the cells 1 through 4 counterclockwise, starting with the cell containing $\phi_o$, as shown in Fig. 7. Detailed configurations of the constituent subvolumes resulting from the projection line $\tau$ are shown in Figs. 8-11.

The extension of Eq. 25 to three-dimensional flow field may be written as

$$\phi_N = \phi_p = \left(\frac{V_1}{V_{tot}}\right)\phi_1 + \left(\frac{V_2}{V_{tot}}\right)\phi_2 + \left(\frac{V_3}{V_{tot}}\right)\phi_3 + \left(\frac{V_4}{V_{tot}}\right)\phi_4 \ , \tag{26}$$

where

$$V_{tot} = V_1 + V_2 + V_3 + V_4 \tag{26a}$$

and $V_1$, $V_2$, $V_3$, and $V_4$ are shown in Fig. 7.

## 4. NUMERICAL RESULTS

### 4.1 Steady-State Validations

Several numerical experiments are conducted to assess the performances of the pure-upwind, skew-upwind, and volume-weighted skew-upwind schemes implemented in COMMIX-1B. To have a solid base for comparison, we have selected problems with known analytic solutions.

#### 4.1.1 Two-Dimensional Corner-to-corner Flow (Test Problem 1)

Consider the steady mixing of two streams at different temperatures shown in Fig. 12. Each is flowing at the same velocity, but at a 90° angle to each other. The two streams are introduced at the left and bottom of a two-dimensional rectangular grid. The problem was discussed by Patankar,[19] Leschziner,[20] and Raithby.[4] If the thermal conductivity is zero, the problem reduces to solving

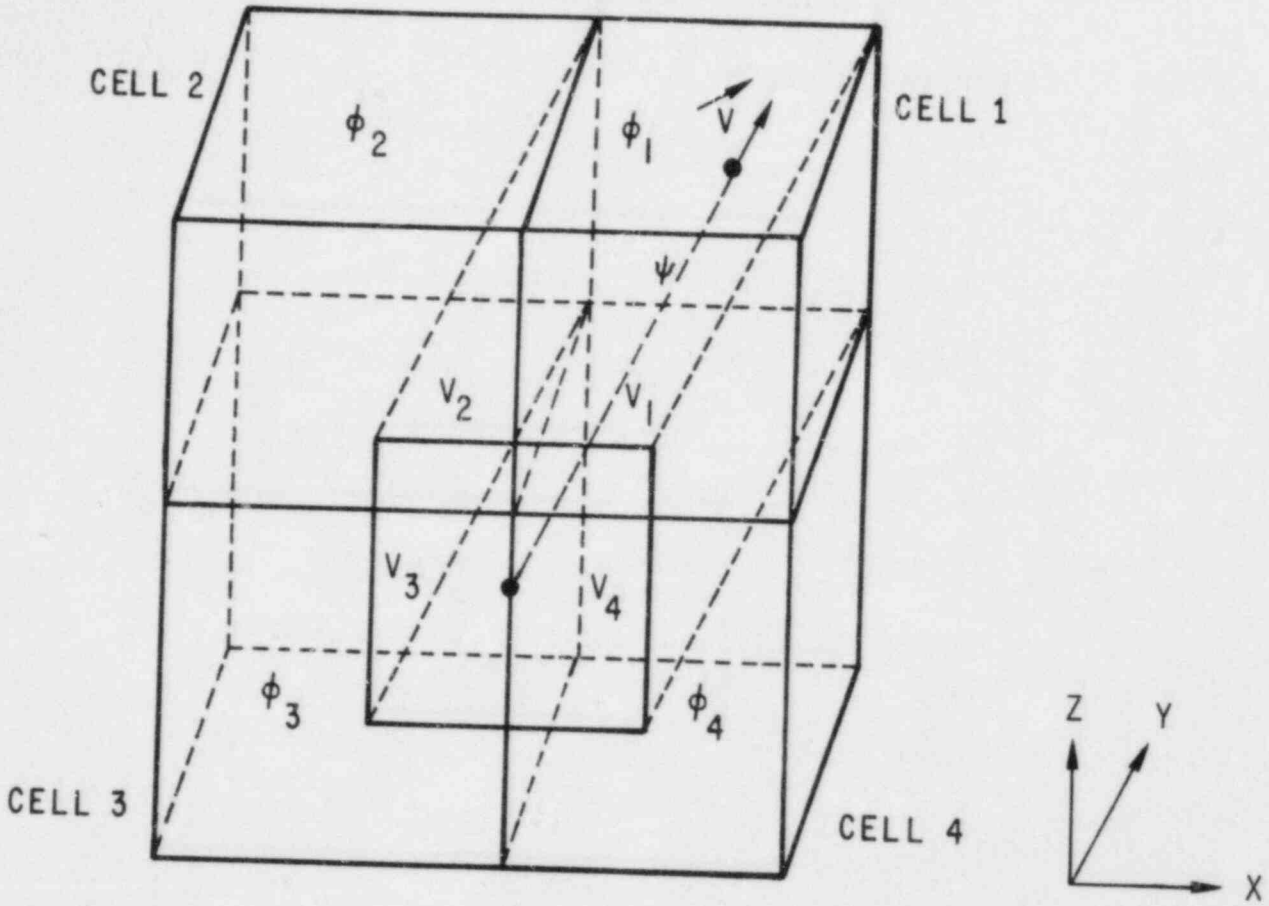


$$V_{TOT} = V_1 + V_2 + V_3 + V_4$$

$$\phi_{y+} = \left(\frac{V_1}{V_{TOT}}\right)\phi_1 + \left(\frac{V_2}{V_{TOT}}\right)\phi_2 + \left(\frac{V_3}{V_{TOT}}\right)\phi_3 + \left(\frac{V_4}{V_{TOT}}\right)\phi_4$$

Fig. 7. Three-Dimensional Volume-Weighted Difference Scheme

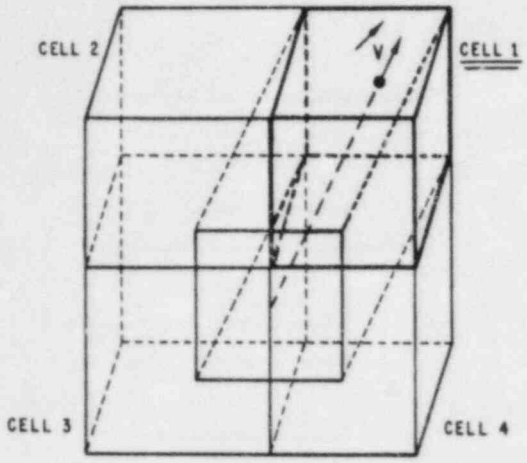


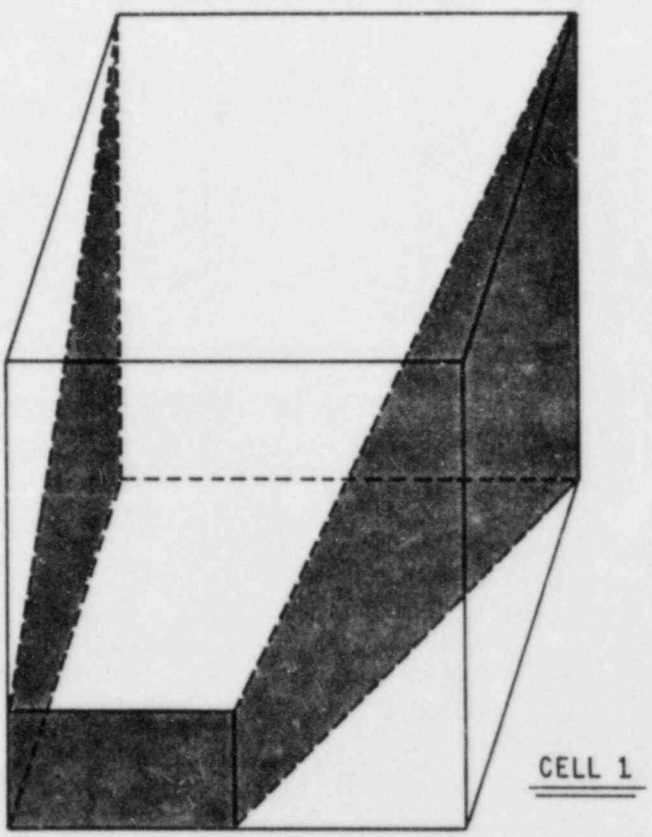


Fig. 8. Projected Element in Cell 1

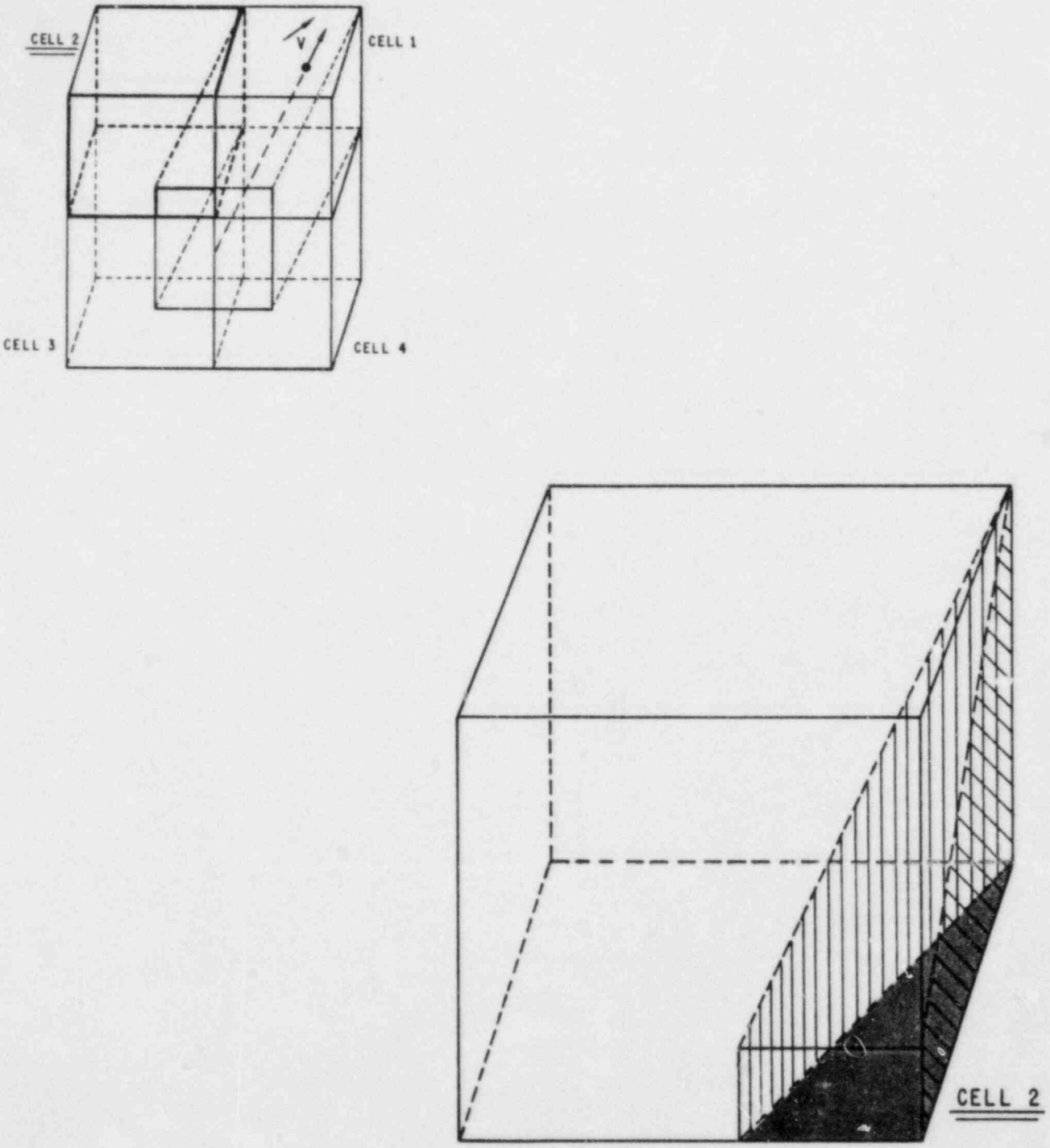


Fig. 9. Projected Element in Cell 2

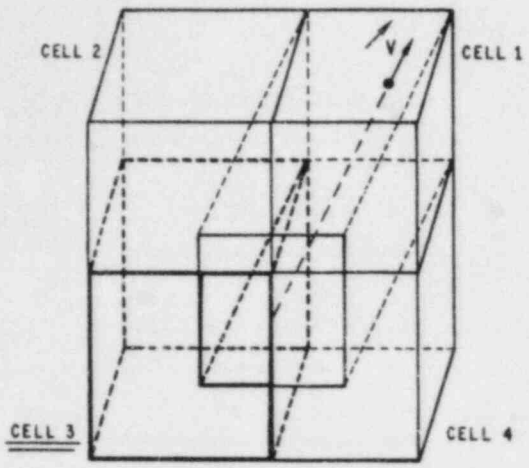


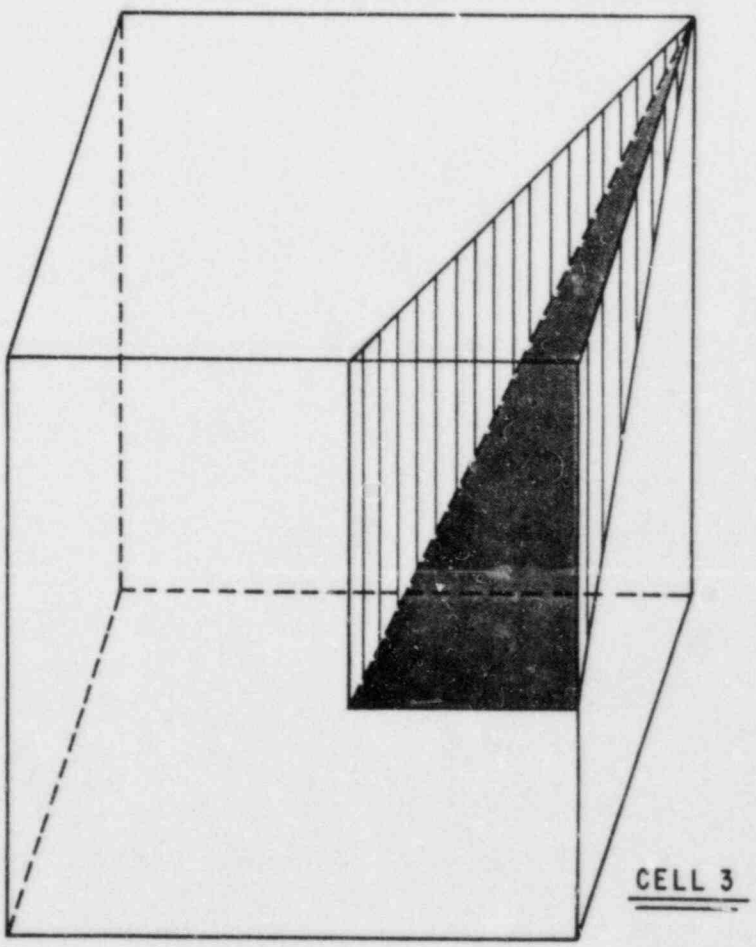


Fig. 10. Projected Element in Cell 3

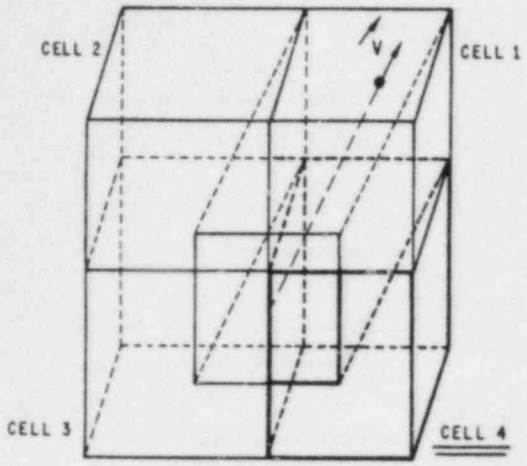


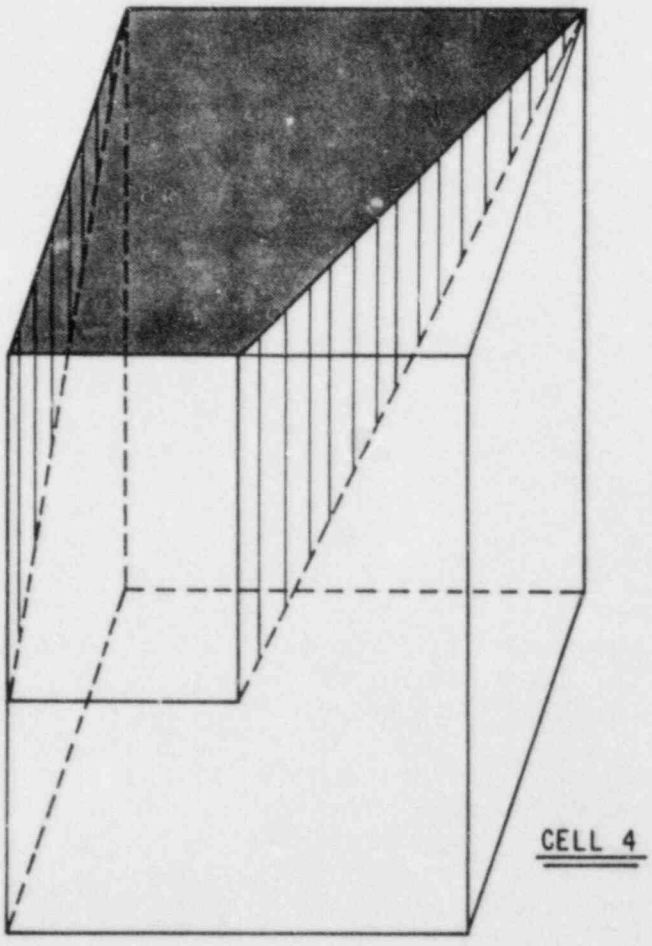


Fig. 11. Projected Element in Cell 4

$$u \frac{\partial T}{\partial x} + v \frac{\partial T}{\partial y} = 0 \ , \tag{27}$$

with

$$T = 0°C \text{ at } x = 0 \tag{28a}$$

and

$$T = 100°C \text{ at } y = 0 \ . \tag{28b}$$

We used the velocities u and v equal to 0.01 m/s, and a grid size of $\Delta x = \Delta y = 0.01$ m.

The results obtained with the different schemes are presented in Fig. 12 and are compared in Table 1. The numbers in the corners of each square correspond to temperature values (numerical results) obtained with different schemes. For easy comparison, we have also included the analytical (true) solution, i.e.,

$T = 0°$ above the diagonal,

$T = 100°$ below the diagonal, and

$T = 50°$ on the diagonal.

Note that the SUD scheme has the best performance in this test problem. The results are identical to the analytical solution, implying that the SUD scheme has no numerical diffusion for this problem. However, in subsequent problems we will see the deficiency of the SUD scheme. The pure-upwind difference scheme has the worst performance, while the VWSUD scheme has intermediate performance.

### 4.1.2 Two-Dimensional Highly Angled Flow (Test Problem 2)

The steady mixing of two streams with different velocity components is selected as a second numerical experiment. As shown in Fig. 13, the magnitude of the velocity of the flow from the bottom is twice that from the left. All other conditions are identical to that of Test problem 1.

The results are shown in Fig. 13 and the comparisons are shown in Table 2. A deficiency of the SUD scheme is brought out in this problem: a significant overshoot of 16°C is detected. However, it still achieves a substantial reduction of 30% of the numerical diffusion over the pure-upwind scheme in terms of the standard deviation. The VWSUD scheme, like the pure-upwind difference scheme, has no overshoots, but has a better performance of 30% over the pure-upwind scheme.

### 4.1.3 Three-Dimensional Corner-to-Corner Flow (Test Problem 3)

Extension of the two-dimensional benchmark problem described in Sec. 4.1.1 to three-dimensional flow is considered as the third test problem. As shown in Fig. 14, the three streams are introduced at the left, front, and the bottom of a three-dimensional cube.

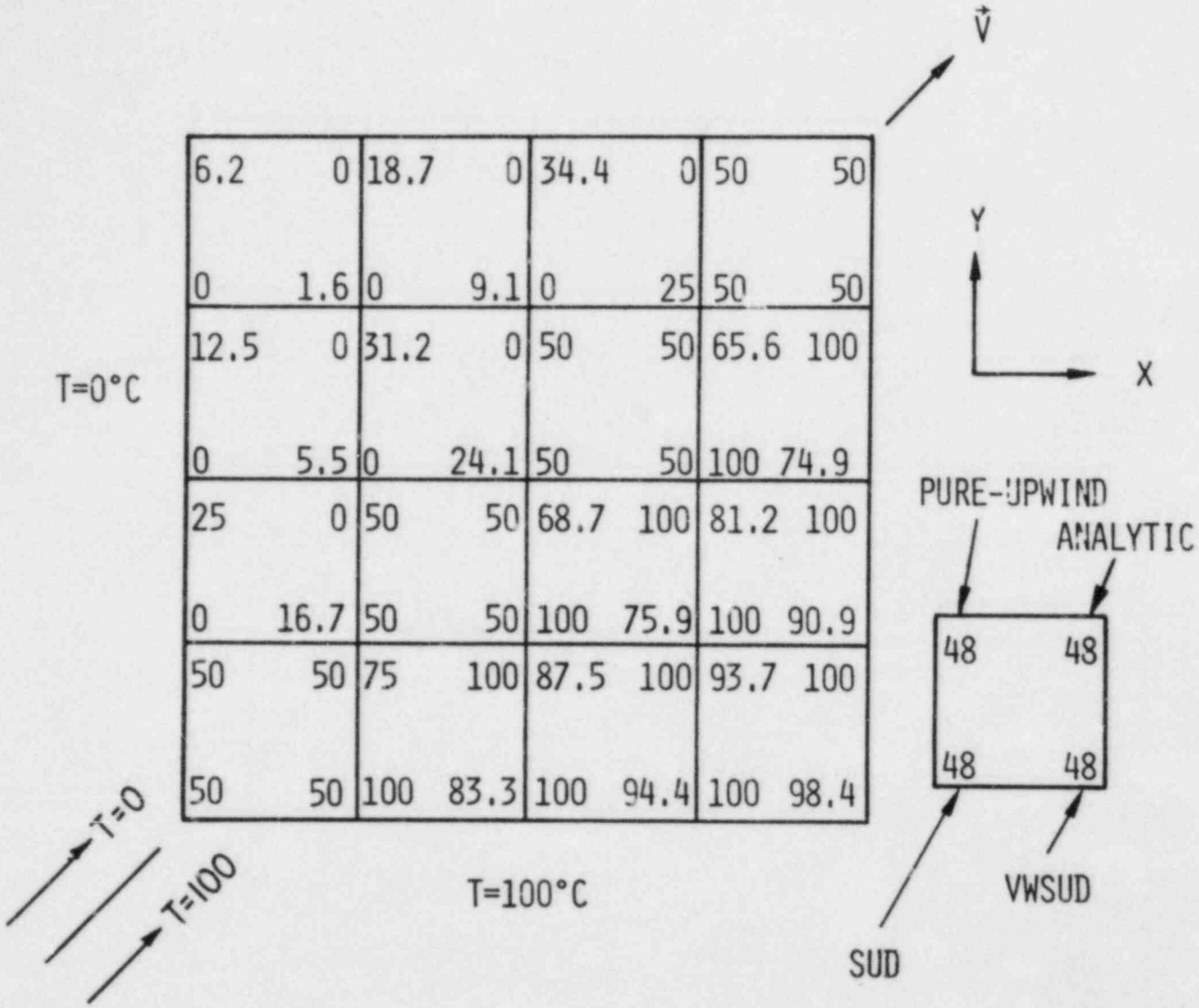


Fig. 12. Two-Dimensional Corner-to-Corner Flow

Table 1. Comparison of Pure-Upwind, Skew-Upwind, and Volume-Weighted Skew-Upwind Difference Schemes (Two-Dimensional Corner-to-Corner Flow

| OPTION | IESKEW | STANDARD DEVIATION $\sigma$(°C) | IMPROVEMENT OVER PURE-UPWIND % | MAX. ERROR (°C) | OVER SHOOT |
|---|---|---|---|---|---|
| PURE UPWIND | 0 | 21 | — | 34.4 | NO |
| SIMPLE SKEW UPWIND | 1 | 0.0 | 100 | 0.0 | NO |
| VOLUME-WEIGHTED | 2,3 | 14.6 | 30 | [illegible].0 | NO |

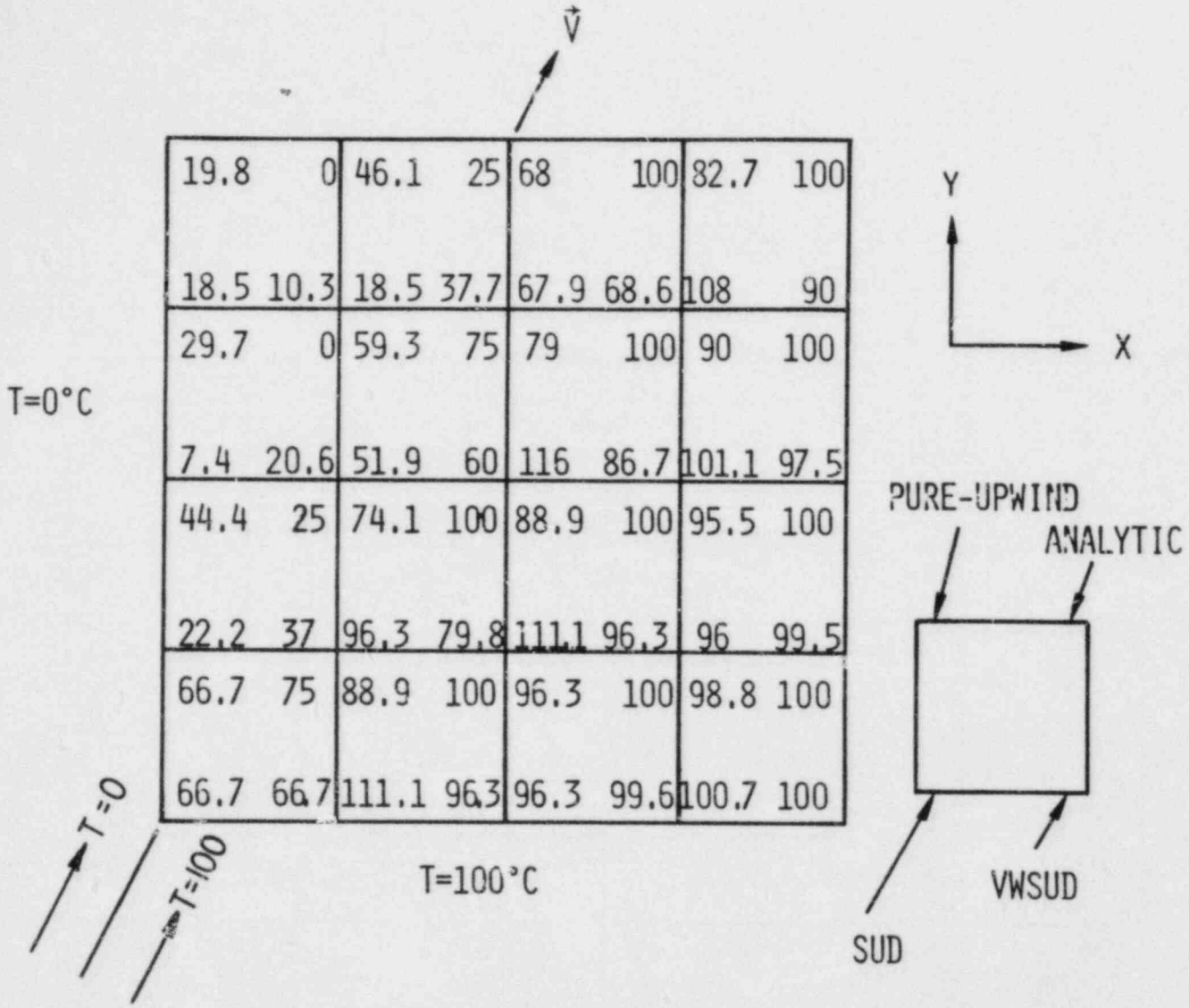


Fig. 13. Two-Dimensional Flow with w = 2v

Table 2. Comparison of Pure-Upwind, Skew-Upwind, and Volume-Weighted Skew-Upwind Difference Schemes (Two-Dimensional Flow with $w = 2v$)

| OPTION | IESKEW | STANDARD DEVIATION $\sigma$(°C) | IMPROVEMENT OVER PURE-UPWIND % | MAX. ERROR (°C) | OVER SHOOT |
|---|---|---|---|---|---|
| PURE UPWIND | 0 | 19.39 | — | 32 | NO |
| SIMPLE SKEW UPWIND | 1 | 13.51 | 30 | 32.1 | YES |
| VOLUME-WEIGHTED | 2,3 | 13.75 | 30 | 31.4 | NO |

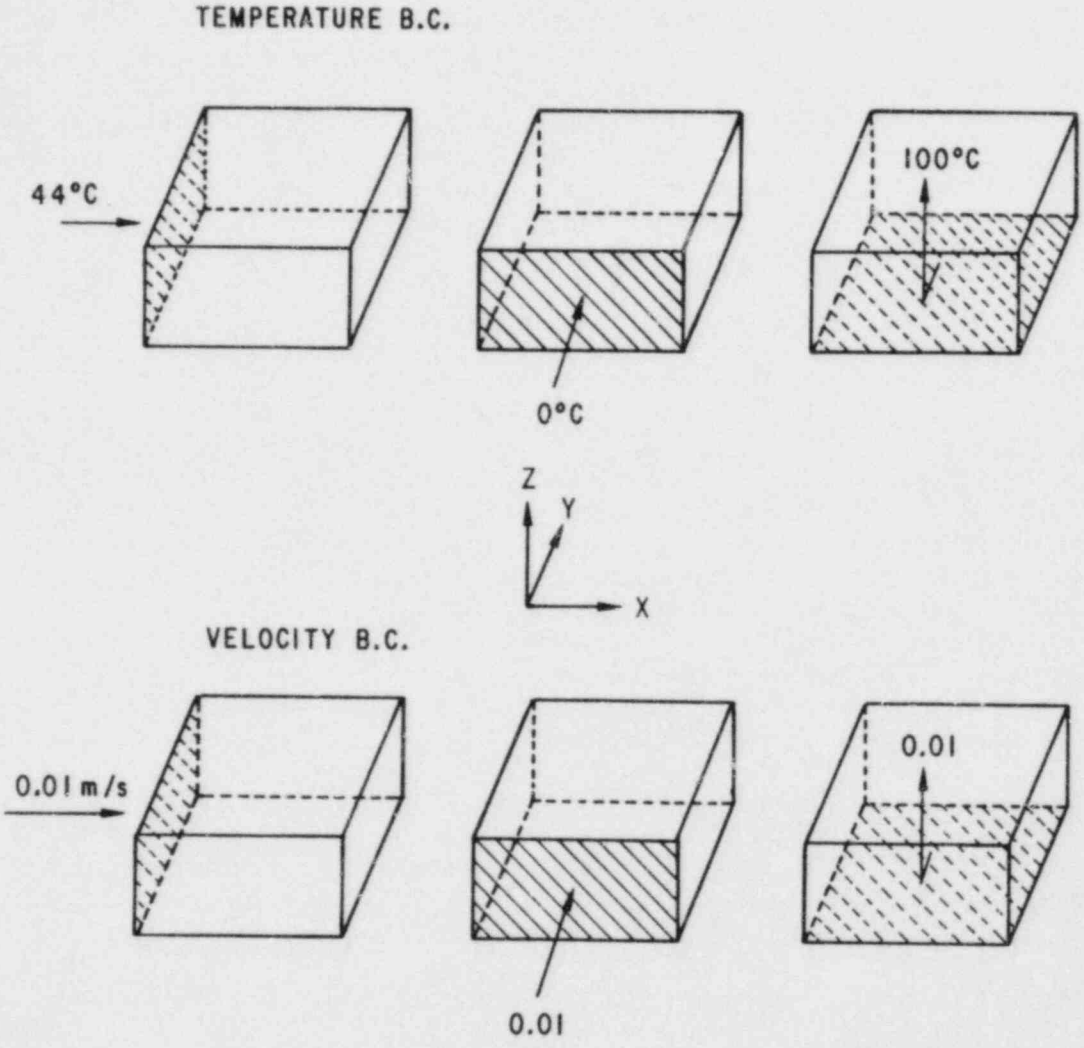


Fig. 14. Three-Dimensional Corner-to-Corner Flow

The streams are assigned with temperatures of 44, 0, and 100°C, respectively. The three components of the velocity are equal to 0.01 m/s and the grid sizes are all equal to 0.01 m. Assuming that the thermal conductivity is equal to zero, the analytic solution is easily derived; the results are shown in Fig. 15. Results for each K-level are shown in Figs. 16-18. Comparisons and analysis are presented in Table 3. Improvement of the SUD scheme over the pure-upwind difference scheme is substantial. Seventy percent of the error in terms of standard deviation has been reduced and maximum error has been reduced from 28.9 to 7.4°C. However, overshoots are observed. It should be emphasized that the SUD scheme produces under- and overshoots for the three-dimensional corner-to-corner problem but not in the analogous two-dimensional problem (Sec 4.1.1). The WSUD scheme, however, provides an overall and balanced improvement in terms of reduction of numerical diffusion and still maintains the simulated result within bounds.

## 4.2 Transient Validation

### 4.2.1 SAI Experiment (Test Problem 4)

#### 4.2.1.1 Problem Description

The experiment analyzed here is Test No. 1 of the SAI full-height experiment[21] which EPRI had sponsored to SAI for understanding thermal mixing relevant to the pressurized thermal shock. A simple rectangular geometry was constructed to simulate the cold leg and the downcomer of a PWR. The geometry of the cold leg and the downcomer used in the SAI thermal and fluid mixing experiment is illustrated in Fig. 19. The small dots in the cold leg as shown in Fig. 19 represent the locations of thermocouples used in the experiment. In the experiment, loop flow enters the cold leg at 70°C and flows down the cold leg to the downcomer. Approximately one-fifth of the way down from the entrance, cold fluid at 17°C (from HPI) enters the cold leg at an angle of 60° as shown in Fig. 19. The test conditions and relevant parameters are summarized in Table 4.

In the experiment, there were variations in the flow rates of the cold leg and HPI, and heat losses from the walls of the test section. But in our analysis, we assumed them to be negligible.

#### 4.2.1.2 Solution Procedure

Numerical simulation of the SAI experiment was performed by Lin et al[22] using COMMIX-1A[8]. A simple turbulence model with constant turbulent viscosity was used in their study. The numerical scheme used was the pure-upwind difference scheme. Regular rectangular control volume was used, creating a "zig-zag" approximation in modeling the angled HPI injector and the diverging nozzle section in the cold leg. Downstream of the HPI outlet, their simulation showed penetration of the cold fluid much deeper than that of experimental observations for Test No. 1 of the SAI experiment. Furthermore, thermal stratification should be stable (continuously increasing temperature from bottom to top) instead of unstable (having some cold fluid above the hot fluid) in the cold leg near the HPI outlet.

To improve the numerical modeling, the concept of irregular cells instead of "zig-zag" approximation was used in modeling the

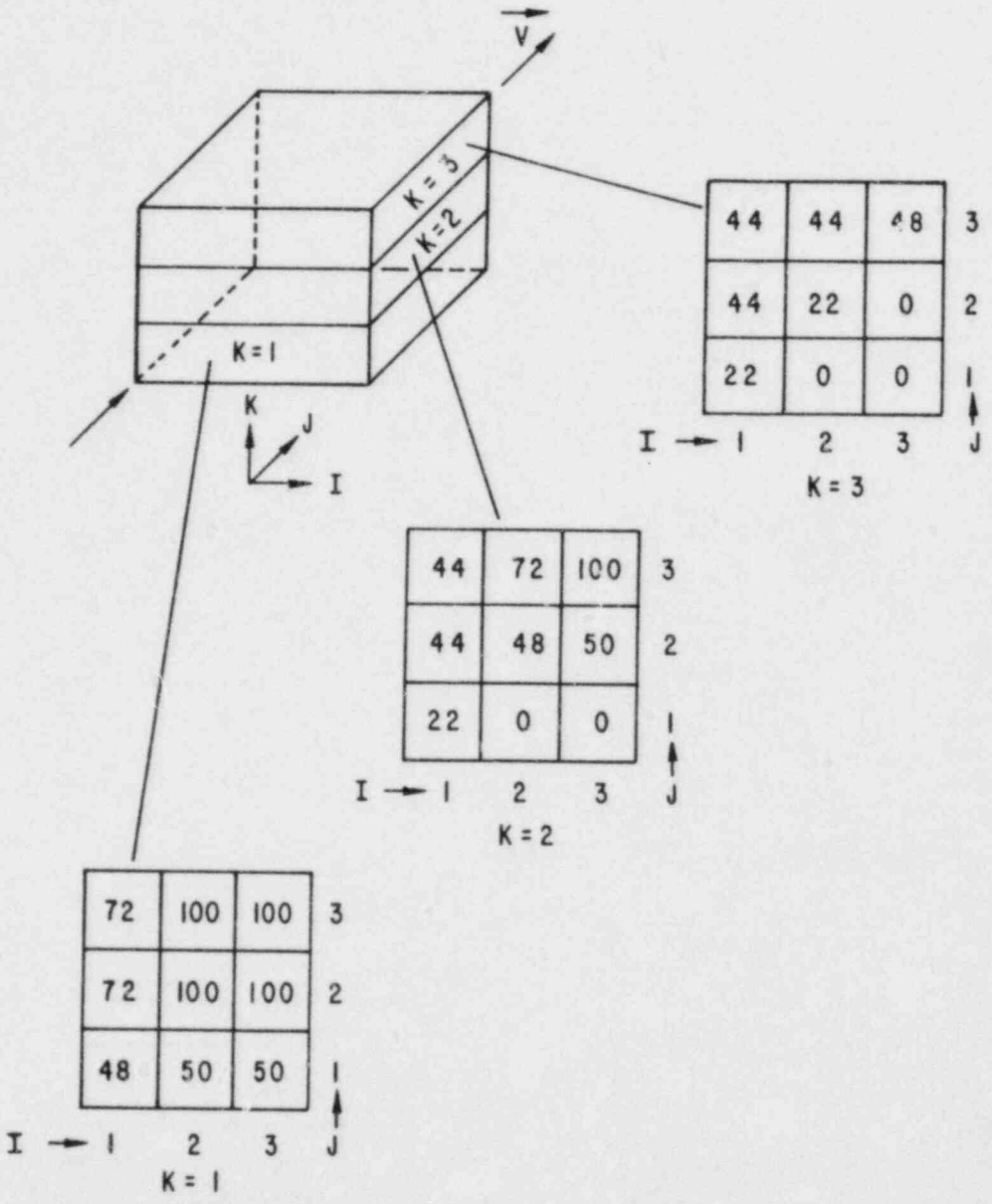


Fig. 15. Analytical Solution for Three-Dimensional Corner-to-Corner Flow

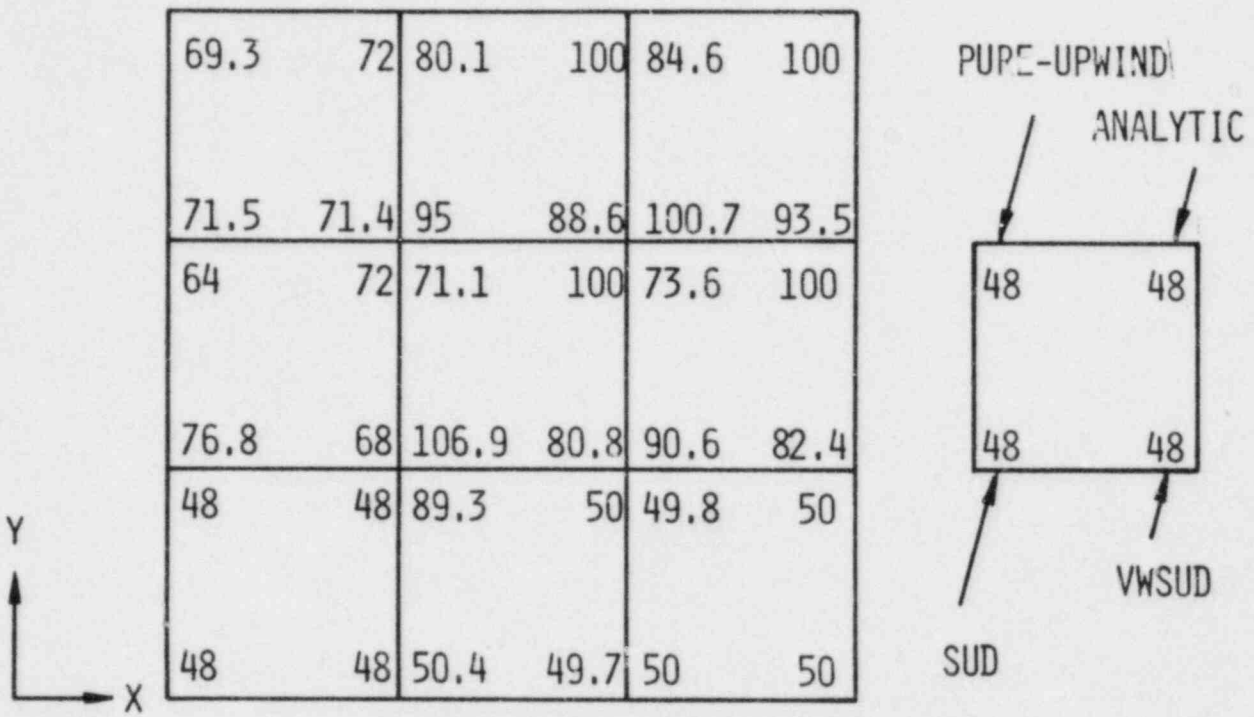


Fig. 16. Three-Dimensional Corner-to-Corner Flow (K=1)

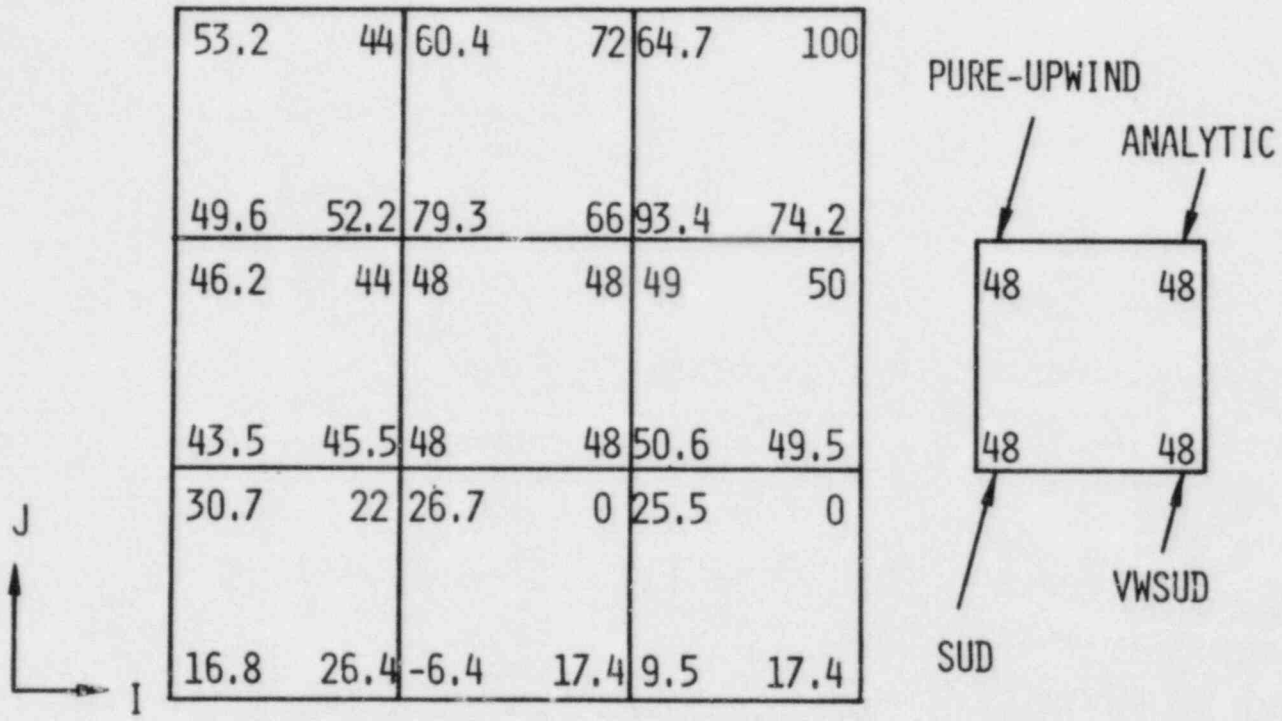


Fig. 17. Three-Dimensional Corner-to-Corner Flow (K = 2)

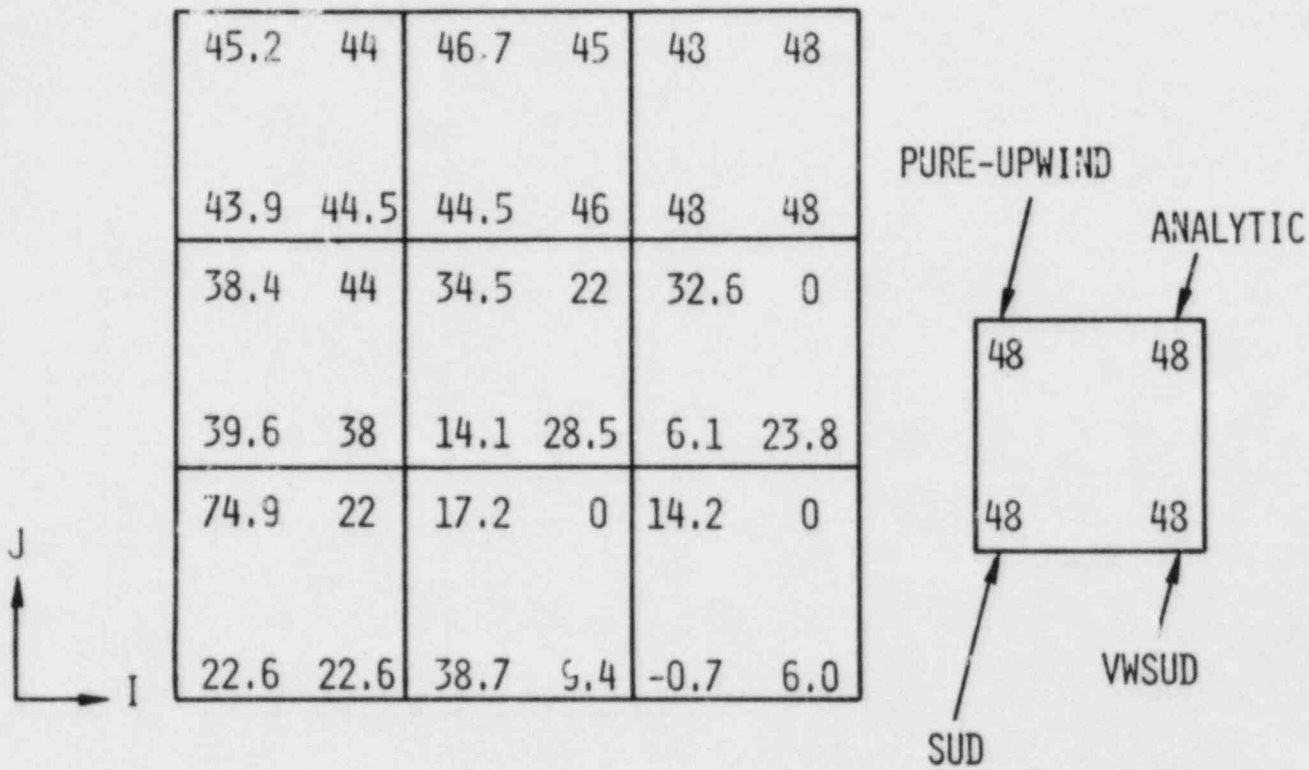


Fig. 18. Three-Dimensional Corner-to-Corner Flow (K = 3)

Table 3. Comparison of Pure-Upwind, Skew-Upwind, and Volume-Weighted Skew-Upwind Difference Schemes (Three-Dimensional Corner-to-Corner Flow)

| OPTION | IESKEW | STANDARD DEVIATION $\sigma$(°C) | IMPROVE-MENT OVER PURE-UP-WIND % | MAX. ERROR (°C) | OVER SHOOT |
|---|---|---|---|---|---|
| PURE UP-WIND | 0 | 15.41 | — | 28.9 | NO |
| SIMPLE SKEW UP-WIND | 1 | 4.71 | 70 | 9.42 | NO |
| VOLUME-WEIGHTED | 2,3 | 9.82 | 35 | 19.2 | NO |

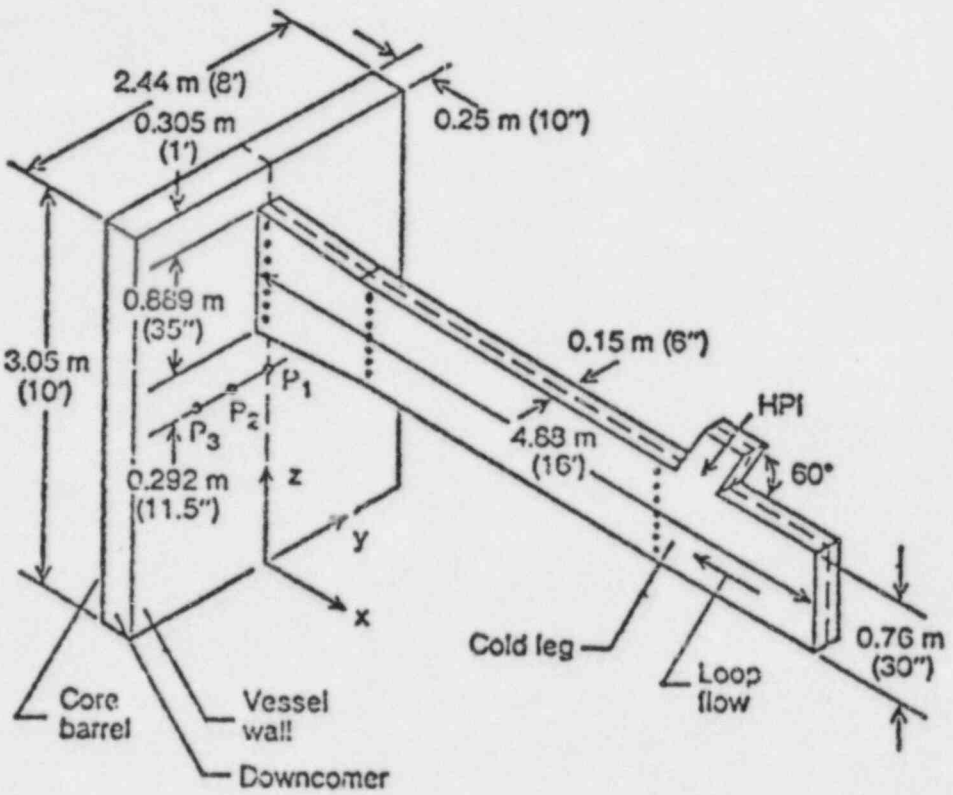


Fig. 19. Model Geometry for Cold Leg and Downcomer used in SAI Thermal and Fluid Mixing Test ('.' indicates Thermocouple Location).

Table 4. Summary of Test Conditions and Relevant Parameters for Test No. 1 of SAI Full-Scale Thermal Mixing Experiment

| Parameter | Value |
|---|---|
| Average flow rate of cold leg | 10.6 ℓ/s (168.5 gpm) |
| Average flow rate of HPI (after injection) | 1.0 ℓ/s (16 gpm) |
| Inlet temperature of cold leg | 70°C |
| Inlet temperature of HPI (after injection) | 17°C |
| Ratio of loop flow rate to HPI flow rate | 10.6 |
| Inlet velocity of cold leg | 0.0913 m/s |
| Inlet velocity of HPI | 0.0258 m/s |
| $Re_{CL} = \frac{\rho_{CL} V_{CL} D_{CL}}{\mu_{CL}}$ | $3.8 \times 10^4$ |
| $Fr_{CL} = \frac{V_{CL}}{g D_{CL} \frac{\rho_{HPI} - \rho_{CL}}{(\rho_{HPI} + \rho_{CL})/2}}$ | 0.44 |
| $Fr_{MIX} = \frac{V_{HPI} \frac{A_{HPI}}{A_{CL}}}{g D_{CL} \frac{\rho_{HPI} - \rho_{CL}}{\rho_{HPI}}}$ | 0.04 |

angled HPI injector and the diverging nozzle section of the cold leg. In addition, three different numerical difference schemes were used to quantify the numerical diffusion in the PTS problem:

- Pure-upwind Difference Scheme.
- Skew-upwind Difference (SUD) Scheme.
- Volume-weighted Skew-upwind Difference (VWSUD) Scheme.

All three simulations were performed using the fully-implicit scheme[2] and constant turbulent viscosity $\mu_t = 0.0$ pa-s.

In our analysis, we assumed a symmetry with respect to the central plane ($y = 0$); therefore, only half of the geometry was

modeled. We used a total of 950 cells (IMAX = 28, JMAX = 8, KMAX = 23) to model the half geometry.

Prior to the initiation of HPI, isothermal steady-state conditions were obtained first. After that, the HPI was introduced at time t = 0, and the transient computations up to t = 256 s were performed.

#### 4.2.1.3 Results and Discussions

The velocity distribution along the centerline of the downcomer and cold leg at t = 256 s after the initiation of HPI is shown in Fig. 20 to illustrate the flow field induced by the fluid mixing in the SAI experiment. Large amounts of numerical diffusion are generated primarily for regions with highly angled flow. Because the velocity profile is very similar for the results using VWSUD and the results using pure-upwind difference, only the flow field using VWSUD is presented here to illustrate the characteristics of the flow pattern.

- Near the injector of HPI, the cold fluid (17°C) from the HPI heavily mixes with the hot fluid (70°C) in the cold leg. However, the mixing is limited to the top portion of the cold fluid. The penetration of the cold fluid is small. This is the region with highly angled flow where numerical diffusion may be severe. This region is denoted as region A.

- As the mixed fluid flows down the cold leg from Region A to Region B, the cold fluid from the top of the cold leg tends to penetrate to the bottom. The flow direction is also highly angled in this region.

- At the junction of the cold leg straight and diverging section (Region C), the flow direction is nearly leveled off. This indicates that penetration of the cold fluid is nearly complete. The thermocouple response also indicated that a stable thermal stratification was observed in the experiment.

- At the junction of the cold leg and the downcomer (Region D), hot stagnant fluid from the downcomer tends to enter the cold leg at the top, resulting in counter-current flow. Because of the turning of flow from the cold leg towards the downcomer, most of the flow direction is also highly angled in this region.

- In the downcomer, cold fluid impinges directly on the core-barrel side of the downcomer like a wall jet. After hitting the wall, cold fluid moves down along the core-barrel side until the downward motion is overcome by the upward momentum of the buoyancy driven hot fluid. This creates a recirculating flow in the bottom section of the downcomer.

From the description of the mixing pattern, it can be noted that the most probable regions where the numerical diffusion due to highly angled flow may be significant are Regions A, B, and D. In order to illustrate this, a comparison of the vertical temperature profiles at the cold

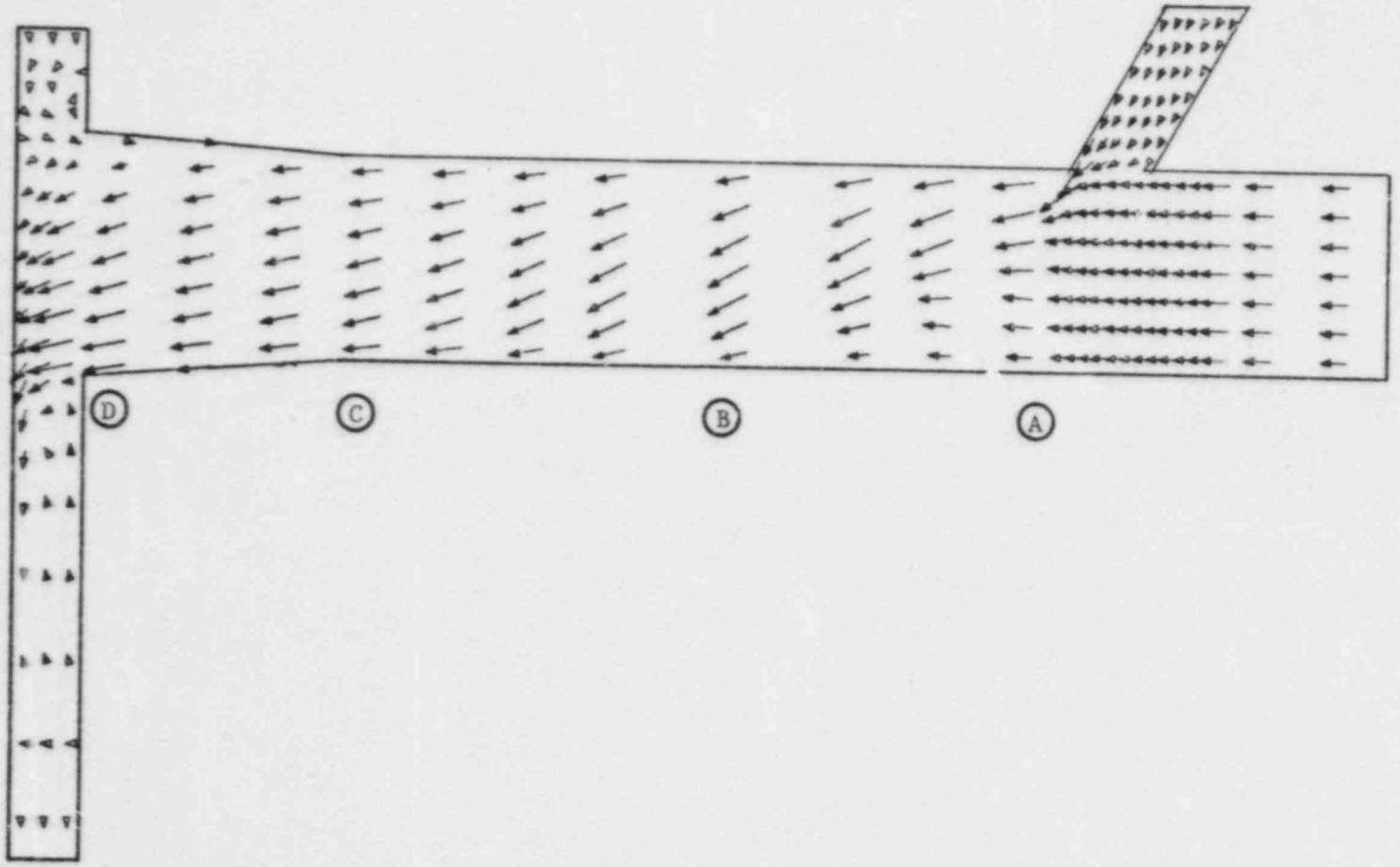


Fig. 20. Velocity Distribution along Centerline of Downcomer and Cold Leg for SAI Test 1 at t = 256 s (Computation with VWSUD only)

leg downstream of the HPI outlet (in Region A) is shown in Fig. 21. Since the trends of thermal stratification have been established approximately 80 s after initiation of HPI, the instantaneous temperature profiles at 100 s after initiation of HPI are illustrated here for the purpose of comparison. The ordinate in Fig. 21 is y/H, H being the height of the cold leg.

Figure 21 shows that at the cold leg downstream of the HPI outlet, penetration of the cold fluid with pure-upwind difference is much deeper than that of the experimental observations due to the large amount of numerical diffusion. The results of SUD and VWSUD indicated that penetration of the cold fluid is only limited to the top portion of the cold leg that is consistent with the experiment. The use of SUD and VWSUD did eliminate a substantial amount of numerical diffusion to prevent the "false" penetration of the cold fluid.

At Region B where the amount of numerical diffusion may be significant due to the highly angled flow, the use of SUD results in overshooting behavior in the middle of the cold leg. A comparison of temperature profiles for three different models is presented in Table 5. Unfortunately, experimental data are not available for comparison at this location.

TABLE 5. Comparison of Temperature Profile in Cold Leg Downstream of HPI (Region B) for Three Numerical Difference Schemes (time = 100 sec after HPI)

| Height (Y/H) | Pure-Upwind | SUD | VWSUD |
|---|---|---|---|
| (13/14) | 52.0°C | 67.5°C | 62.8°C |
| (11/14) | 63.0°C | 68.3°C | 63.0°C |
| (9/14) | 63.3°C | 70.7°C | 63.0°C |
| (1/2) | 63.3°C | 72.6°C | 62.7°C |
| (5/14) | 63.3°C | 63.5°C | 62.2°C |
| (3/14) | 63.6°C | 69.4°C | 62.5°C |
| (1/14) | 64.3°C | 66.2°C | 63.9°C |

In Table 5, it can be noted that the temperature at the middle of the cold leg (Y/H = 0.5) predicted by the SUD scheme is higher than 70°C (the maximum possible temperature). This is one of the deficiencies of the SUD scheme. Consequently, the temperature profile is distorted. The results of the pure-upwind difference scheme indicate good mixing in the top portion of the cold leg. The results of the VWSUD scheme indicate that more cold fluid penetrates to the bottom of the cold leg. This is the location where the thermal stratification is in transition from unstable to stable. Computations using the SUD scheme were terminated at 100 s because of these observed overshoots.

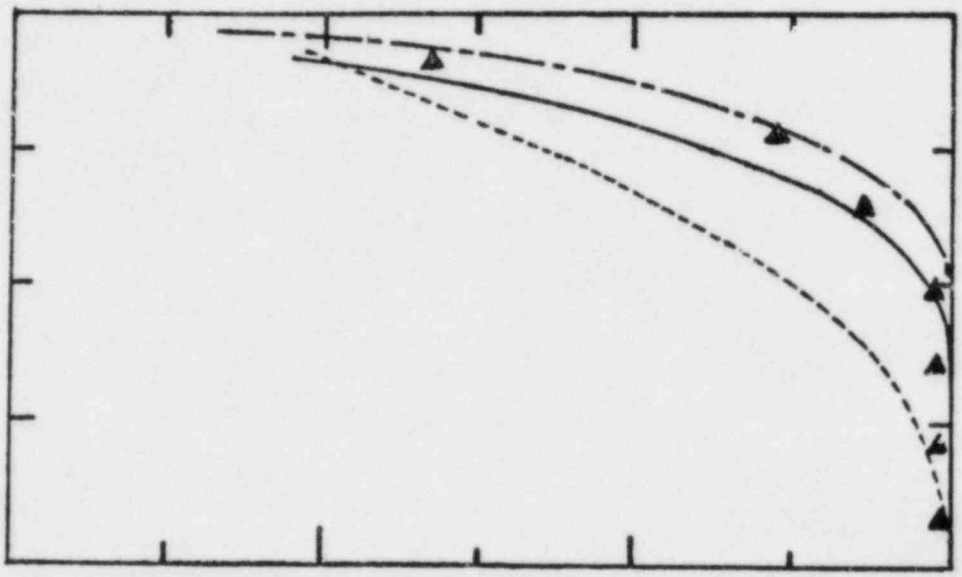

▲ SAI Test Data

---------- Pure-upwind Calculations

——·——· SUD Calculations

———— VWSUD Calculations

Fig. 21. Comparison of Temperature Profile in Cold Leg Downstream of HPI (Region A) for three Numerical Difference Schemes (time = 100 s after HPI)

The temperature distribution along the centerline of the downcomer and cold leg at t = 256 s after initiation of the HPI is shown in Fig. 22. At the junction of the cold leg straight and diverging sections, cold fluid already penetrated to the bottom of the cold leg, resulting in a stable thermal stratification. The results of Model 3 (VWSUD) clearly illustrate the correct trend of thermal stratification. The results of Model 1 (pure-upwind difference) is nearly uniform. The disagreement with experimental observation can be attributed to the large amount of numerical diffusion of the upwind difference scheme. At the entrance of the downcomer, due to the effect of buoyancy, hot stagnant fluid at the top of the downcomer is sucked back into the top portion of the cold leg as described in Fig. 20. As a result, significant stable thermal stratification was observed in the experiment. The temperature difference between the top and bottom of the cold leg in this entrance region is higher than that at the junction of the cold leg straight and diverging sections. The results of using VWSUD illustrate the correct thermal stratification with overall temperature difference (between the top and bottom of the cold leg) of 2.0°C. Although the results of using the pure-upwind difference scheme also illustrate this trend, the maximum temperature difference is small ($\Delta T$ = 0.6°C). The numbers seem small (2.0°C vs 0.6°C), but the maximum temperature drop at this location during the whole transient process is only 6°C.

In the downcomer, there is a hot pocket at the top of the downcomer due to the nearly stagnant flow in that region. Mixing is quite good in the downcomer at t = 256 s after the initiation of HPI, the difference between the results of using VWSUD and the results of using upwind difference is small. At certain locations of the downcomer, there is a discrepancy between the numerical computations and the experiment; the temperature is approximately 3°C lower in the experiment than that in the numerical computations. The reason is the heat loss in the experiment prior to the initiation of HPI results in the lower initial value of thermocouple response.

A comparison of the calculated and experimental temperature profiles at four different sections during the transient are shown in Figs. 23-26. Figure 23 shows the comparison of thermocouple data along the centerline in the cold leg downstream of the HPI with COMMIX-1B calculations. The fluctuation of thermocouple response in the experiment was quite substantial as shown in Fig. 23. Thermocouple $L_{11}$ is located in the middle of the cold leg, $L_{10}$ is one unit above $L_{11}$, $L_9$ is 2 units above $L_{11}$, whereas $L_{12}$ is one unit below $L_{11}$, and $L_{13}$ is two units below $L_{11}$. Each unit is measured as 1/7 of the height of the cold leg. At this location, the temperature profile is virtually unchanged after 60 s of HPI. Due to the large amount of numerical diffusion, the temperature of $L_{10}$ and $L_{11}$ for pure-upwind difference is approximately 5 to 7°C lower than that of the experiment and the results using VWSUD.

Figure 24 shows the comparison of thermocouple data along the centerline of the cold leg at the entrance to the downcomer with COMMIX-1B calculations. Thermocouples $L_{44}$ through $L_{49}$ represent the temperature profiles from the top to the bottom. Thermocouple $L_{43}$ was out of order in the experiment, therefore no reading was reported. The quenching behavior, as indicated by the thermocouple readings near the bottom of the cold leg ($L_{48}$ and $L_{49}$), is very pronounced between 40 to 60 s after the initiation of HPI.

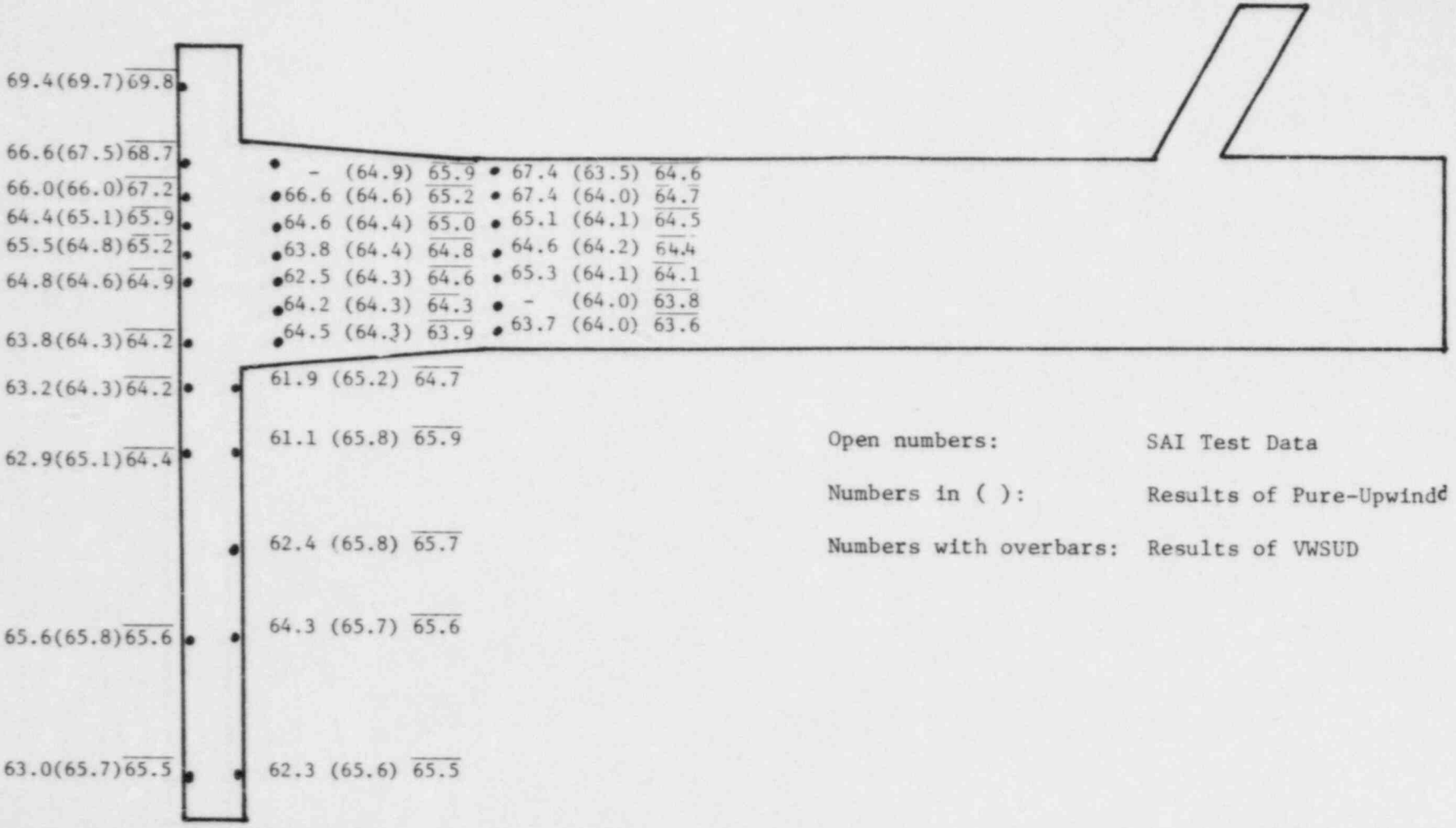


Fig. 22. Temperature Distribution along Centerline of Downcomer and Cold Leg for SAI Test 1 at t = 256 s

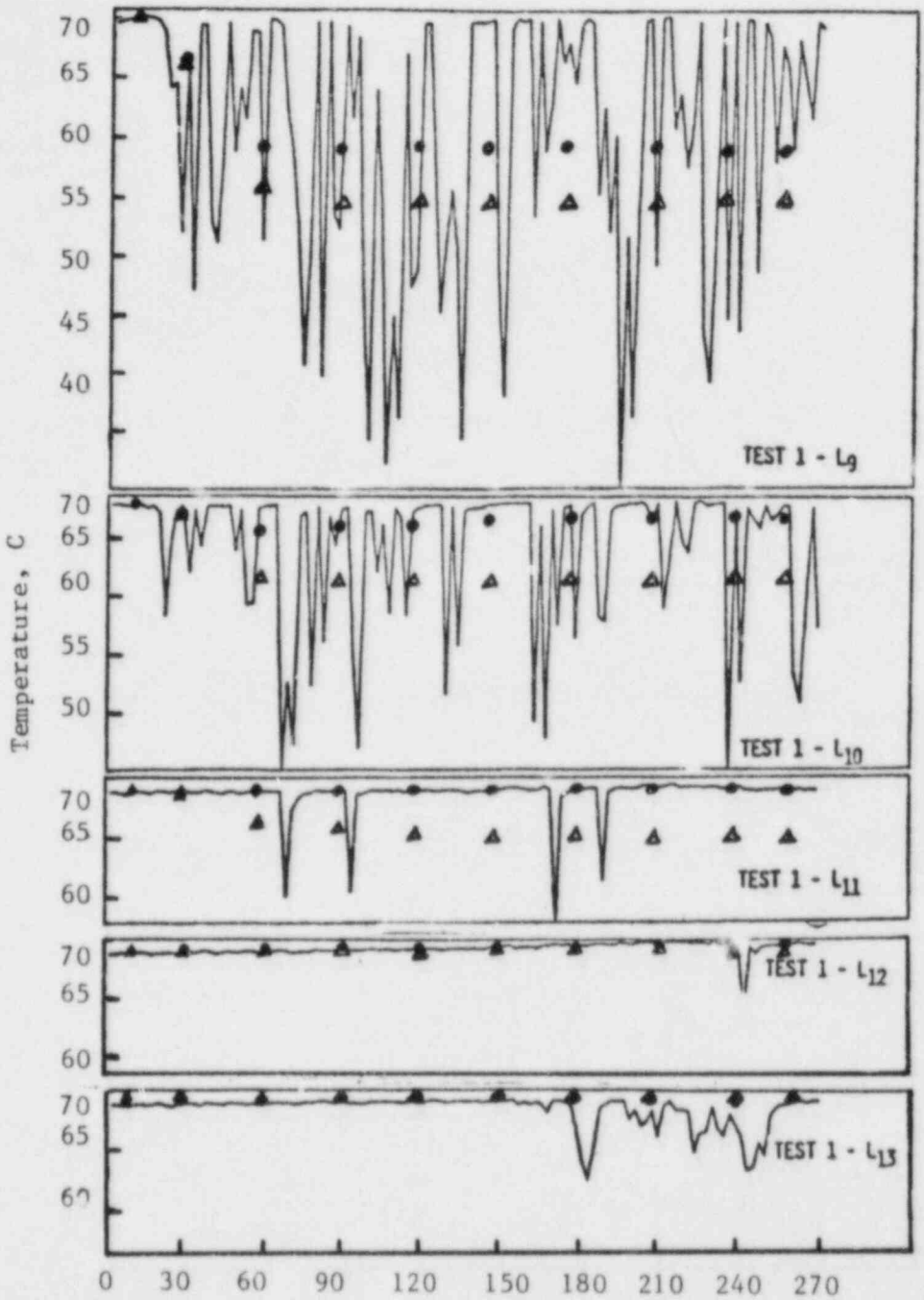


Fig. 23. Comparison of Thermocouple Data along Centerline of Cold Leg Downstream of HPI with COMMIX-1B Calculations

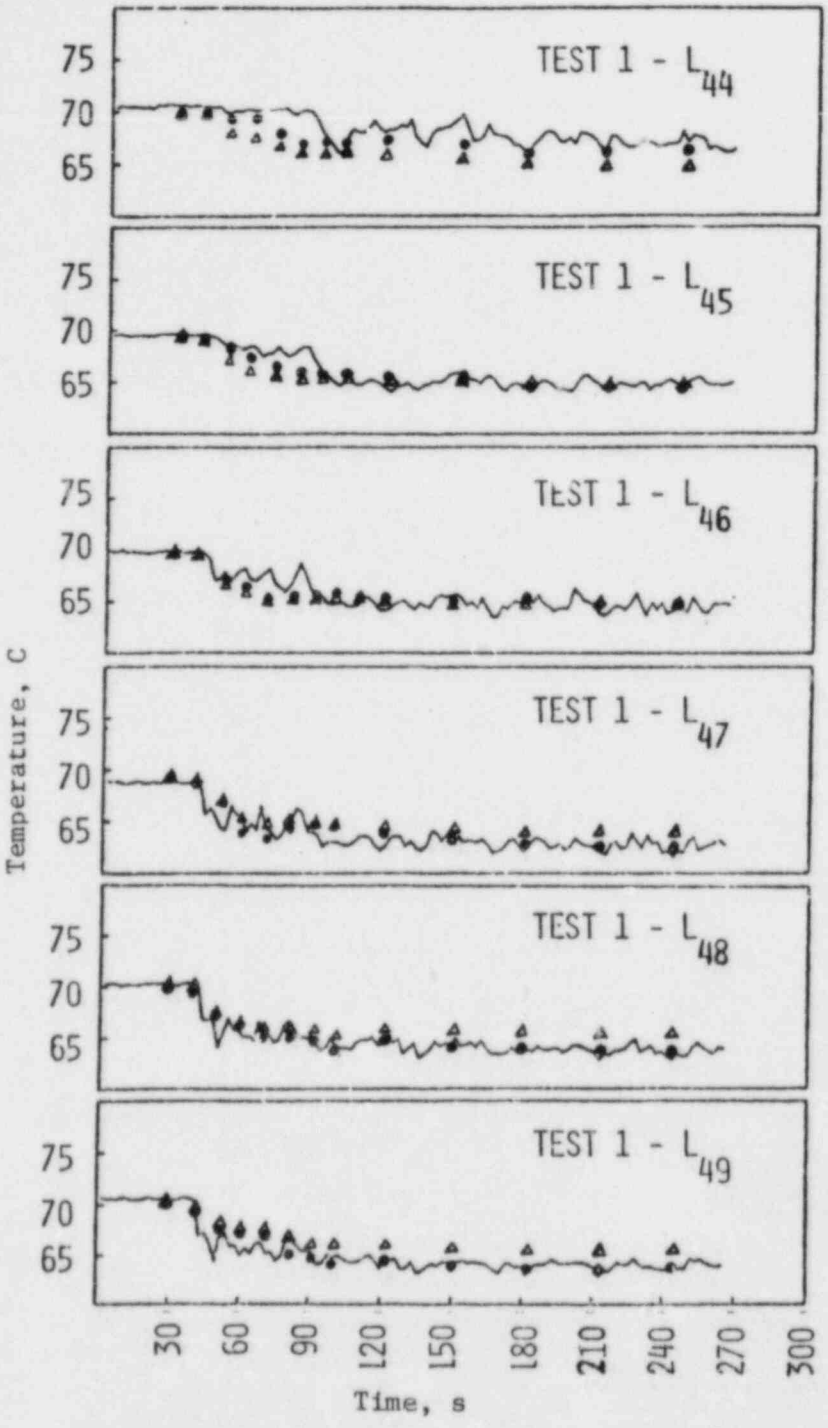


Fig. 24. Comparison of Thermocouple Data along Centerline of Cold Leg at Entrance to Downcomer with COMMIX-1B Calculations

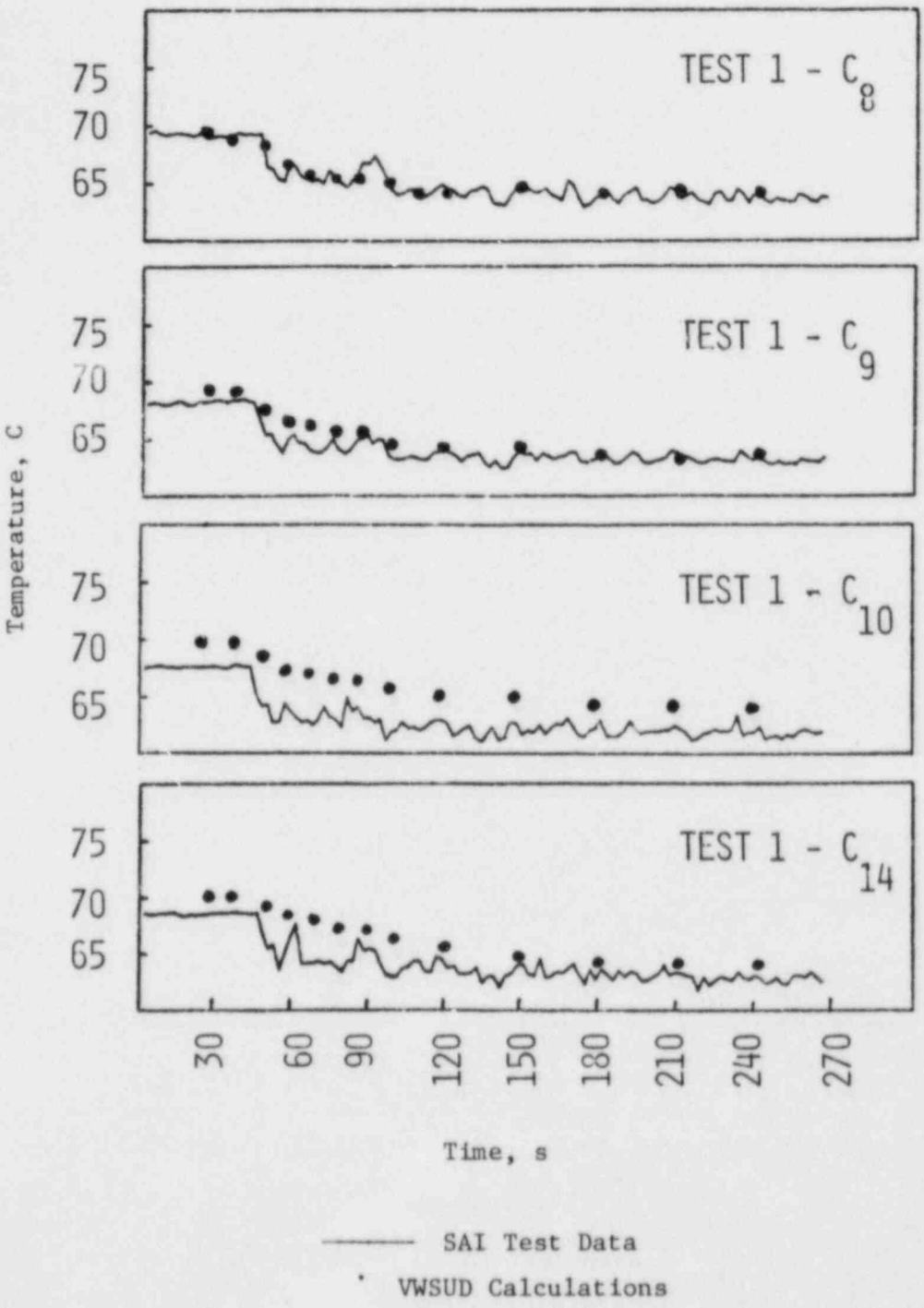


Fig. 25. Comparison of Thermocouple Data on Core-Barrel Side of Downcomer with COMMIX-1B Calculations using VWSUD

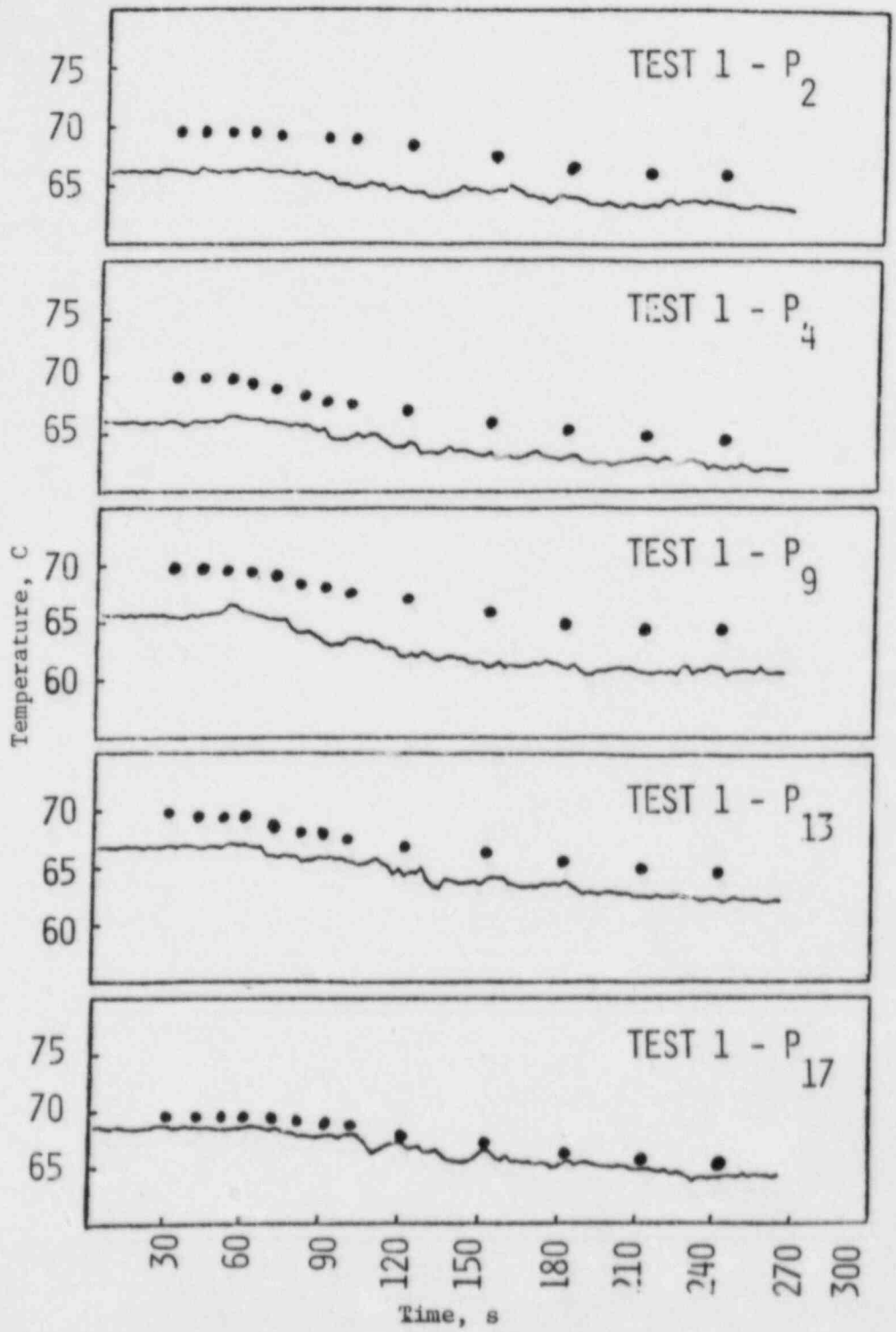


Fig. 26. Comparison of Thermocouple Data on Pressure-Vessel Side of Downcomer with COMMIX-1B Calculations using VWSUD

If the quenching is severe, "thermal shock" will occur. Our computations indicate that the temperature gradient is relatively mild in this test. Use of VWSUD reduces a substantial amount of the numerical diffusion as described before (Fig. 22). Although the greement between the experiment and the results using pure-upwind difference is reasonably good, agreement between the experiment and the numerical computations using VWSUD is significantly improved. For example, at $L_{44}$, results using upwind difference are constantly lower than experimental data, whereas results using VWSUD agrees well with the experiment. At the bottom of the cold leg, such as $L_{47}$ to $L_{49}$, due to the insufficient amou . of thermal stratification, predictions using upwind difference are constantly higher than experimental data. Agreement between the numerical computation with VWSUD and experimental data is quite good for thermocouples $L_{47}$, $L_{48}$, and $L_{49}$.

Comparisons of selected thermocouple data on the core-barrel side and pressure-vessel side of the downcomer with COMMIX-1B calculations are shown in Figs. 25 and 26, respectively. Since the results shown in Fig. 22 indicate close agreement between the VWSUD and pure-upwind difference schemes, the comparisons with the experimental data are limited to the results of VWSUD only. The cold fluid leaving the cold leg directly hits the wall of the downcomer as illustrated by the transient temperature plot of $C_8$ and $C_9$ in Fig. 25. As a result, similar to $L_{48}$ and $L_{49}$ in Fig. 24, there is a quenching behavior between 40 - 60 s after the initiation of HPI. Because thermocouple $C_{14}$ is located at the downcomer well below the exit plane of the cold leg, the quenching behavior is relatively mild.

As mentioned before, in the experiment there were some heat losses from the walls. Prior to initiation of HPI, the temperatures for thermocouples $P_2$, $P_4$, $P_9$, and $P_{13}$ are approximately 66°C only, 4°C below the initial temperature used in the numerical computation. As a result, there is a difference between the experiment and numerical computation. However, the trend of the temperature gradients is very similar; they are all relatively mild. If the initial temperatures were close to 70°C, such as at thermocouple $P_{17}$, then agreement would have been even better.

In conclusion, numerical diffusion is an important source of numerical error in thermal mixing analysis of the pressurized thermal shock problem. The results based on the VWSUD improve the agreement substantially with the experimental data especially in regions with highly angled flows.

### 4.2.2 CREARE Experiment (Test Problem 5)

#### 4.2.2.1 Problem Description

Two analyses were performed for this Creare experiment[23] (Test #51), which EPRI had sponsored to CREARE, Inc. for understanding thermal mixing phenomenon related to pressurized thermal shock. The first analysis used very fine computational meshes, the one-equation turbulence model, and the pure-upwind scheme. The second analysis used coarse computational meshes, the one-equation turbulence model, and the volume-weighted skew-upwind scheme. The two analyses were compared to see the effects of the VWSUD scheme.

The test geometry of the Creare 1/5-scale facility[23] is given in Fig. 27. Major linear dimensions of the facility are reduced from typical prototype values of Westinghouse and Combustion Engineering plants by approximately a factor of 5. The cold leg is simulated by a circular pipe with three injection locations and angles. The downcomer is represented by a planar section having width and height comparable to a 90° sector of a reactor downcomer. The blockage due to the hot-leg pipe also is included in the downcomer, along with a typical step in the vessel wall.

The COMMIX model of the CREARE geometry is given in Fig. 28. The cold leg is modeled by an octagon. The 60° HPI injection is modeled as a square pipe with exactly 60° inclination. Since the injection angle affects greatly the split of flows in the cold leg, accurate representation of the injection angle is important in the analysis. The nozzle at the end of the cold leg was modeled by eight inclined planes. The step in the belt line of the downcomer also was modeled.

Figure 29 shows the computational meshes and the thermocouple locations used in the first analysis. A total of 7477 computational cells was used for the analysis with most of the mesh concentration in the pipe. The number of meshes in the x, y, and z directions are 37, 24, and 36, respectively. The meshes are chosen to accommodate the thermocouples at centers of the computational cells whenever possible. The surface permeabilities in the x and y directions at the bottom of the downcomer was set equal to zero to insure that there was no cross-flow; this was to simulate the manifold at the bottom of the downcomer in the experiment. All inclined surfaces are modeled in COMMIX through the use of irregular geometries. Most of the tedious work in preparing the volume porosity and surface permeabilities for the irregular surfaces automated by a computer program currently is under development.

The conditions for Test 51 are shown in Fig. 30[24]. The initial condition of the test before the transient was at 64.1°C (147.3°F) with a loop flow of $2.52 \times 10^{-4}$ $m^3/s$ (4.0 gpm). At the start of the transient, cold fluid at a temperature of 16.67°C (62.0 °F) and flow rate of $1.35 \times 10^{-4}$ $m^3/s$ (2.14 gpm) was injected into the cold leg through the HPI pipe (5.08d cm ID). By the time the flow reached the nozzle, a significant amount of mixing had taken place. Therefore, the measured temperatures were very close to the mixed mean temperature in the downcomer region below the cold leg. Three important mixing processes were observed in the experiment.

- Part of the cold fluid propagated upstream of the cold leg, while most of it flowed downstream toward the downcomer; the cold fluid eventually propagated all the way to the upstream elbow region of the cold leg,

- Part of the hot fluid on top of the downcomer was sucked into the cold leg to form a recirculation flow in the upper portion of the nozzle; this process enhances the thermal stratification in the nozzle region, and

- The cold fluid from the cold leg jumped over the gap between the vessel wall and the core barrel wall in the downcomer, resulting in a slightly cooler temperature on the barrel side of the downcomer.

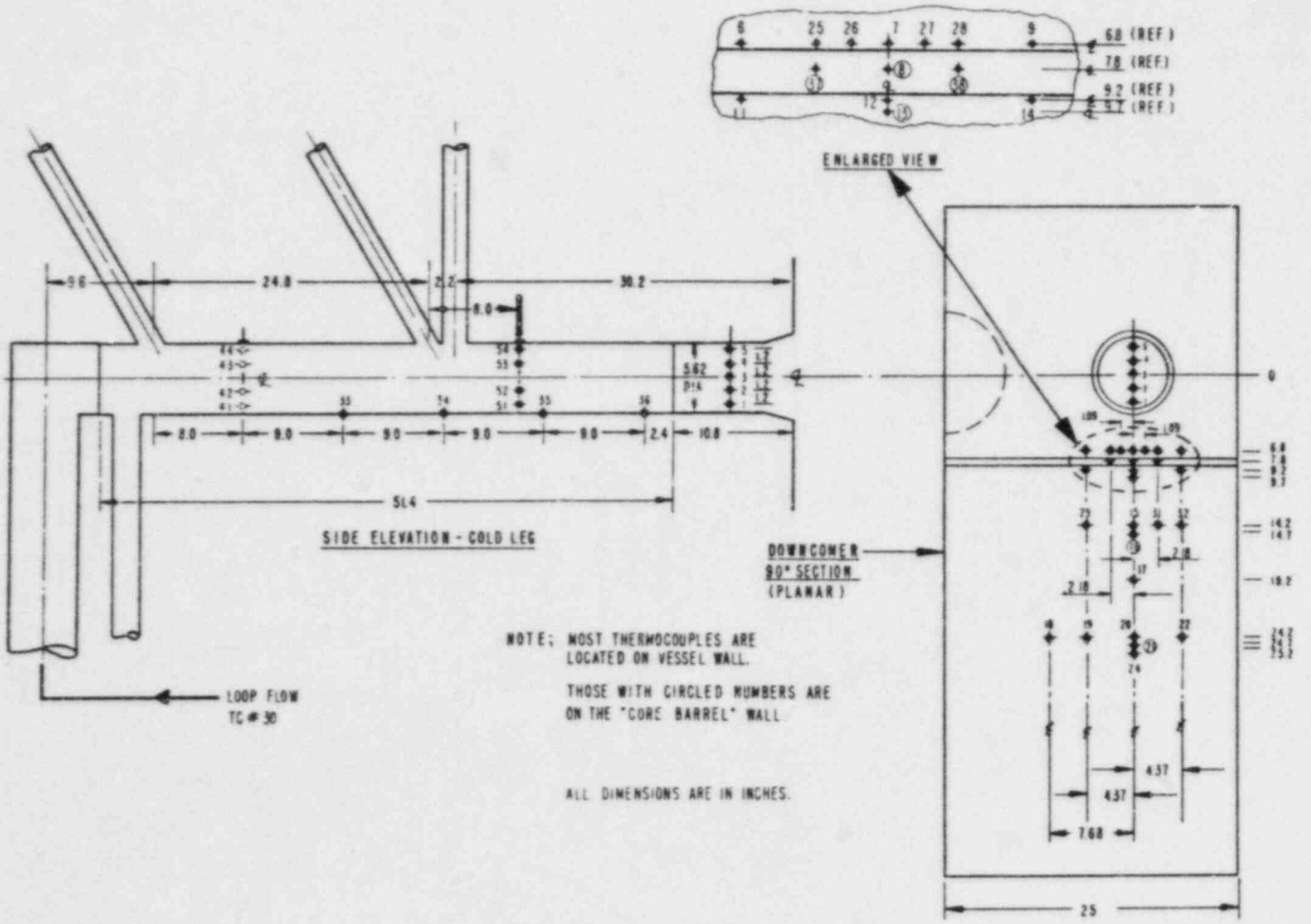


Fig. 27. CREARE 1/5-Scale Test Configuration, Dimensions, and Thermocouple Locations

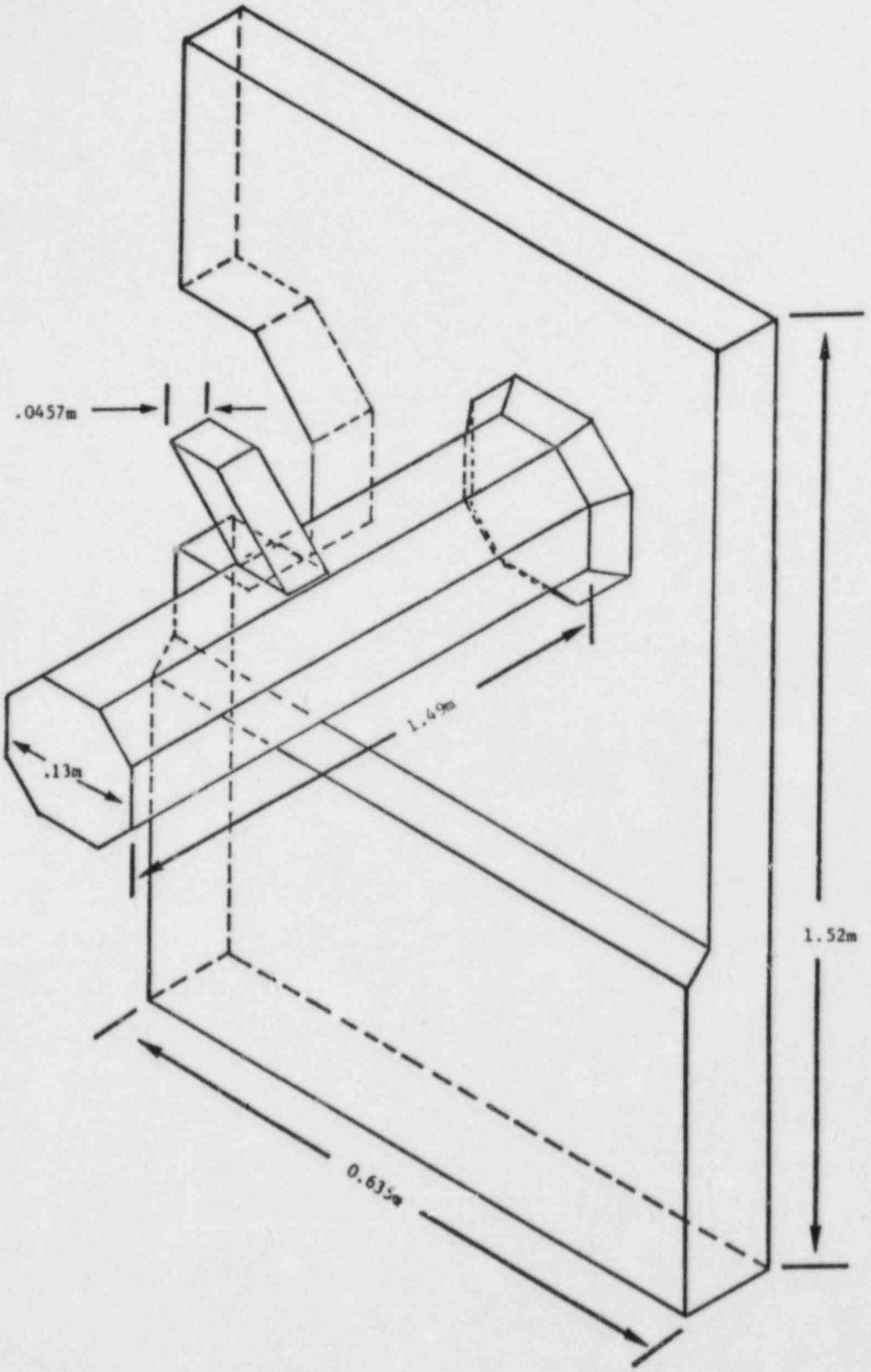


Fig. 28. COMMIX Model of CREARE Test 51 Geometry

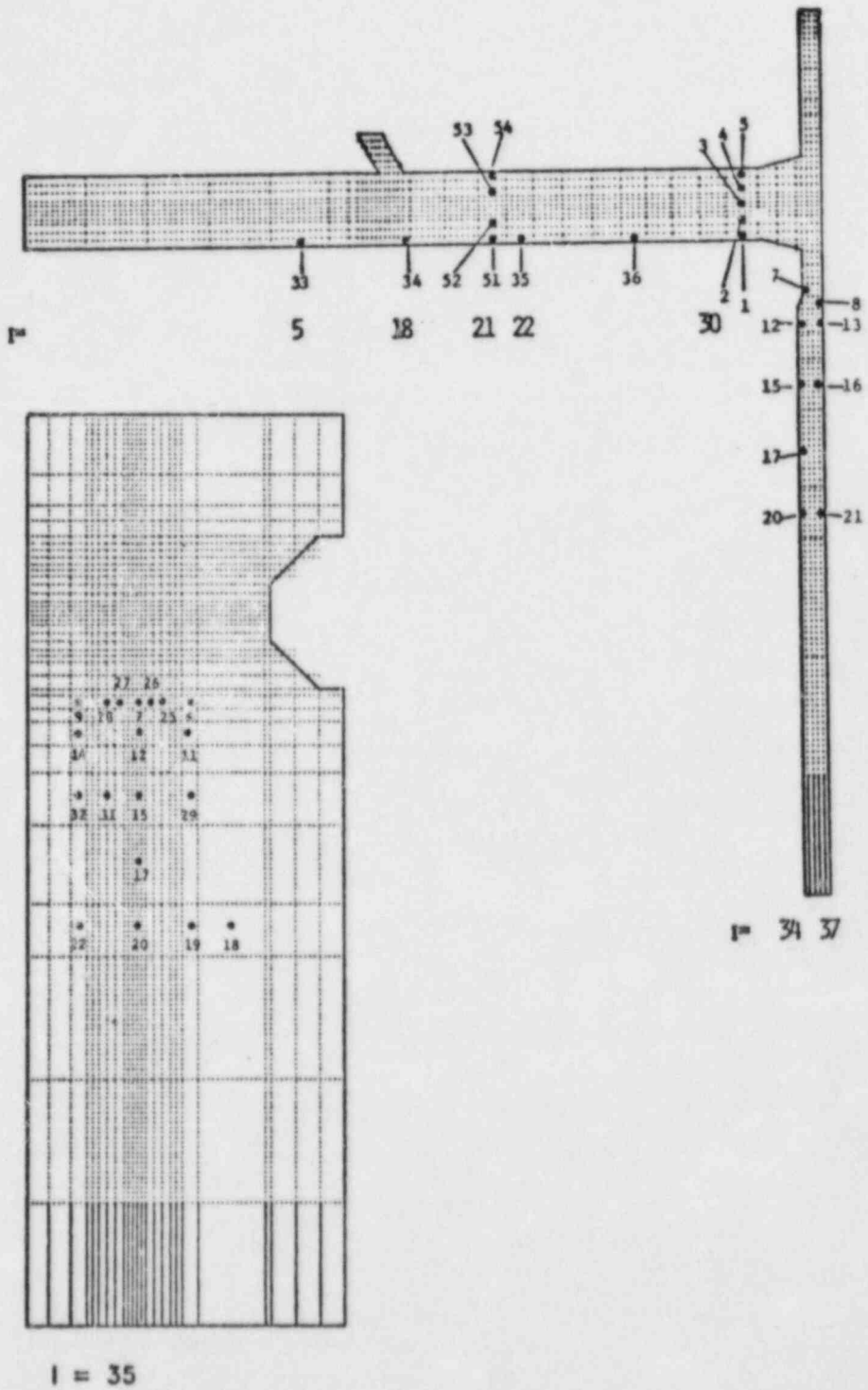


Fig. 29. Computational Meshes used in the COMMIX Calculation, and Thermocouple Locations

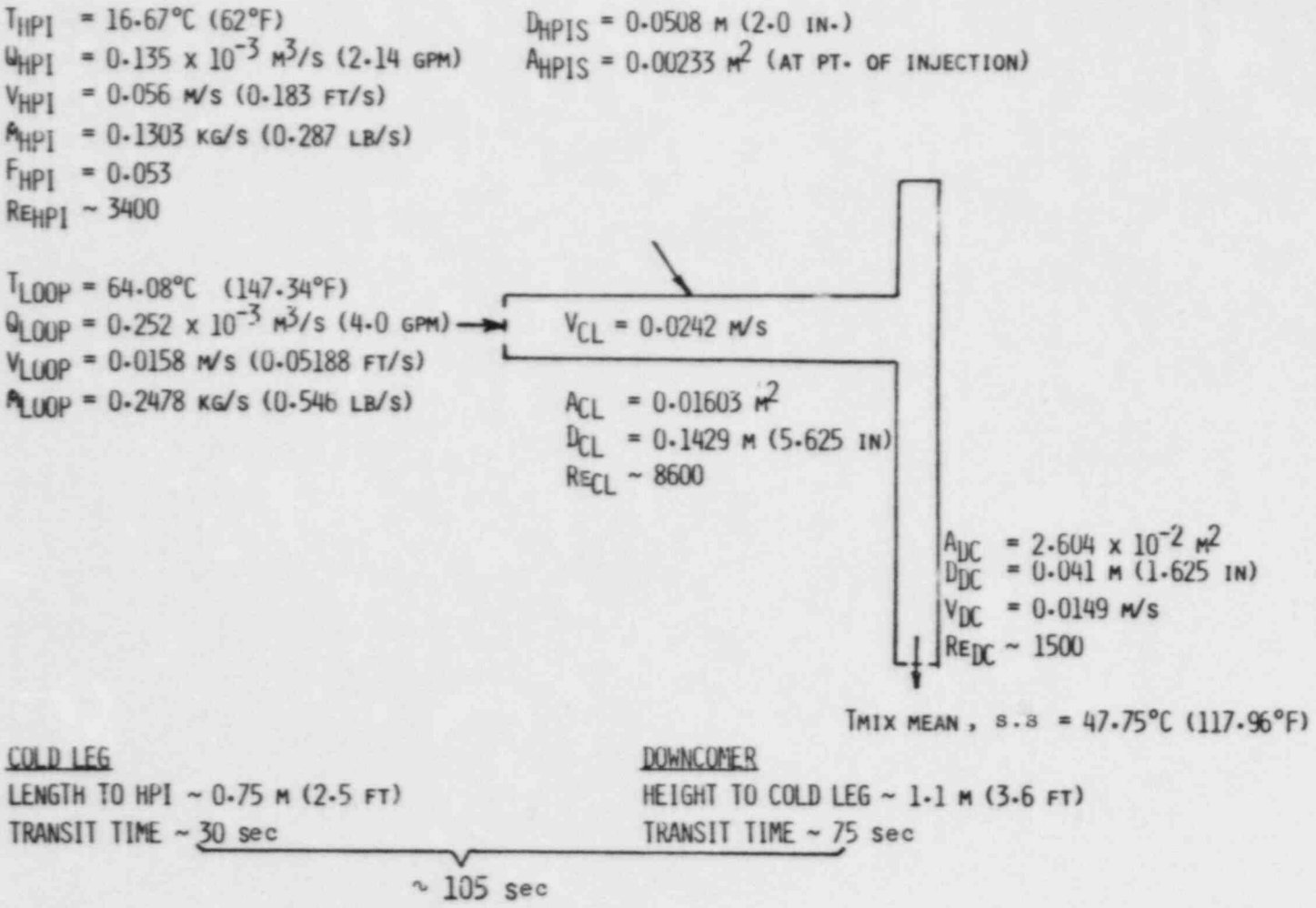


Fig. 30. Summary Data Sheet of 1/5-Scale Experiment Simulated - Test 51 $Q_{loop}/Q_{HPIS}$ = 1.87, Near 60° Top Injection

These three phenomena are reproduced in the COMMIX calculations.

#### 4.2.2.2 Results and Discussion

The present COMMIX calculational results for the first analysis are given in Figs. 31-35. The COMMIX results are given by dots and the experimental data are given by solid lines in these figures. Excellent agreement between the COMMIX calculations and the experimental data was achieved by using the previously mentioned refinements.

Thermocouples T1-T5 are located just before the nozzle region. Experimental readings of these thermocouples showed that the cold fluid penetrated to the bottom of the cold leg and stayed on the bottom toward the downcomer. Therefore, temperature readings on T1 are lower than readings on T5. This flow pattern also is confirmed from the thermocouple readings of T51 and T54, which are right downstream of the high-pressure injection pipe in the cold leg. Therefore, slight thermal stratification existed in the cold leg and the nozzle region. However, significant mixing had occurred in the cold leg. This is manifested by the fact that the overall temperature readings between T1-T5 are much higher than the inlet temperature of 16.67°C at the HPI pipe.

Part of the cold flow penetrated upstream of the cold leg. This is evidenced by the upstream thermocouple reading at T33, which indicated the arrival of the cold fluid at about 12 sec into the transient. Temperature readings for T34-T35 indicated the propagation of the cold front toward the downcomer.

Once the cold fluid reached the downcomer, it jumped over the gap in the downcomer and cooled the core-barrel wall first. This phenomenon can be seen by comparing the temperature readings of T7 and T12 on the vessel wall to T8 and T13 on the core-barrel wall. Temperatures in the core-barrel side are in general slightly cooler. However, these differences diminish when the fluid travels further down the downcomer. This is evident by comparing temperature readings of T15 and T20 on the vessel wall with T16 and T21 on the core-barrel wall.

The second COMMIX analysis for the CREARE experiment was performed with coarse meshes (2304 cells). The mesh structure and the thermocouple locations are shown in Figs. 34-36. All the physical models used in this second analysis are the same as those used in the first, except the finite-differencing scheme; the first analysis used the pure-upwind scheme, while the second used the volume-weighted skew-upwind scheme. The results of this coarse-mesh calculation are given in Figs. 37-41. All the important physical phenomena are reproduced as in the previous analysis. As can be seen from the figures, the accuracy of the computational results are compatible with that of the first analysis; however, the computational time is less than the previous fine-mesh calculation. This reduction in computer running time is due primarily to the reduction in computational cells, which was also observed by other investigators.[17] This is an important improvement due to the VWSUD scheme.

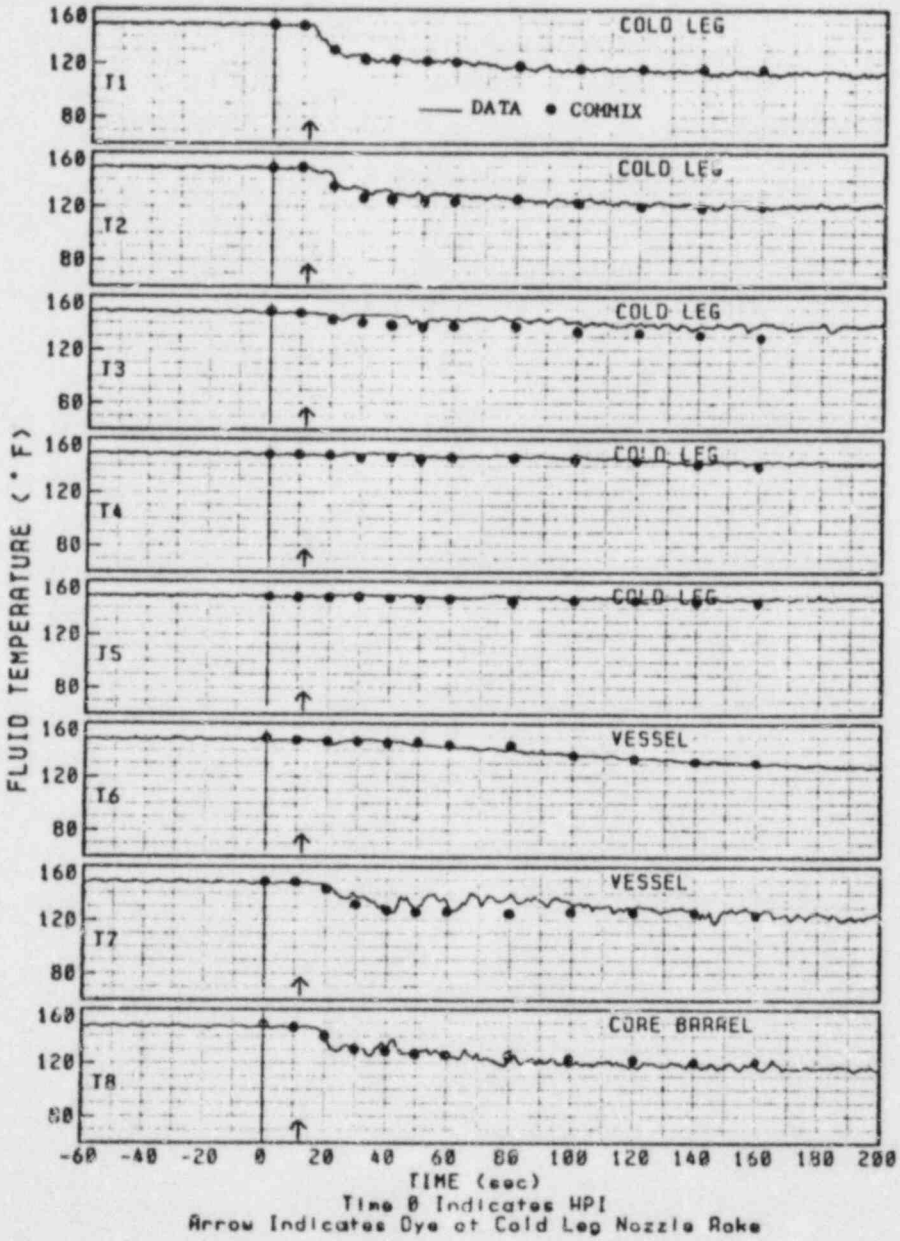


Fig. 31. Transient Temperature Comparison between Fine-Mesh COMMIX Calculations and Experimental Data for Creare Test 51 at Thermocouples T1-T8

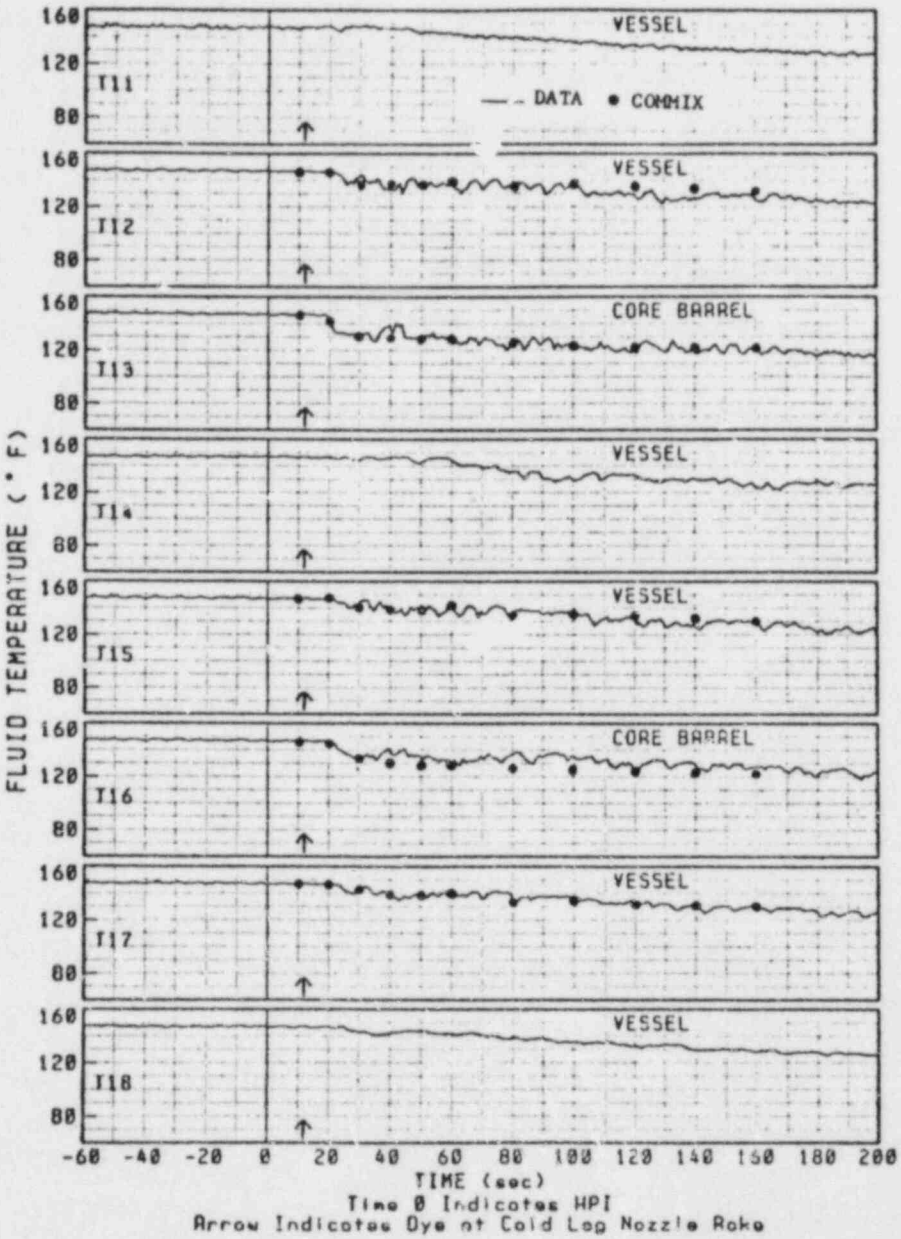


Fig. 32. Transient Temperature Comparison between Fine-Mesh COMMIX Calculations and Experimental Data for Creare Test 51 at Thermocouples T11-T18

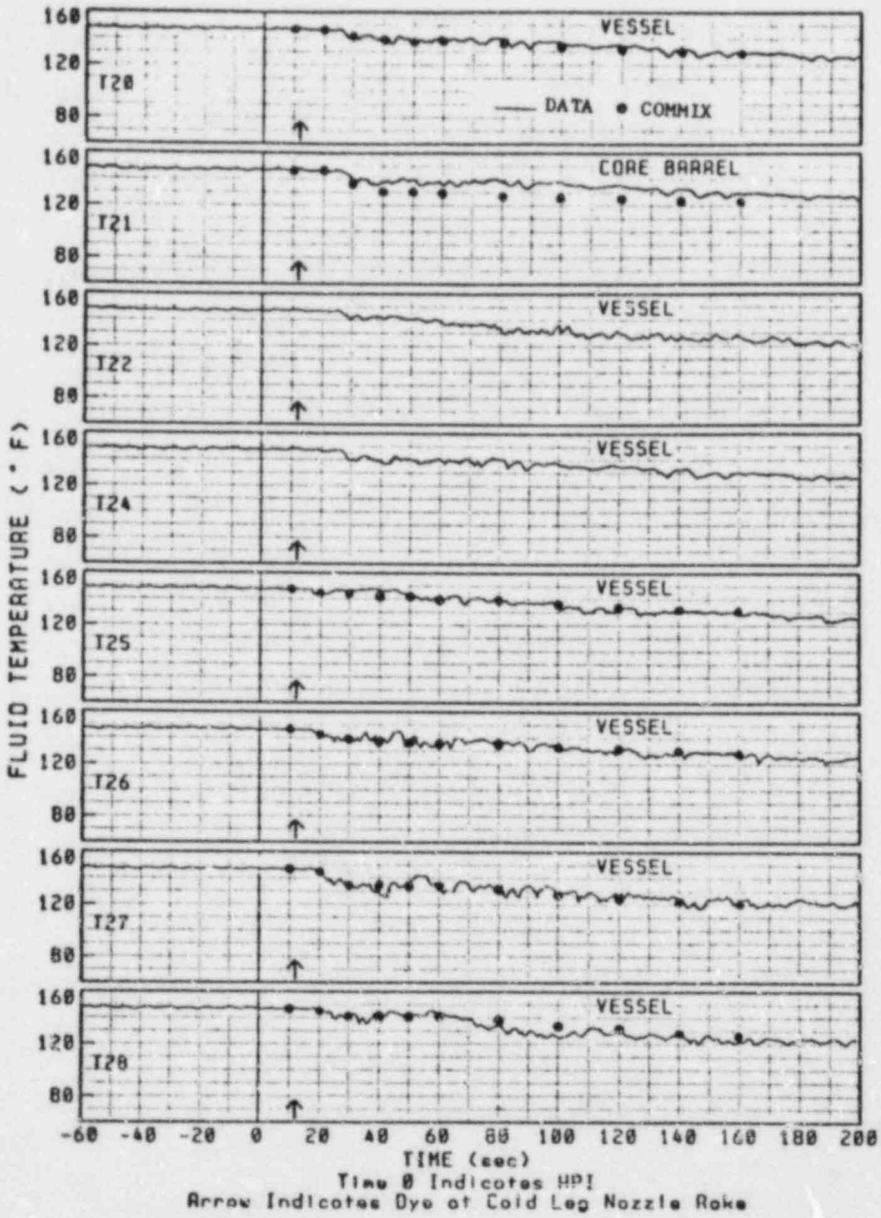


Fig. 33. Transient Temperature Comparison between Fine-Mesh COMMIX Calculations and Experimental Data for Creare Test 51 at Thermocouples T20-T28

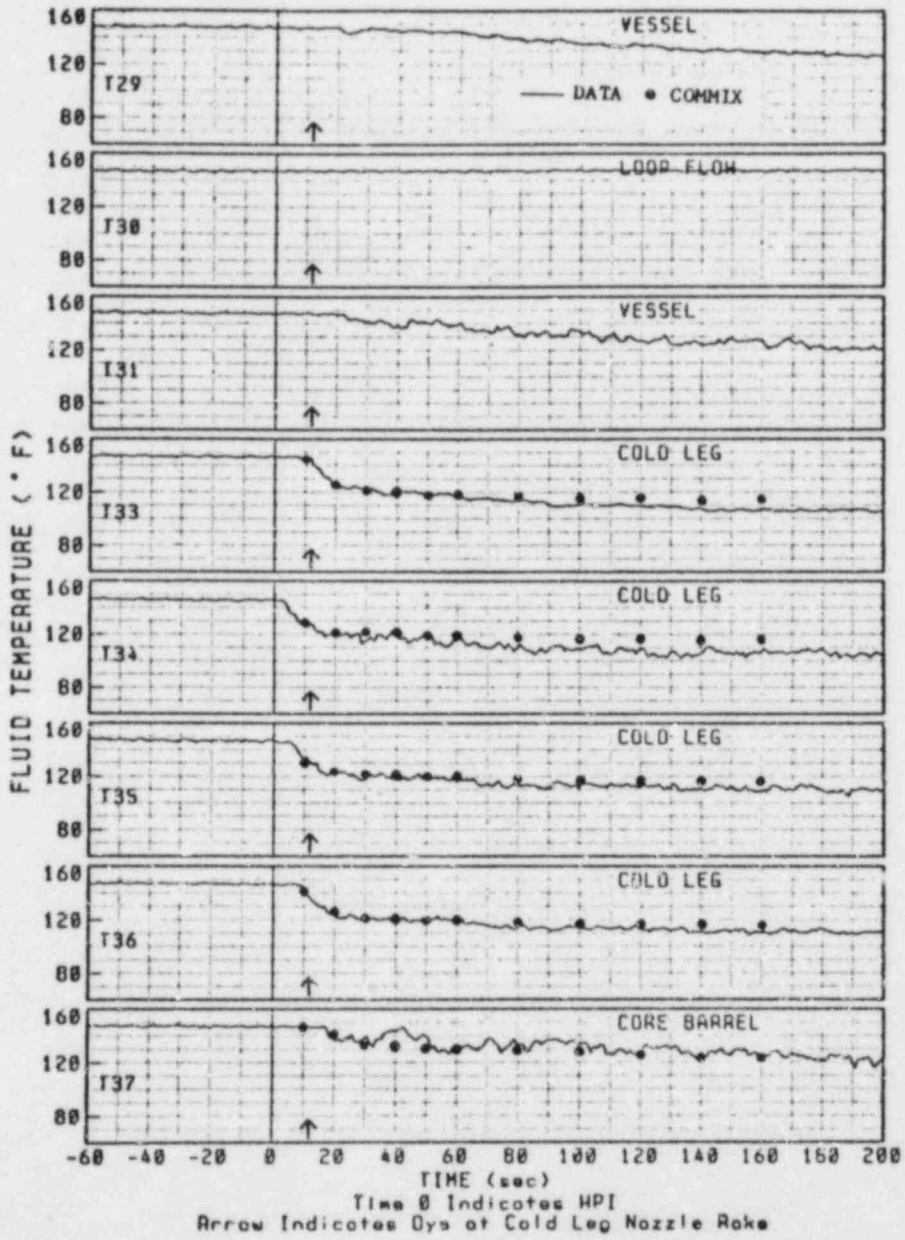


Fig. 34. Transient Temperature Comparison between Fine-Mesh COMMIX Calculations and Experimental Data for Creare Test 51 at Thermocouples T29-T37

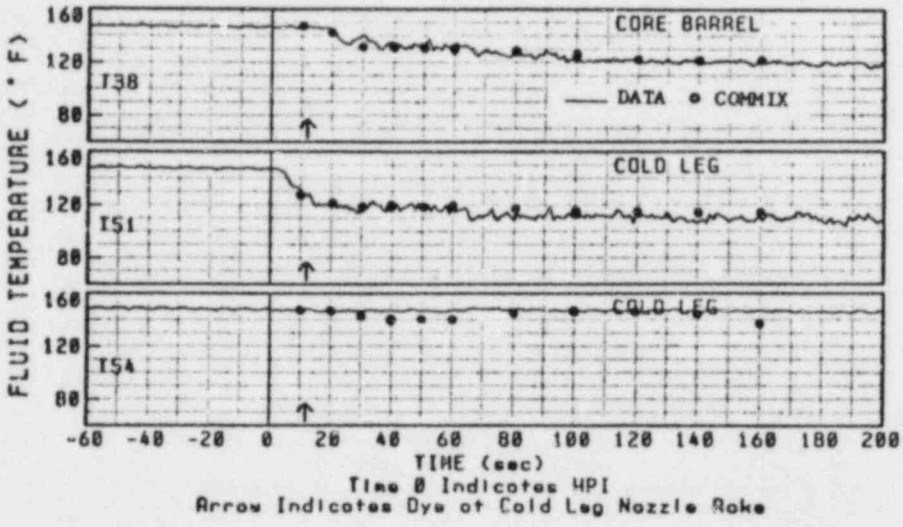


Fig. 35. Transient Temperature Comparison between Fine-Mesh COMMIX Calculations and Experimental Data for Creare Test 51 at Thermocouples T38, T51, and T54

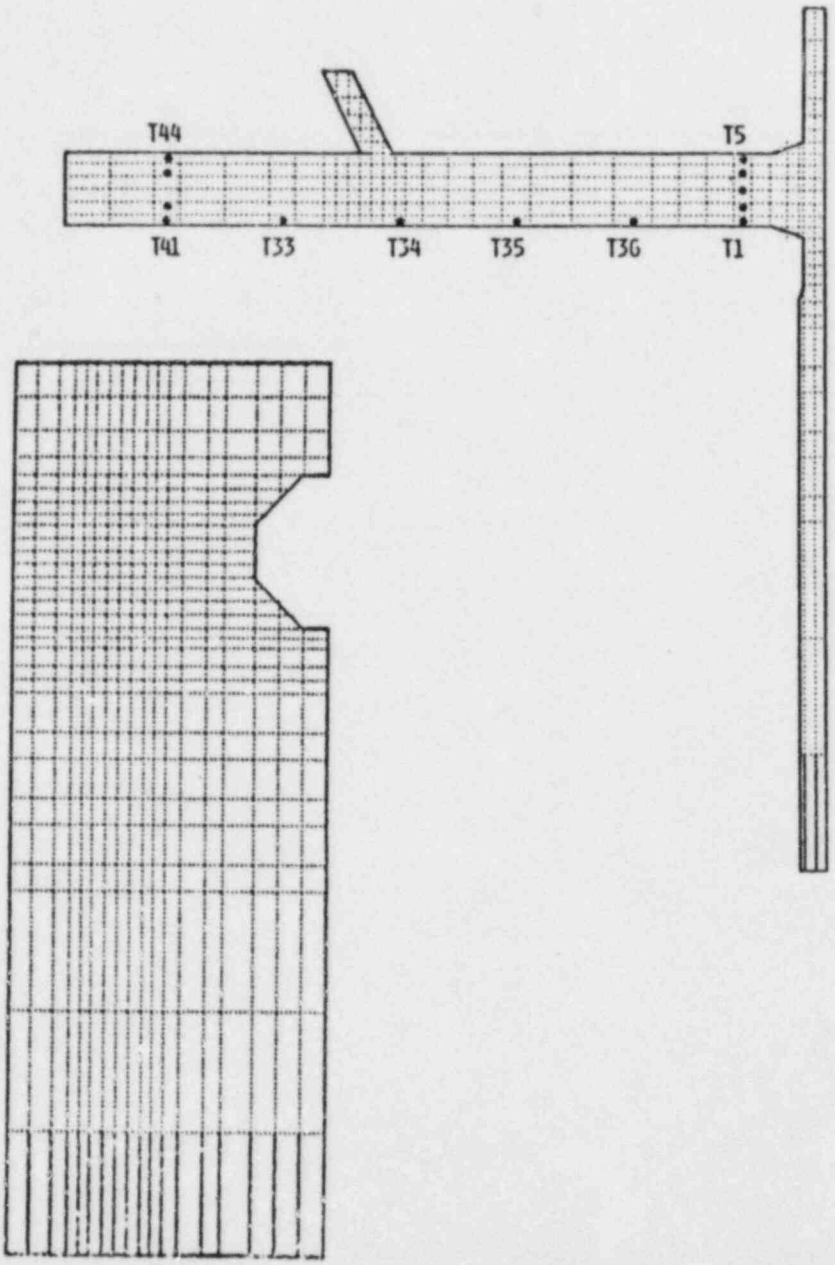


Fig. 36. COMMIX Computational Meshes for CREARE Experiment[23]

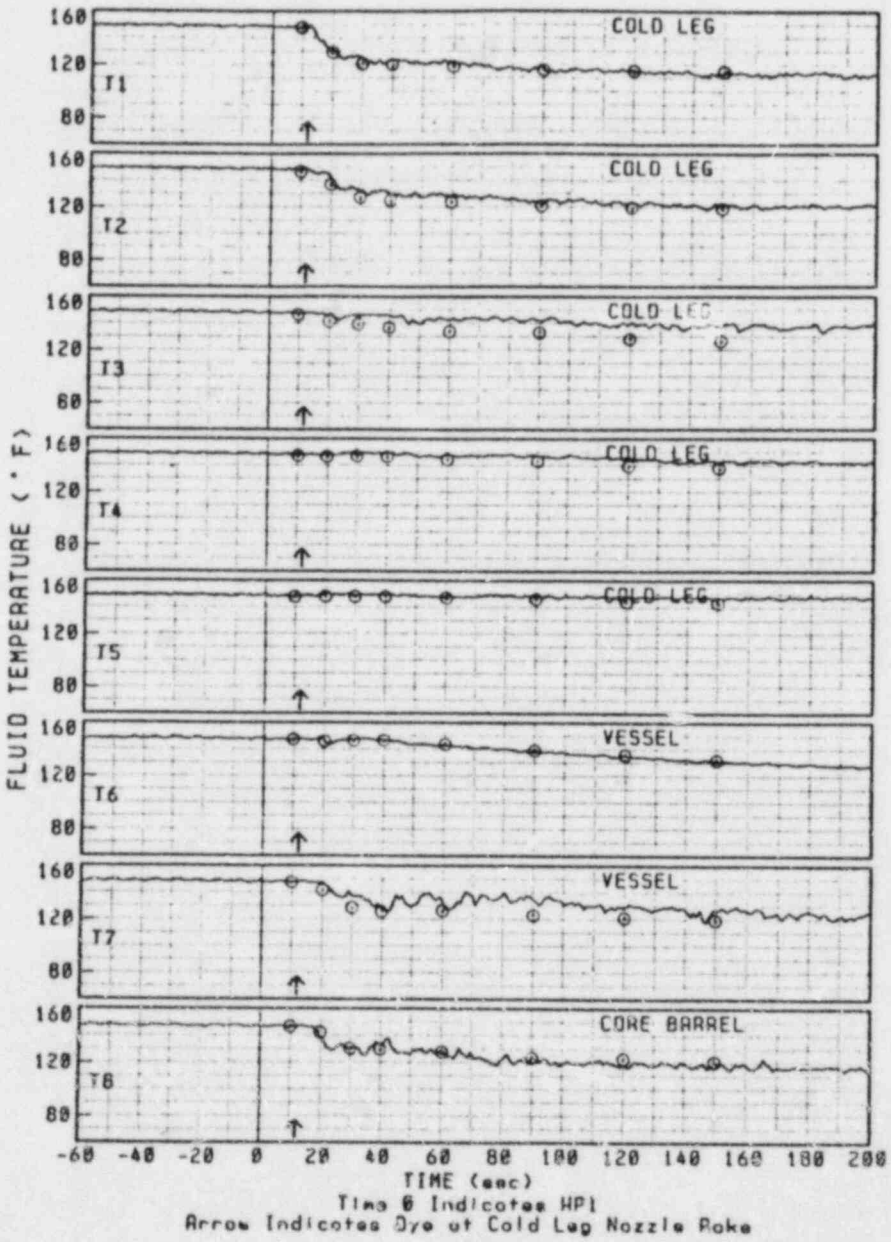


Fig. 37. Transient Temperature Comparison between Coarse-Mesh with VWSUD COMMIX Calculations and Experimental Data for Creare Test 51 at Thermocouples T1-T8

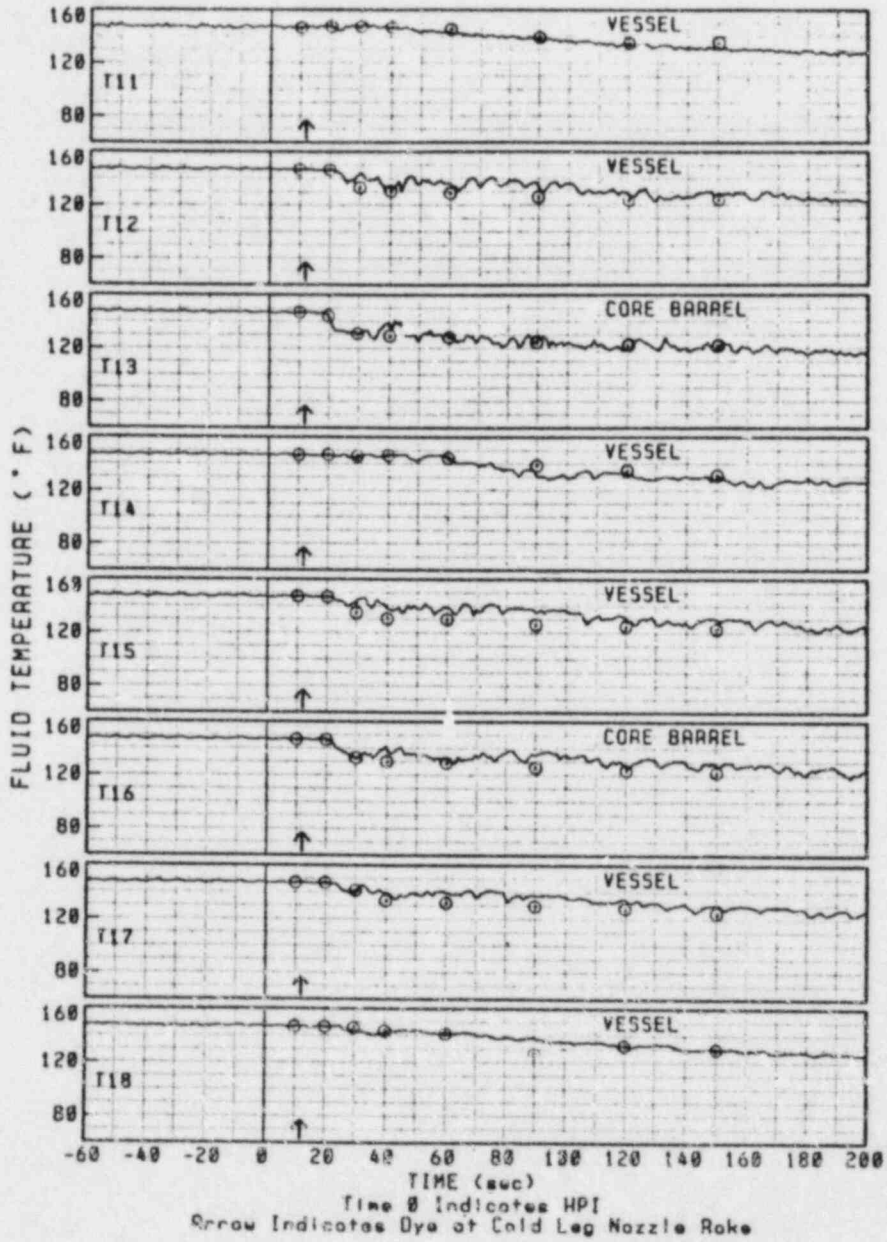


Fig. 38. Transient Temperature Comparison between Coarse-Mesh with VWSUD COMMIX Calculations and Experimental Data for Creare Test 51 at Thermocouples T11-T18

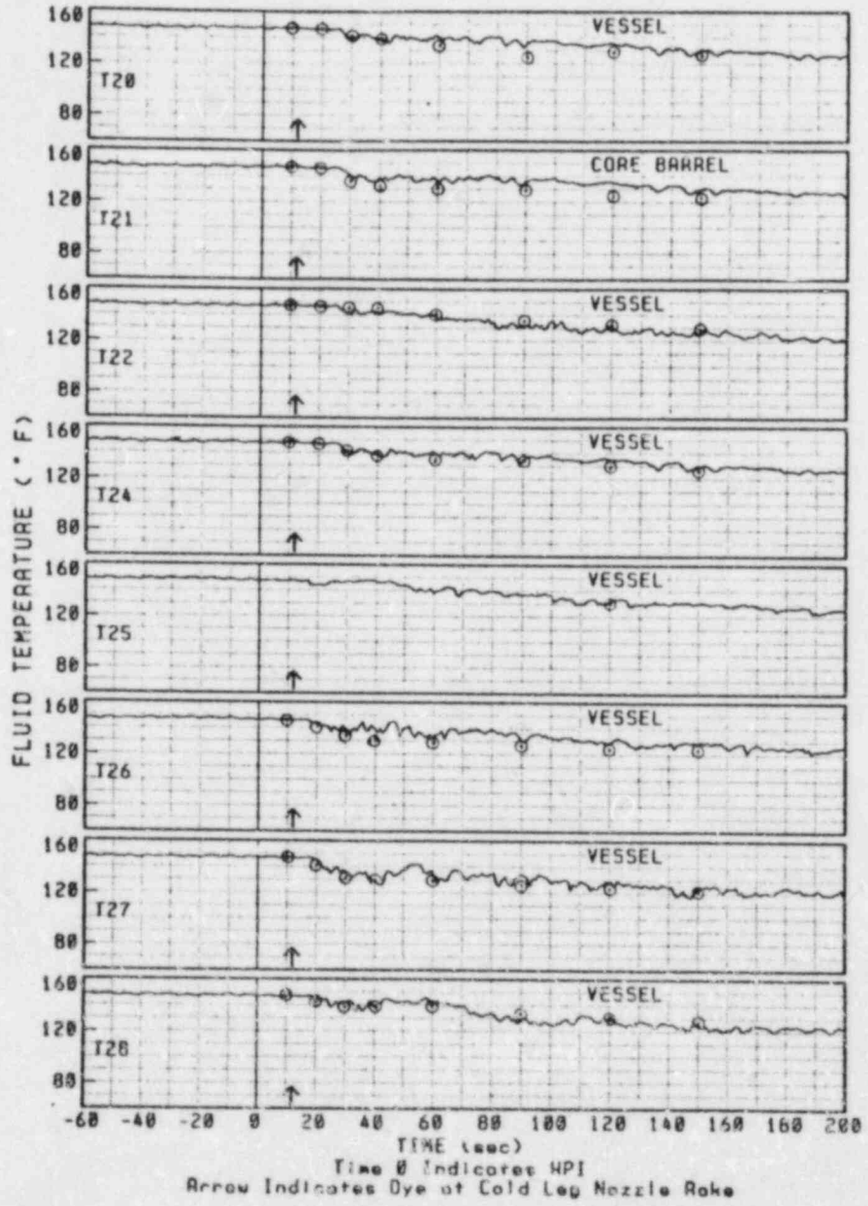


Fig. 39. Transient Temperature Comparison between Coarse-Mesh with VWSUD COMMIX Calculations and Experimental Data for Creare Test 51 at Thermocouples T20-T28

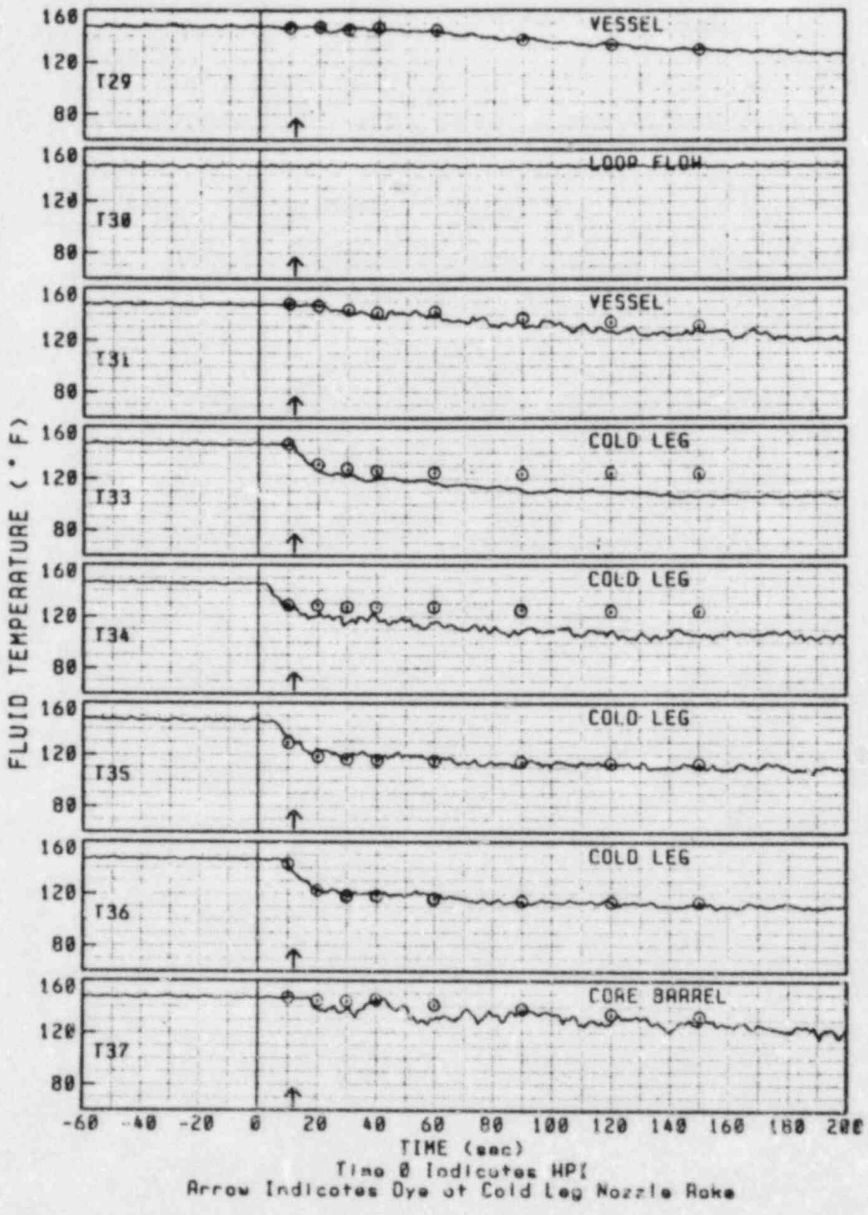


Fig. 40. Transient Temperature Comparison between Coarse-Mesh with VWSUD COMMIX Calculations and Experimental Data for Creare Test 51 at Thermocouples T29-T37

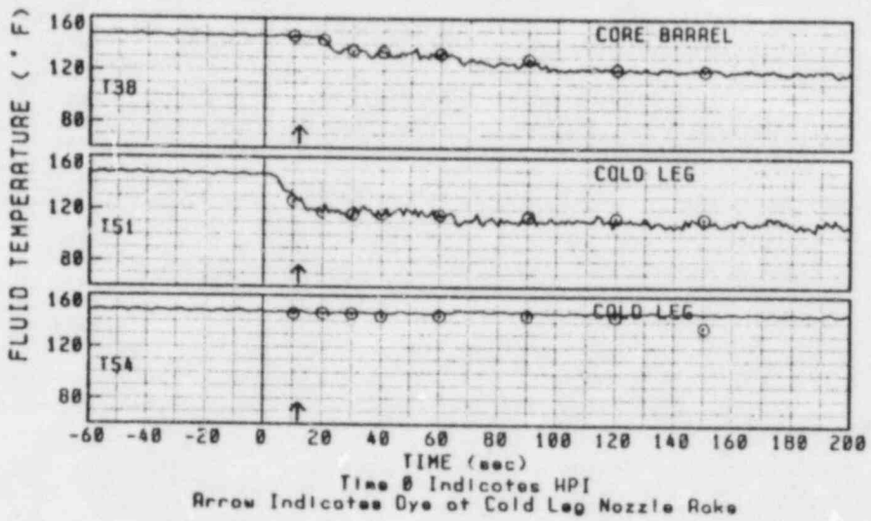


Fig. 41. Transient Temperature Comparison between Coarse-Mesh with VWSUD COMMIX Calculations and Experimental Data for Creare Test 51 at Thermocouples T38, T51, and T54

## 5. CONCLUSIONS

We have implemented the three-dimensional SUD and VWSUD schemes in the energy equation of COMMIX-1B as a user's option. However, in general, we recommend exercising the SUD option with caution. These schemes have been implemented only in the energy equation for the following reasons:

- Numerical experiments have confirmed that numerical diffusion due to the pure-upwind difference scheme is mainly from the energy equation.
- Hassan et al.[17] have found no appreciable difference in the solution of the momentum equation when they changed the order of approximation (upwind to central difference).
- Our numerical simulations confirm that modifications only in the energy equation are sufficient to predict results that are in agreement with experimental data.

The SUD and VWSUD schemes have been debugged and validated by performing several multidimensional steady-state and transient simulations of thermal-mixing benchmark problems and two thermal mixing experiments. The following conclusions have been arrived at from comparisons with analytical solutions and experimental thermocouple response data.

- The SUD scheme can significantly reduce numerical diffusion for steady-state thermal mixing problems with flow oblique to grid lines. However, significant under- and overshoots occur and appear to be greater in three dimensions than in two dimensions.
- The SUD scheme appears to be less stable than the VWSUD scheme and may require high underrelaxation.
- For the same mesh size, the computer running time for the SUD and VWSUD schemes are larger than that for the pure-upwind scheme, but numerical diffusion is less. So there is a price to be paid for reducing numerical diffusion. The additional running time is highly problem-dependent.

Overall, the VWSUD scheme

- is numerically stable. The stability analysis is presented in Appendix A.
- has the same order of accuracy as the SUD scheme, but eliminates all of the under- and overshoots (computational values over and above the limits of physically allowable values) observed in the SUD scheme in this study.
- retains the simplicity of the SUD scheme without resorting to artificial cutoffs needed in the SUD scheme. This advantage is crucial in many thermal-hydraulic applications.

- significantly reduces the numerical diffusion for steady-state and transient thermal mixing with flow oblique to computational grids. Hence, the VWSUD scheme permits more realistic analysis of thermal mixing to help resolve the pressurized thermal shock issue.

- permits use of a coarser mesh than with pure-upwind and still provides results that are of the same order of accuracy, saving significant computer running time by a factor of 4 to 8.

Further validation of the VWSUD scheme will require many more applications of the scheme.

## ACKNOWLEDGEMENTS

We are indebted to all our colleagues in the ATHRP and especially to Dr. C. I. Yang for submitting discussions and constructive comments; to Mrs. S. A. Moll and Miss B. D. Wright for typing the manuscript; to Drs. R. T. Curtis, C. N. Kelber, and Mr. P. M. Wood of the U. S. Nuclear Regulatory Commission for their support in the development work; and to Drs. J. H. Kim, B. K. H. Sun, and W. B. Loewenstein for their support in the validation work.

# REFERENCES


1. W. T. Sha, H. M. Domanus, R. C. Schmitt, J. J. Oras, and E. I. H. Lin, "COMMIX-1: A Three-Dimensional Transient Single-Phase Component Computer Program for Thermal-Hydraulic Analysis," NUREG/CR-0785, ANL-77-86 (Sept. 1978).

2. H. M. Domanus, W. T. Sha, R. C. Schmitt, and V. L. Shah, "COMMIX-1A: A Three-Dimensional Transient Single-Phase Computer Program for Thermal Hydraulic Analysis of Single and Multicomponent Systems", ANL-82-25, NUREG/CR-2896, (December 1983).

3. W. T. Sha et al., "COMMIX-1B: A Three-Dimensional Transient Single-Phase Computer Program for Thermal-Hydraulic Analysis of Single and Multicomponent Systems," to be published.

4. G. D. Raithby, "A Critical Evaluation of Upstream Differencing Applied to Problems involving Fluid Flow," Comp. Methods Appl. Mech. Eng. 9, pp. 75-103 (1976).

5. G. D. Raithby, "Skew Upstream Differencing Schemes for Problems involving Fluid Flow," Comp. Methods Appl. Mech. Eng. 9, pp. 153-164 (1976).

6. H. M. Domanus, R. C. Schmitt, W. T. Sha, and V. L. Shah, "Implicit Solution Scheme in the COMMIX-1A Computer Program," ATHRP-16 (Sept. 1983).

7. F. F. Chen, H. M. Domanus, W. T. Sha, and V. L. Shah, "Turbulence Modeling in the COMMIX-Computer Code," ANL-83-65 (March 1984).

8. W. C. Rivard, O. A. Farmer, T. D. Butler, and P. J. O'Rourke, "A Method for Increased Accuracy in Eulerian Fluid Dynamic Calculations," Los Alamos Report LA-5426-MS (Oct. 1973).

9. J. P. Boris and D. L. Book, "Flux-Corrected Transport. III. Minimal-Error FCT Algorithms," J. Comp. Phys. 20, pp 397-431 (1976).

10. S. T. Zalesak, "Fully Multidimensional Flux-Corrected Transport Algorithms for Fluids," J. Comp. Phys. 31, pp. 335-362 (1979).

11. P. Romstedt and W. Werner, "Efficient High-Order Method for the Solution of Fluid Dynamics Equations," Nucl. Sci. and Eng. 64 (1977).

12. R. G. Steinke, "Triangular Geometry Fluid Dynamics with Reduced Artificial Diffusion," ANS Trans. 34, pp. 310-311 (1980).

13. M. J. Chapman, "FRAM - Nonlinear Dumping Algorithms for the Continuity Equation," J. Comp. Phys. 44, pp 84-103 (1981).

14. W. P. Crowley, "Second-Order Numerical Advection," J. Comp. Phys. 1, pp. 471-484 (1967).

15. W. P. Crowley, "PUFL: An Almost Lagrangian Gasdynamic Calculation for Pipe Flows with Mass Entrainment," J. Comp. Phys. 2, pp. 61-86 (1967).

16. J. N. Lillington," A Vector Upstream Differencing Scheme for Problems in Fluid Flow involving Significant Source Terms in Steady-State Linear Systems," Int. J. for Numer. Methods Fluids 1, pp. 3-16 (1981).

17. Y. A. Hassan, J. G. Rice, and J. H. Kim, "A Stable Mass Flow Weighted Two-Dimensional Skew-Upwind Scheme," Numer. Heat Transfer 6, pp. 395-408 (1983).

18. P. J. Roache, Computational Fluid Dynamics, Hermosa Publ., Albuquerque, New Mexico (1972).

19. S. V. Patankar, Numerical Heat Transfer and Fluid Flow, Hemisphere Publ. Corp. (1980).

20. M. A. Leschziner, "Practical Evaluation of Three Finite Difference Schemes for the Computation of Steady-State Recirculatory Flows," Comp. Methods Appl. Mech. Eng. 23, pp. 293-312 (1980).

21. A. Hashemi and J. Goodman, "Thermal Mixing in a Rectangular Geometry Model of a Cold Leg with High Pressure Injection and a Downcomer," EPRI NP-2924 (March 1983).

22. C. L. Lin, J. H. Kim, and Bill K. H. Sun, "Numerical Simulation of Thermal and Fluid Mixing in the Cold Leg and Downcomer of a Model Geometry during a PWR Primary Side Overcooling," Thermal-Hydraulics of Nuclear Reactors, Vol. II, The Second International Topical Meeting on Nuclear Reactor Thermal-Hydraulics, Santa Barbara, California, pp. 988-996 (Jan. 11-14, 1983).

23. P. H. Rothe, M. F. Ackerson, and J. A. Block, "Fluid and Thermal Mixing in a Model Cold Leg and Downcomer with Loop Flow," EPRI NP-2312 (April 1982).

24. R. W. Lyczkowski, C. C. Miao, H. M. Domanus, J. R. Hull, W. T. Sha, and R. C. Schmitt, "Three-Dimensional Analysis of Thermal and Fluid Mixing in Cold Leg and Downcomer of PWR Geometries," EPRI NP-3321, (December 1983).

## APPENDIX A. ACCURACY AND STABILITY ANALYSIS OF THE VOLUME-WEIGHTED SKEW-UPWIND DIFFERENCE SCHEME

Our discussion of the volume-weighted skew-upwind difference scheme is limited to two dimensions; however, the results can be readily extended to three dimensions. The weighting scheme is shown in Fig. A.1 for the north and east faces. Two flows are shown, one at 30° and the other at 60°. The situations on the south and west faces follow from this figure. In this discussion we shall assume that u and v velocities are positive and uniform with Courant numbers $\alpha$ and $\beta$ defined as $\alpha = u\delta t/\delta x$ and $\beta = v\delta t/\delta y$, where $\delta x$ and $\delta y$ are the cell sizes in the x and y direction, respectively. The scheme uses volume weighting to determine the value of $\phi$ at the calculational faces. That is, the scheme is like Raithby's but uses volume weighting rather than linear interpolation. Our first task is to write expressions for the volumes in terms of the Courant numbers.

East and West Face:

$$A_0 = \begin{cases} \frac{1}{2}\delta x\delta y\left(1 - \beta/4\alpha\right) & \text{when } \beta/2 < \alpha \\ \frac{1}{2}\delta x\delta y\,\alpha/\beta & \text{when } \alpha < \beta/2 \end{cases} \tag{A-1a}$$

$$A_1 = \begin{cases} \frac{1}{4}\delta x\delta y\,\beta/2\alpha & \text{when } \beta < \alpha \\ \frac{1}{4}\delta x\delta y\left(1 - \alpha/2\beta\right) & \text{when } \alpha < \beta \end{cases} \tag{A-1b}$$

North and South Face:

$$A_0 = \begin{cases} \frac{1}{2}\delta x\delta y\left(1 - \alpha/4\beta\right) & \text{when } \beta > \alpha/2 \\ \frac{1}{2}\delta x\delta y\,\beta/\alpha & \text{when } \beta < \alpha/2 \end{cases} \tag{A-2a}$$

$$A_1 = \begin{cases} \frac{1}{8}\delta x\delta y\,\alpha/\beta) & \text{when } \beta > \alpha/2 \\ \frac{1}{2}\delta x\delta y\left(1 - \beta/2\alpha\right) & \text{when } \beta < \alpha/2 \end{cases} \tag{A-2b}$$

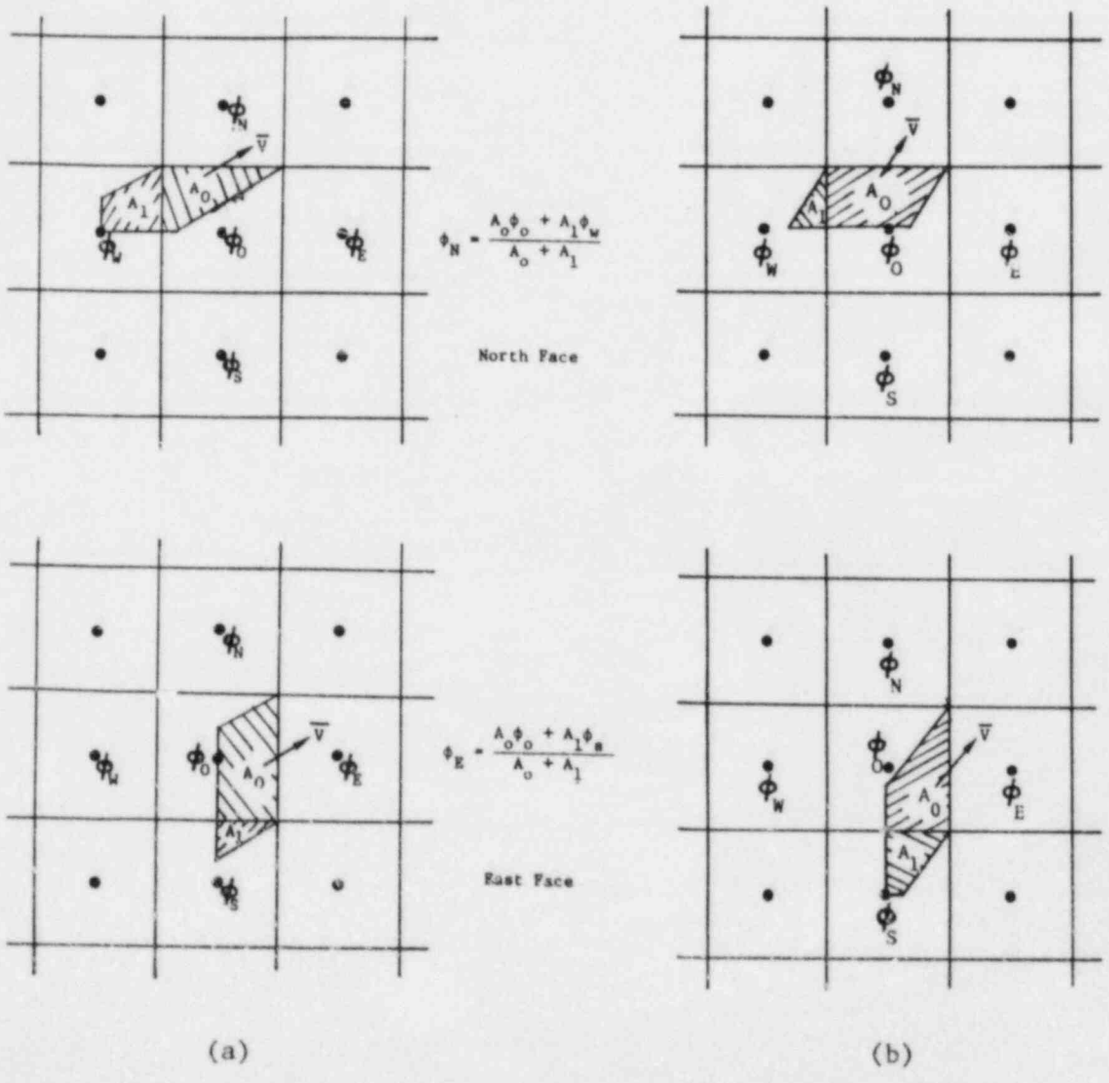


Fig. A.1. Volume-Weighted Skew-Upwind Scheme for North and East Faces at (a) 30° Angle and (b) 60° Angle

Having found the areas, we can approximate $\phi_e$, $\phi_w$, $\phi_n$, and $\phi_s$ just as in Raithby's scheme. Thus, we have

$$\phi_{ij}^{n+1} = \phi_{ij}^{n} - \frac{\delta t}{\delta x \delta y}\left\{F_e - F_w + F_n - F_s\right\}, \tag{A-3}$$

where we approximate the fluxes as

$$F_e \doteq u\delta y\phi_e^*, \quad F_w \doteq u\delta y\phi_w^*, \quad F_n \doteq v\delta x\phi_n^*, \quad F_s \doteq v\delta x\phi_s^* .$$

In the VWSUD scheme, we use ($u, v > 0$):

$$\phi_e^* = \frac{A_0\phi_0 + A_1\phi_S}{A_0 + A_1},$$

$$\phi_w^* = \frac{A_0\phi_W + A_1\phi_{SW}}{A_0 + A_1},$$

$$\phi_n^* = \frac{A_0\phi_0 + A_1\phi_W}{A_0 + A_1},$$

and

$$\phi_s^* = \frac{A_0\phi_S + A_1\phi_{SW}}{A_0 + A_1}, \tag{A-4}$$

Here it is understood that $A_0$ and $A_1$ are calculated in accordance with Eq. A-1 for the appropriate face.

Using Eq. A-1 with Eq. A-4, setting $\omega = \beta/\alpha$, and

$$\phi_0 = \phi_{ij}^{n}, \ \phi_S = \phi_{ij-1}^{n}, \ \phi_W = \phi_{i-1,j}^{n}, \ \phi_{SW} = \phi_{i-1,j-1}^{n},$$

we find

$$\phi_e^* = \begin{cases} 1 - \frac{\omega}{4}\ \phi_0 + \frac{\omega}{4}\phi_S & \text{for } 0 < \omega < 1 \\ \dfrac{1 - \frac{\omega}{4}\ \phi_0 + \frac{1}{2}\ 1 - \frac{1}{2\omega}\ \phi_S}{\frac{3}{2} - \frac{\omega}{4} - \frac{1}{4\omega}} & \text{for } 1 < \omega < 2 \\ \dfrac{\frac{1}{\omega}\phi_0 + \frac{1}{2}\ 1 - \frac{1}{2\omega}\ \phi_S}{\frac{1}{2} + \frac{3}{4\omega}} & \text{for } 2 < \omega \end{cases} \tag{A-5}$$

$$\phi_w^* = \begin{cases} 1 - \frac{\omega}{4}\ \phi_W + \frac{\omega}{4}\ \phi_{SW} & \text{for } 0 < \omega < 1 \\ \dfrac{1 - \frac{\omega}{4}\ \phi_W + \frac{1}{2}\ 1 - \frac{1}{2\omega}\ \phi_{SW}}{\frac{3}{2} - \frac{\omega}{4} - \frac{1}{4\omega}} & \text{for } 1 < \omega < 2 \\ \dfrac{\frac{1}{\omega}\ \phi_W + \frac{1}{2}\ 1 - \frac{1}{2\omega}\ \phi_{SW}}{\frac{1}{2} + \frac{3}{4\omega}} & \text{for } 2 < \omega \end{cases} \tag{A-6}$$

$$\phi_n^* = \begin{cases} \dfrac{\omega\phi_o + \frac{1}{2}\ 1 - \frac{\omega}{2}\ \phi_W}{\frac{1}{2} + \frac{3}{4}\ \omega} & \text{for } 0 < \omega < \frac{1}{2} \\ \dfrac{1 - \frac{1}{4\omega}\ \phi_0 + \frac{1}{2}\ 1 - \frac{\omega}{2}\ \phi_W}{\frac{3}{2} - \frac{1}{4\omega} - \frac{\omega}{4}} & \text{for } \frac{1}{2} < \omega < 1 \\ 1 - \frac{1}{4\omega}\ \phi_0 + \frac{1}{4\omega}\ \phi_W & \text{for } 1 < \omega \end{cases} \tag{A.7}$$

$$\phi_s^* = \begin{cases} \dfrac{\omega\phi_S + \frac{1}{2}\ 1 - \frac{\omega}{2}\ \phi_{SW}}{\frac{1}{2} + \frac{3}{4}\ \omega} & \text{for } 0 < \omega < 1 \\ \dfrac{1 - \frac{1}{4\omega}\ \phi_0 + \frac{1}{2}\ 1 - \frac{\omega}{2}\ \phi_{SW}}{\frac{3}{2} - \frac{1}{4\omega} - \frac{\omega}{4}} & \text{for } \frac{1}{2} < \omega < 1 \\ 1 - \frac{1}{4\omega}\ \phi_s + \frac{1}{4\omega}\ \phi_{SW} & \text{for } 1 < \omega \end{cases} \tag{A-8}$$

Just as in Raithby's scheme, we use the approximation

$$\frac{\delta t}{\delta x \delta y} F_e \doteq \alpha\phi_e^*,\ \frac{\delta t}{\delta x \delta y} F_w \doteq \alpha\phi_w^*,\ \frac{\delta t}{\delta x \delta y} F_n \doteq \beta\phi_n^*,\ \frac{\delta t}{\delta x \delta y} F_s \doteq \beta\phi_s^* \tag{A-9}$$

to obtain

$$\phi_{ij}^{n+1} = \phi_{ij}^n - \{\alpha\phi_e^* - \alpha\phi_w^* + \beta\phi_n^* - \beta\phi_s^*\}\ , \tag{A-10}$$

which can be written for each of the four cases

$$0 < \omega \leq \frac{1}{2} \ , \ \frac{1}{2} < \omega \leq 1 \ , \ 1 < \omega \leq 2 \ , \ 2 < \omega \ .$$

Case I: $0 < \omega < \frac{1}{2} \quad (\omega = \beta/\alpha)$

$$\phi_{ij}^{n+1} = \left(1 - \alpha + \frac{\beta}{4} - \frac{\beta^2/\alpha}{\frac{1}{2} + \frac{3}{4}\frac{\beta}{\alpha}}\right)\phi_{ij}^{n} + \left(-\frac{\beta}{4} + \frac{\beta^2/\alpha}{\frac{1}{2} + \frac{3}{4}\frac{\beta}{\alpha}}\right)\phi_{i,j-1}^{n}$$

$$+ \left[\alpha - \frac{\beta}{4} - \frac{\frac{\beta}{2}\left(1 - \frac{\beta}{2\alpha}\right)}{\frac{1}{2} + \frac{3}{4}\frac{\beta}{\alpha}}\right]\phi_{i-1,j}^{n} + \left[\frac{\beta}{4} + \frac{\frac{\beta}{2}\left(1 - \frac{\beta}{2\alpha}\right)}{\frac{1}{2} + \frac{3}{4}\frac{\beta}{\alpha}}\right]\phi_{i-1,j-1}^{n} \qquad \text{(A-11)}$$

Case II: $\frac{1}{2} < \omega < 1$

$$\phi_{ij}^{n+1} = \left[1 - \alpha + \frac{\beta}{4} - \frac{\beta\left(1 - \frac{\alpha}{4\beta}\right)}{\frac{3}{2} - \frac{\alpha}{4\beta} - \frac{\beta}{4\alpha}}\right]\phi_{ij}^{n} + \left[-\frac{\beta}{4} + \frac{\beta\left(1 - \frac{\alpha}{4\beta}\right)}{\frac{3}{2} - \frac{\alpha}{4\beta} - \frac{\beta}{4\alpha}}\right]\phi_{i,j-1}^{n}$$

$$+ \left[\alpha - \frac{\beta}{4} - \frac{\frac{\beta}{2}\left(1 - \frac{\beta}{2\alpha}\right)}{\frac{3}{2} - \frac{\alpha}{4\beta} - \frac{\beta}{4\alpha}}\right]\phi_{i-1,j}^{n} + \left[\frac{\beta}{4} + \frac{\frac{\beta}{2}\left(1 - \frac{\beta}{2\alpha}\right)}{\frac{3}{2} - \frac{\alpha}{4\beta} - \frac{\beta}{4\alpha}}\right]\phi_{i-1,j-1}^{n} \qquad \text{(A-12)}$$

Case III: $1 < \omega < 2$

$$\phi_{ij}^{n+1} = \left[1 - \beta + \frac{\alpha}{4} - \frac{\alpha\left(a - \frac{\beta}{4\alpha}\right)}{\frac{3}{2} - \frac{\beta}{4\alpha} - \frac{\alpha}{4\beta}}\right]\phi_{ij}^{n} + \left[\beta - \frac{\alpha}{4} - \frac{\frac{\alpha}{2}\left(1 - \frac{\alpha}{2\beta}\right)}{\frac{3}{2} - \frac{\beta}{4\alpha} - \frac{\alpha}{4\beta}}\right]\phi_{i,j-1}^{n}$$

$$+ \left[-\frac{\alpha}{4} + \frac{\alpha\left(1 - \frac{\beta}{4\alpha}\right)}{\frac{3}{2} - \frac{\beta}{4\alpha} - \frac{\alpha}{4\beta}}\right]\phi_{i-1,j}^{n} + \left[\frac{\alpha}{4} + \frac{\frac{\alpha}{2}\left(1 - \frac{\alpha}{2\beta}\right)}{\frac{3}{2} - \frac{\beta}{4\alpha} - \frac{\alpha}{4\beta}}\right]\phi_{i-1,j-1}^{n} \qquad \text{(A-13)}$$

Case IV: $2 < \omega$

$$\phi_{ij}^{n+1} = \left(1 - \beta + \frac{\alpha}{4} - \frac{\alpha^2/\beta}{\frac{1}{2} + \frac{3}{4}\frac{\alpha}{\beta}}\right)\phi_{ij}^{n} + \left[\beta - \frac{\alpha}{4} - \frac{\frac{\alpha}{2}\left(1 - \frac{\alpha}{2\beta}\right)}{\frac{1}{2} + \frac{3}{4}\frac{\alpha}{\beta}}\right]\phi_{i,j-1}^{n}$$

$$+\left(-\frac{\alpha}{4}+\frac{\alpha^2/\beta}{\frac{1}{2}+\frac{3}{4}\frac{\alpha}{\beta}}\right)\phi^n_{i-1,j}+\left[\frac{\alpha}{4}+\frac{\frac{\alpha}{2}\left(1-\frac{\alpha}{2\beta}\right)}{\frac{1}{2}+\frac{3}{4}\frac{\alpha}{\beta}}\right]\phi^n_{i-1,j-1} \qquad \text{(A-14)}$$

Just as for Raithby's scheme, we can interpret this difference scheme as an interpolation scheme. We again recall that the interpolation point in the xy (spatial) plane is $R^*$: $(\xi^*,\eta^*)$ where $\xi^* = -\alpha$, $\eta^* = -\beta$. Thus, the right side of Eqs. A-11 through A-14 can be regarded as interpolants of $\phi$ evaluated at $(\xi^*, \eta^*)$. We shall call this interpolant $\tilde{\phi}(\xi,\eta)$, but we will not write it out because the expressions are quite involved. However, one obtains it from Eqs. A-11 through A-14 by replacing $\alpha$ by $-\xi$ and $\beta$ by $-\eta$. Thus,

$$\phi^{n+1}_{ij} = \tilde{\phi}\,(\xi^*, \eta^*)\ . \qquad \text{(A-15)}$$

The interpolation domain is the square shown in Fig. A.2, and this domain is subdivided into four subregions. We note that the VWSUD scheme involves 4 points whereas the Raithby scheme involved 6 points. The domain is now divided into 4 parts whereas in the Raithby scheme the domain was divided into 3 parts. The VWSUD scheme is entirely rational whereas the Raithby scheme was partially polynomial and partially rational.

On the question of order of accuracy, we see immediately that $\tilde{\phi}$ is a continuous interpolant that will reproduce the set $\begin{matrix}1\\ \xi\\ \eta\end{matrix}$, but will not reproduce $\xi\eta$. Thus, we are again considering a first-order scheme just as Raithby's.

We next consider the stability of the VWSUD scheme. (Again, the regions R1 - R4 are in the $\alpha,\beta$ plane reflected through the origin and we denote the corresponding regions in the $\alpha,\beta$ plane by $\hat{R1}$ - $\hat{R4}$.) Consider a Fourier mode $\rho^n_{k\ell}\ \exp(\hat{i}kx_i + \hat{i}\ell y_j)$ and set $\theta = k\delta x$ and $\phi = \ell\delta y$; then from Eqs. A-11 through A-14, we find

Case I: $0 < p/k < \frac{1}{2}, \alpha, p > 0$, Region 1 $(\hat{R1})$

$$\rho_{k,\ell} = 1 - \alpha + \frac{\beta}{4} - \frac{\beta^2/\alpha}{\frac{1}{2}+\frac{3}{4}\frac{\beta}{\alpha}} + \left[\alpha - \frac{\beta}{4} - \frac{\frac{\beta}{2}\left(1-\frac{\beta}{2\alpha}\right)}{\frac{1}{2}+\frac{3}{4}\frac{\beta}{\alpha}}\right]\cos\theta$$

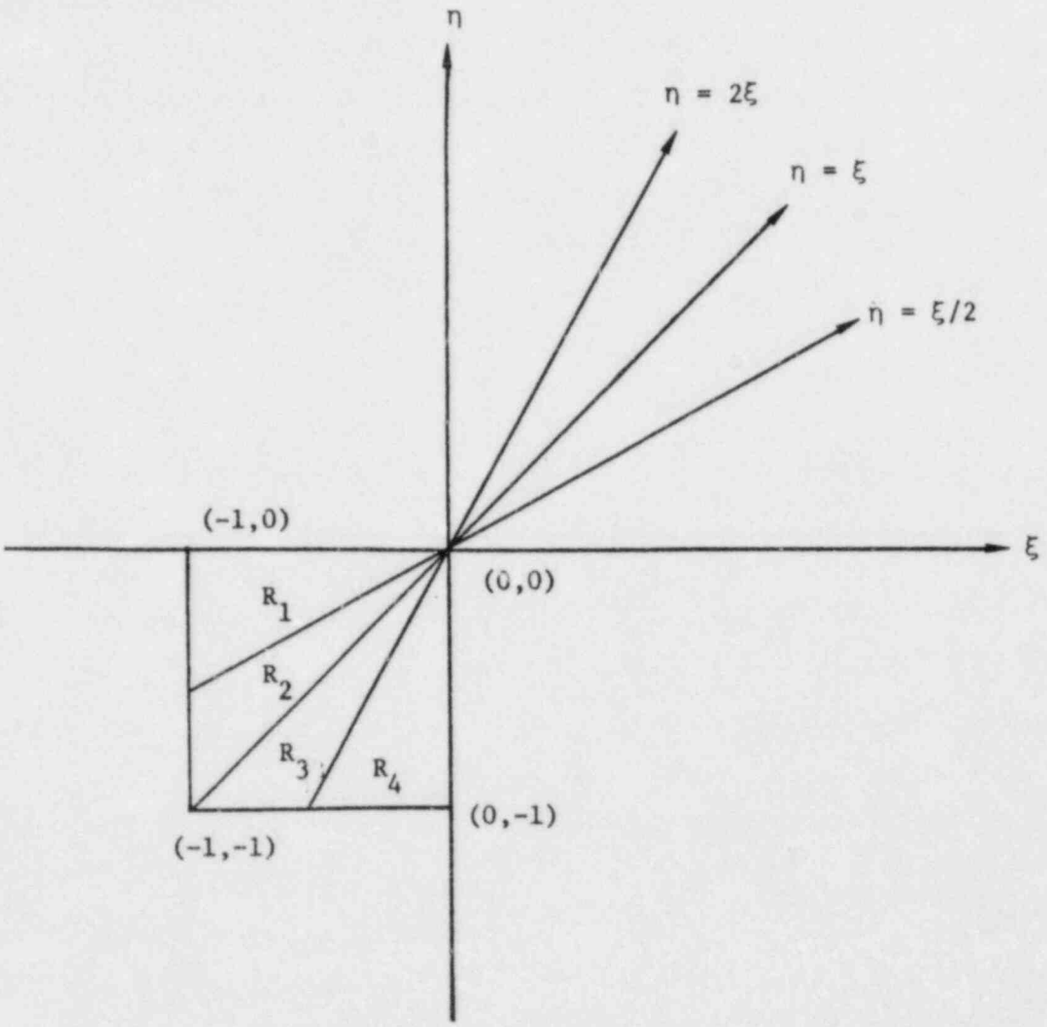


Fig. A.2. Interpolation Domain

$$+\left(-\frac{\beta}{4}+\frac{\beta^2/\alpha}{\frac{1}{2}+\frac{3}{4}\frac{\beta}{\alpha}}\right)\cos\phi+\left[\frac{\beta}{4}+\frac{\frac{\beta}{2}\left(1-\frac{\beta}{2\alpha}\right)}{\frac{1}{2}+\frac{3}{4}\frac{\beta}{\alpha}}\right]\cos(\theta+\phi)$$

$$-i\left\{\left[\alpha-\frac{\beta}{4}-\frac{\frac{\beta}{2}\left(1-\frac{\beta}{2\alpha}\right)}{\frac{1}{2}+\frac{3}{4}\frac{\beta}{2\alpha}}\right]\sin\theta+\left[-\frac{\beta}{4}+\frac{\beta^2/\alpha}{\frac{1}{2}+\frac{3}{4}\frac{\beta}{\alpha}}\right]\sin\phi\right.$$

$$\left.+\left[\frac{\beta}{4}+\frac{\frac{\beta}{2}\left(1-\frac{\beta}{2\alpha}\right)}{\frac{1}{2}+\frac{3}{4}\frac{\beta}{\alpha}}\right]\sin(\theta+\phi)\right\} \qquad \text{(A-16)}$$

Case II: $\frac{1}{2}<\frac{\beta}{\alpha}<\frac{1}{2}$, $\alpha,\beta>0$ Region 2$(\hat{R}2)$

$$\rho_{k,\ell}=1-\alpha+\frac{\beta}{4}-\frac{\beta\left(1-\frac{\alpha}{4\beta}\right)}{\frac{3}{2}-\frac{\alpha}{4\beta}-\frac{\alpha}{4\alpha}}+\left[\alpha-\frac{\beta}{4}-\frac{\frac{\beta}{2}\left(1-\frac{\beta}{2\alpha}\right)}{\frac{3}{2}-\frac{\alpha}{4\beta}-\frac{\beta}{4\alpha}}\right]\cos\theta$$

$$+\left[-\frac{\beta}{4}+\frac{\beta\left(1-\frac{\alpha}{4\beta}\right)}{\frac{3}{2}-\frac{\alpha}{4\beta}-\frac{\beta}{4\alpha}}\right]\cos\phi+\left[\frac{\beta}{4}+\frac{\frac{\beta}{2}\left(1-\frac{\beta}{2\alpha}\right)}{\frac{3}{2}-\frac{\alpha}{4\beta}-\frac{\beta}{4\alpha}}\right]\cos(\theta+\phi)$$

$$-i\left\{\left[\alpha-\frac{\beta}{4}-\frac{\frac{\beta}{2}\left(1-\frac{\beta}{2\alpha}\right)}{\frac{3}{2}-\frac{\alpha}{4\beta}-\frac{\beta}{4\alpha}}\right]\sin\theta+\left[-\frac{\beta}{4}+\frac{\beta\left(1-\frac{\alpha}{4\beta}\right)}{\frac{3}{2}-\frac{\alpha}{4\beta}-\frac{\beta}{4\alpha}}\right]\sin\phi\right.$$

$$\left.+\left[\frac{\beta}{4}+\frac{\frac{\beta}{2}\left(1-\frac{\beta}{2\alpha}\right)}{\frac{3}{2}-\frac{\alpha}{4\beta}-\frac{\beta}{4\alpha}}\right]\sin(\theta+\phi)\right\} \qquad \text{(A-17)}$$

Case III: $1<\frac{\beta}{\alpha}<2$, $\alpha,\beta>0$, Region 3$(\hat{R}3)$

$$\rho_{k,\ell}=1-\beta+\frac{\alpha}{4}-\frac{\alpha\left(1-\frac{\beta}{4\alpha}\right)}{\frac{3}{2}-\frac{\beta}{4\alpha}-\frac{\beta}{4\beta}}+\left[-\frac{\alpha}{4}-\frac{\alpha\left(1-\frac{\beta}{4\alpha}\right)}{\frac{3}{2}-\frac{\beta}{4\alpha}-\frac{\alpha}{4\beta}}\right]\cos\theta$$

$$+\left[\beta-\frac{\alpha}{4}-\frac{\frac{\alpha}{2}\left(1-\frac{\alpha}{2\beta}\right)}{\frac{3}{2}-\frac{\beta}{4\alpha}-\frac{\alpha}{4\beta}}\right]\cos\phi+\left[\frac{\alpha}{4}+\frac{\frac{\alpha}{2}\left(1-\frac{\alpha}{2\beta}\right)}{\frac{3}{2}-\frac{\beta}{4\alpha}-\frac{\alpha}{4\beta}}\right]\cos(\theta+\phi)$$

$$-i\left\{\left[+\frac{\alpha}{4}-\frac{\alpha\left(1-\frac{\beta}{4\alpha}\right)}{\frac{3}{2}-\frac{\beta}{4\alpha}-\frac{\alpha}{4\beta}}\right]\sin\theta+\left[\beta-\frac{\alpha}{4}-\frac{\frac{\alpha}{2}\left(1-\frac{\alpha}{2\beta}\right)}{\frac{3}{2}-\frac{\beta}{4\alpha}-\frac{\alpha}{4\beta}}\right]\sin\phi\right.$$

$$\left.+\left[\frac{\alpha}{4}+\frac{\frac{\alpha}{2}\left(1-\frac{\alpha}{2\beta}\right)}{\frac{3}{2}-\frac{\beta}{4\alpha}-\frac{\alpha}{4\beta}}\right]\sin(\theta+\phi)\right\} \qquad \text{(A-18)}$$

Case IV: $2<\frac{\beta}{\alpha}$, $\alpha,\beta>0$, Region 4 $(\hat{R}4)$

$$\rho_{k,\ell}=1-\beta+\frac{\alpha}{4}-\frac{\alpha^2/\beta}{\frac{1}{2}+\frac{3}{4}\frac{\alpha}{\beta}}+\left(-\frac{\alpha}{4}+\frac{\alpha^2/\beta}{\frac{1}{2}+\frac{3}{4}\frac{\alpha}{\beta}}\right)\cos\theta$$

$$+\left[\beta-\frac{\alpha}{4}+\frac{\frac{\alpha}{2}\left(1-\frac{\alpha}{2\beta}\right)}{\frac{1}{2}+\frac{3}{4}\frac{\alpha}{\beta}}\right]\cos\phi+\left[\frac{\alpha}{4}+\frac{\frac{\alpha}{2}\left(1-\frac{\alpha}{2\beta}\right)}{\frac{1}{2}+\frac{3}{4}\frac{\alpha}{\beta}}\right]\cos(\theta+\phi)$$

$$-i\left\{\left(-\frac{\alpha}{4}+\frac{\alpha^2/\beta}{\frac{1}{2}+\frac{3}{4}\frac{\alpha}{\beta}}\right)\sin\theta+\left[\beta-\frac{\alpha}{4}-\frac{\frac{\alpha}{2}\left(1-\frac{\alpha}{2\beta}\right)}{\frac{1}{2}+\frac{3}{4}\frac{\alpha}{\beta}}\right]\sin\phi\right.$$

$$\left.+\left[\frac{\alpha}{4}+\frac{\frac{\alpha}{2}\left(1-\frac{\alpha}{2\beta}\right)}{\frac{1}{2}+\frac{3}{4}\frac{\alpha}{\beta}}\right]\sin(\theta+\phi)\right\} \qquad \text{(A-19)}$$

In the $\alpha,\beta$ plane we have four regions defined, as shown in Fig. A.3. For each region, $\rho_{k,\ell}$ has the form

$$\rho_{k,\ell}=A_m+B_m e^{-i\phi}+C_m e^{-i\theta}+D_m e^{-i\theta}e^{-i\phi}\ ,\quad m=1,2,3,4\ , \qquad \text{(A-20)}$$

where $A_m$, $B_m$, $C_m$, $D_m$ can be read off from Eqs. A-16 through A-19. Consider any one of the four regions and drop the subscript m for now. Because this interpolation procedure reproduces the set of monomials $\begin{Bmatrix}1\xi\\n\end{Bmatrix}$ and because $\xi^*=-\alpha$ and $\eta^*=-\beta$, we have the following relations:

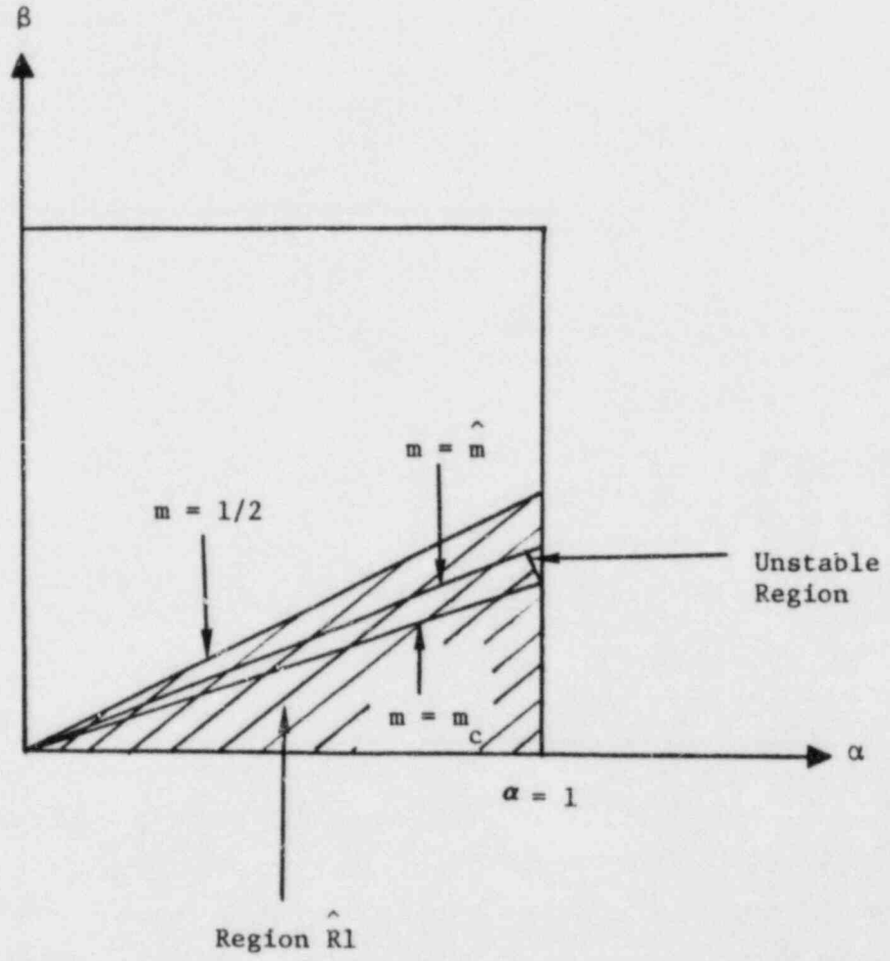


Fig. A.3. Domain Showing Unstable Region for Case $\theta = \phi$ in $\hat{R}1$

$$A + B + C + D = 1,$$

$$C + D = \alpha,$$

$$B + D = \beta. \tag{A-21}$$

Thus, we can write any $\rho$ in Eq. A-20 as

$$\rho = 1 - \alpha - \beta + D + (\alpha - D)e^{-i\theta} + (\beta - D)e^{-i\phi} + De^{-i\theta}e^{-i\phi} . \tag{A-22}$$

Set

$$C(\theta) = 1 - \cos\theta = 2 \sin \frac{\theta}{2} ;$$

then from Eq. A-22, we find

$$\begin{aligned} |\rho|^2 = 1 &- 2\alpha C(\theta) + 2\alpha^2 C(\theta) - 2\beta C(\phi) + 2\beta^2 C(\phi) \\ &+ 2\alpha\beta \ [C(\theta) + C(\phi) - C(\theta - \phi)] \\ &+ 2D \ [C(\theta) + C(\phi) - C(\theta + \phi)] , \end{aligned} \tag{A-23}$$

i.e.,

$$\begin{aligned} |\rho|^2 = 1 &- 2[(\alpha - \alpha^2 - \alpha\beta) \ C(\theta) - DC(\theta) + D(\alpha + \beta - D)C(\theta)C(\phi) \\ &+ (\beta - \beta^2 - \alpha\beta) \ C(\phi) - DC(\phi) + D(\alpha + \beta - D) \ C(\theta) \ C(\phi) \\ &+ \alpha\beta \ C(\theta - \phi) + DC(\theta + \phi)] . \end{aligned} \tag{A-24}$$

We are going to rewrite this expression in a form more convenient for checking stability. Before doing this, we note that any four parameter interpolating scheme which reproduces the set of monomials $1, \xi, \eta$ will produce Eqs. A-21 through A-23. In particular, a bilinear-donor-cell scheme corresponds to setting $D = \alpha\beta$. A linear-donor-cell scheme corresponds to the choice $D \equiv 0$. So at this point we are looking at the question of stability for general four-point schemes. Raithby's skew-upwind scheme, as we have seen, is a six-point scheme rather than a four-point scheme, so it does not fit this discussion. The form in Eq. A-24 is a convenient form when $D = 0$, because in this case one can see that

$$|\rho|^2 = 1 - 2f , \tag{A-25}$$

where

$$f = \alpha(1 - \alpha - \beta) \ C(\theta) + \beta \ (1 - \alpha - \beta) \ C(\phi) + \alpha\beta \ C(\theta - \phi) \tag{A-26}$$

and one sees that a sufficient condition for $f \geq 0$ (i.e., linear-donor-cell scheme is stable) is that

$$0 \leq \alpha,\ 0 \leq \beta,\ \alpha + \beta \leq 1 \ . \tag{A-27}$$

However, Eq. A-24 is not convenient when $D = \alpha\beta$ (bilinear-donor-cell scheme) and we do not think this form would be convenient for the D's associated with the VWSUD scheme. For this reason, we will rewrite Eq. A-24. To this end, we start with the identity

$$\begin{aligned}
&[1 - 2(\alpha - \alpha^2 + D - \alpha\beta)\ C(\theta)]\ [1 - 2(\beta - \beta^2 + D - \alpha\beta)\ C(\phi)] \\
&\equiv [\text{fac}\ \alpha]\ [\text{fac}\ \beta] \\
&= 1 - 2(\alpha - \alpha^2)\ C(\theta) - 2(\beta - \beta^2)\ C(\phi) \\
&\quad + 4(\alpha - \alpha^2)\ (\beta - \beta^2)\ C(\theta)\ C(\phi) \\
&\quad - 2(D - \alpha\beta)\ C(\theta)\ [1 - 2(\beta - \beta^2)\ C(\phi)] \\
&\quad - 2(D - \alpha\beta)\ C(\phi)\ [1 - 2(\alpha - \alpha^2)\ C(\theta)] \\
&\quad + 4(D - \alpha\beta)^2\ C(\theta)\ C(\phi) \ .
\end{aligned} \tag{A-28}$$

Use Eq. A-38 in Eq. A-23 to obtain

$$\begin{aligned}
|\rho|^2 &= [\text{fac}\ \alpha]\ [\text{fac}\ \beta] - 2\alpha\beta\ C(\theta - \phi) - 2DC(\theta + \phi) + 4DC(\theta) + 4DC(\phi) \\
&\quad + C(\theta)\ C(\phi)\ [-4(\alpha - \alpha^2)\ (\beta - \beta^2) - 4(D - \alpha\beta)\ (\beta - \beta^2) \\
&\quad - 4(D - \alpha\beta)\ (\alpha - \alpha^2) - 4(D - \alpha\beta)^2 - 4\alpha D - 4\beta D + 4D^2] \ .
\end{aligned} \tag{A-29}$$

Now use the relation

$$C(\theta + \phi) + C(\theta - \phi) = 2C(\theta) + 2C(\phi) - 2C(\theta)\ C(\phi) \ . \tag{A-30}$$

Then after some algebra, we find

$$|\rho|^2 = 1 - 2f \ , \tag{A-31}$$

where

$$\begin{aligned}
f &= [\alpha(1 - \alpha) + D - \alpha\beta]\ \{1 - [\beta(1 - \beta) + D - \alpha\beta]\ C(\phi)\}\ C(\theta) \\
&\quad + [\beta(1 - \beta) + D - \alpha\beta]\ \{1 - [\alpha(1 - \alpha) + D - \alpha\beta]\ C(\theta)\}\ C(\phi) \\
&\quad + (\alpha\beta - D)\ C(\theta - \phi) \ .
\end{aligned} \tag{A-32}$$

The form in Eq. A-32 is very convenient for the bilinear-donor scheme where $D = \alpha\beta$. In this case, it is easily shown that $f \geq 0$ if and only if $0 \leq \alpha \leq 1$, and $0 \leq \beta \leq 1$. When considering stability for the VWSUD scheme, we shall use Eq. A-32. For the VWSUD scheme we shall consider $(\alpha,\beta) \in \hat{R1} = \{(\alpha,\beta):\ 0 \leq \alpha/\beta \leq 1/2,\ \beta \geq 0,\ 0 \leq \alpha \leq 1\}$. In this case, D is defined from Eq. A-11, that is,

$$D(\alpha,\beta) = \frac{\beta}{4} + \frac{\frac{\beta}{2}\left(1 - \frac{\beta}{2\alpha}\right)}{\frac{1}{2} + \frac{3}{4}\frac{\beta}{\alpha}} = \frac{\beta}{4}\left(\frac{10 - \beta/\alpha}{2 + 3\beta/\alpha}\right) . \tag{A-33}$$

To investigate stability, we use this expression for D in Eq. A-32 and ask whether f is greater than or less than 0 for $(\alpha\beta)\varepsilon\hat{R}1$ and $0 \leq \theta \leq \pi$, $0 \leq \phi \leq \pi$. The most obvious approach would be to look at sufficiency conditions for $f > 0$. For example, a set of sufficient conditions for $f > 0$ would be

$$\begin{aligned} &0 \leq \alpha(1 - \alpha) + D - \alpha\beta \leq 1/2 \qquad \text{for } (\alpha,\beta)\varepsilon\hat{R}1 \\ &0 \leq \beta(1 - \beta) + D - \alpha\beta \leq 1/2 \\ &0 \leq \alpha\beta - D , \end{aligned} \tag{A-34}$$

where D is defined by Eq. A-33. Unfortunately, these conditions define a small domain $D_1 \wedge \hat{R}1 \varepsilon \hat{R}1$ that is too small to be useful. If $D_1 \wedge \hat{R}1$ denotes the set $(\alpha,\beta)\varepsilon\hat{R}1$ where $f \geq 0$, then we shall call $D \wedge \hat{R}1$ the stability domain. The problem is that conditions in Eq. A-34 define a domain $D_1 C D_1$ where $D_1$ is too small to be able to use as an indication of when we have stability.

Set

$$\beta = m\alpha, \quad 0 \leq \alpha \leq 1, \quad 0 \leq m \leq 1/2$$

$$\begin{aligned} a_1(\alpha;m) &= \alpha\tilde{a}_1(\alpha;m) = \alpha\left[\frac{8 + 22m - m^2}{8 + 12m} - (1 + m)\alpha\right] \\ a_2(\alpha;m) &= \alpha\tilde{a}_2(\alpha;m) = m\alpha\left[\frac{18 + 11m}{8 + 12m} - (1 + m)\alpha\right] \\ a_3(\alpha;m) &= \alpha\tilde{a}_3(\alpha;m) = m\alpha\left(\alpha - \frac{10 - m}{8 + 12m}\right) . \end{aligned} \tag{A-35}$$

Then Eq. A-32 can be written

$$\begin{aligned} f = \alpha h = \alpha\{&\tilde{a}_1\left[1 - \alpha\tilde{a}_2\, C(\phi)\right] C(\theta) + \tilde{a}_2\left[1 - \alpha\tilde{a}_1\, C(\theta)\right] C(\phi) \\ &+ \tilde{a}_3\, C(\theta - \phi)\} . \end{aligned} \tag{A-36}$$

The central question is whether $h(\alpha;m;\theta,\phi)$ defined in Eq. A-36 is positive for $0 \leq \alpha \leq 1$, $0 \leq \theta$, $\phi \leq \pi$, and $0 \leq m \leq 1/2$. Consider a special case when $\theta = \phi$. Setting $x = C(\theta)$, we have

$$h(\alpha;m;\theta) = \tilde{a}_1(\alpha;m)\,[1 - \alpha\tilde{a}_2(\alpha;m)\,X]\,X + \tilde{a}_2(\alpha;m)\,[1 - \alpha\tilde{a}_1(\alpha;m)\,X]\,X$$

$$= X\{[\tilde{a}_1(\alpha;m) + \tilde{a}_2(\alpha;m)] - 2\alpha x\tilde{a}_1(\alpha;m)\,\tilde{a}_2(\alpha;m)\}$$

$$= X[g_1(\alpha;m) - 2\alpha x g_2(\alpha;m)]\,, \qquad \text{(A-37)}$$

where

$$g_1(\alpha;m) = \frac{8 + 40m + 10m^2}{8 + 12m} - (1 + m)^2\alpha \qquad \text{(A.38)}$$

and

$$g_2(\alpha;m) = \frac{(8 + 22m - m^2)(18m + 11m^2)}{(8 + 12m)^2}$$

$$- \frac{m(m+1)}{8 + 12m}(26 + 33m - m^2)\,\alpha + m(1 + m)^2\,\alpha^2\,,$$

$$= \frac{m(144 + 484m + 224m^2 - 11m^3)}{(8 + 12m)^2}$$

$$- \frac{m}{8 + 12m}(1 + m)(26 + 33m - m^2)\,\alpha + m(1 + m)^2\,\alpha^2\,. \qquad \text{(A-39)}$$

The function $g_1(\alpha;m)$ is a straight line $m\alpha$ with a negative slope:

$$g_1(0;m) > 0,\ 0 < m < 1/2$$

$$g_1(1;m) = \frac{m(6 - 11m - 6m^2)}{4 + 6m}\,.$$

We observe that

$$g_1(1;m) > 0 \text{ when } 0 < m < m_c \triangleq 0.43990171634$$

$$g_1(1;m) < 0 \text{ when } m_c < m < 1/2. \qquad \text{(A-40)}$$

Hence, when $0 < m < m_c$, $g_1(\alpha;m) < 0$ for $0 \leq \alpha \leq 1$. When $m_c < m < 1$, then $g_1[\alpha;m]$ has a root in $[0,1]$. The root is

$$\alpha_{11} = \frac{8 + 40m + 10m^2}{(8 + 12m)(1 + m)^2} = \frac{4 + 20m + 5m^2}{4 + 14m + 16m^2 + 6m^3} \qquad \text{(A-41)}$$

and when $m_c < m < 1$, then

$$g_1(\alpha;m) > 0 \text{ for } 0 < \alpha < \alpha_{11}$$

$$g_1(\alpha;m) < 0 \text{ for } \alpha_{11} < \alpha < 1. \tag{A-42}$$

Note $\alpha_{11}(m_c) = 1$, $\alpha_{11}(1/2) = 0.968253968$.

Next we consider the nature of $g_2(\alpha;m)$. Because

$$g_2(\alpha;m) = \tilde{a}_1(\alpha;m)\, \tilde{a}_2(\alpha;m) \tag{A-43}$$

we can gain some information from the properties of $\tilde{a}_1$ and $\tilde{a}_2$.

Consider $\tilde{a}_2$, from Eq. A-35, we have

$$\tilde{a}_2(0;m) = \frac{18m + 11m^2}{8 + 12m}$$

$$\tilde{a}_2(1;m) = \frac{m(10 - 9m - 12m^2}{8 + 12m} \geq 0 \text{ for all } 0 \leq m \leq 1/2 .$$

Hence, the sign of $g_2(\alpha;m)$ is determined by the sign $\tilde{a}_1$.

From Eq. A-35, we have

$$\tilde{a}_1(0;m) = \frac{8 + 22m - m^2}{8 + 12m} > 0 \text{ for } 0 < m < 1/2$$

$$\tilde{a}_1(1;m) = \frac{m\,(2 - 13m)}{8 + 12m}$$

Hence, when $0 < m < 2/13 \triangleq 0.15385$, then

$$\tilde{a}_1(\alpha;m) < 0 \text{ for } 0 \leq \alpha \leq 1 . \tag{A-44}$$

And when $2/13 < m < 1/2$, then $\tilde{a}_1(\alpha;m)$ changes sign in $[0,1]$.

$$\tilde{a}_1(\alpha;m) > 0 \text{ when } 0 < \alpha < \alpha_{01}$$

$$\tilde{a}_1(\alpha;m) < 0 \text{ when } \alpha_{01} < \alpha < 1 , \tag{A-45}$$

where

$$\alpha_{01} = \frac{8 + 22m - m^2}{8 + 20m + 12m^2} . \tag{A-46}$$

Now the sign of $g_1(\alpha;m)$ is the same as the sign of $\tilde{a}_1$. Thus, when $0 < m \leq 2/13$, then

$$g_2(\alpha;m) > 0 \text{ for } 0 \leq \alpha \leq 1 \ . \tag{A-47}$$

When $2/13 < m \leq 1/2$, then

$$g_2(\alpha;m) > 0 \text{ when } 0 < \alpha < \alpha_{01}$$

$$g_2(\alpha;m) < 0 \text{ when } \alpha_{01} < \alpha < 1 \ . \tag{A-48}$$

Table A.1 combines this information. Note: $\alpha_{01} < \alpha_{11}$ when $m_c < m < 1/2$.

From Table A.1, we see that our task is to check whether $g_1 - 4g_2 > 0$ for various ranges of m and $\alpha$. If necessary, we look at $g_1 - 4\alpha g_2$, which is greater than $g_1 - 4g_2$. However, we note from Case III that when $m_c < m < 1/2$ and $\alpha_{11} < \alpha < 1$, then the quantity of interest is

$$\hat{H}(\alpha;m;x) = - \left|g_1(\alpha;m)\right| + 2\alpha x \left|g_2(\alpha;m)\right| \ .$$

Clearly for a given m, $m_c < m < 1/2$, and a given $\alpha$, $\alpha_{11} < \alpha < 1$, there is a value of x such that $\hat{H}(\alpha;m;x) < 0$. The question is whether this value of x satisfies $0 < x \leq 2$, i.e., whether $\left|g_1(\alpha;m)\right| < 4\alpha \left|g_2(\alpha;m)\right|$ for some $\alpha_{11} < \alpha < 1$, $m_c < m < 1/2$. In any event, it is clear that we have to investigate the functions

$$H(\alpha;m) = g_1(\alpha;m) - 4\alpha g_2(\alpha;m) \tag{A-49}$$

and/or

$$H_1(\alpha;m;) = g_1(\alpha;m) - 4g_2(\alpha;m) \ . \tag{A-50}$$

$H(\alpha;m)$ provides a stronger estimate and is cubic $m\alpha$; whereas, $H_1(\alpha;m)$ provides a weaker estimate and is quadratic in $\alpha$.

$$H(\alpha;m) = C_4(m) - C_3(m)\alpha + C_2(m)\alpha^2 - C_1(m)\alpha^3 \ , \tag{A-51}$$

where

$$C_4(m) = \frac{8 + 40m + 10m^2}{8 + 12m}$$

$$C_3(m) = \frac{\left(16 + 224m + 632m^2 + 344m^3 + 25m^4\right)}{4\left(2 + 3m\right)^2}$$

$$C_2(m) = \frac{4m(1 + m)\ (26\ + 33m - m^2)}{8 + 12m} = \frac{m(1 + m)\left(26 + 33m - m^2\right)}{2 + 3m}$$

$$C_1(m) = 4m(1 + m)^2 \ ;$$

and

TABLE A.1 Sign Properties of the Function H

| Case | m-Range | Properties $g_1, g_2$ | Question of Sign |
|---|---|---|---|
| I | $0 < m < 2/13$ | $g_1 > 0,\ g_2 > 0,\ \alpha$ | $g_1 - 2\alpha x g_2 > g_1 - 4g_2 > 0?,\ 0 \leq \alpha \leq 1$ |
| II | $2/13 < m < m_c$ | $g_1 > 0,\ \alpha$ | $g_1 - 2\alpha x g_2 > g_1 - 4g_2 > 0?,\ 0 < \alpha < \alpha_{01}$ |
| | | $g_2 \gtrless 0$, root $\alpha_{01}$ | $g_1 - 2\alpha x g_2 = g_1 + 2\alpha x\lvert g_2\rvert > 0,\ \alpha_{01} < \alpha < 1$ |
| III | $m_c < m < 1/2$ | $g_1 \gtrless 0$, root $\alpha_{11}$ | $g_1 - 2\alpha x g_2 > g_1 - 4g_2 > 0?,\ 0 < \alpha < \alpha_{01}$ |
| | | $g_2 \gtrless 0$, root $\alpha_{01}$ | $g_1 - 2\alpha x g_2 = g_1 + 2\alpha x\lvert g_2\rvert > 0,\ a_{01} < \alpha < \alpha_{11}$ |
| | | | $g_1 - 2\alpha x g_2 = -\lvert g_1\rvert + 2\alpha x\lvert g_2\rvert,\ \alpha_{11} < \alpha < 1$ |

$$H_1(\alpha;m) = D_3(m) + D_2(m)\alpha - D_1(m)\alpha^2 ,$$

where

$$D_3(m) = \frac{4}{(8 + 12m)^2}\left(16 - 40m - 344m^2 - 194m^3 + 11m^4\right)$$

$$D_2(m) = \frac{\left(-2 + 19m + 51m^2 + 29m^3 - m^4\right)}{2 + 3m}$$

$$D_1(m) = 4m(1 + m)^2 .$$

Now, whenever $g_1 > 0$, $g_2 > 0$, then $H > H_1$; so if we can show $H_1 > 0$, we have established stability for these values of $\alpha$,m. From Table A.1, we see that $g_1 > 0$, $g_2 > 0$ in all cases of interest except the last subcase for Case III. However, the coefficient $D_3(m)$ changes sign in the interval [0,1/2]; so we find it more convenient to work with the cubic function $H(\alpha m)$. When $0 \leq m \leq 1/2$, this cubic has exactly <u>one</u> real positive root $\alpha_{00}(m)$. Moreover, for

$$0 \leq m < 0.490250 , \tag{A-52}$$

the root $\alpha_{00}(m)$ satisfies

$$1 < \alpha_{00}(m).$$

Thus, referring to Table A.1, we see that $g_1 - 2\alpha x g_2 > 0$ in every case except possibly the last subcase of Case III. Consider $m_c < m < 1/2$ and $\alpha_{11}(m) < \alpha < 1$. Thus we have $g_1(\alpha;m) < 0$ and $g_2(\alpha;m) < 0$. Thus, the equation

$$g_1 - 2\alpha x g_2 = -|g_1| + 2\alpha x|g_2| = 0 \tag{A-54}$$

has the solution

$$x = \frac{|g_1|}{2\alpha|g_2|} = \frac{-g_1}{-2\alpha g_2} . \tag{A-55}$$

Now we must have $0 < x < 2$; therefore, we must have

$$x = \frac{|g_1|}{2\alpha|g_2|} < 2, \text{ for } \alpha_{11} < \alpha < 1$$

or $|g_1| < 4\alpha|g_2| \Rightarrow -g_1 < -4\alpha g_2 \Rightarrow g_1 > 4\alpha g_2$,

i.e., $H(\alpha;m) = g_1 - 4\alpha g_2 > 0$.

Now we have $H(\alpha;m) > 0$ on $0 < \alpha < 1$ for $m < 0.49025 = \hat{m}$. Thus, if $m_c = 0.4399017 < m < \hat{m} = 0.49025$ and $\alpha_{11} < \alpha < 1$, then $H(\alpha;m) > 0$ for $\alpha_{11} < \alpha < 1$. Therefore, $x = \frac{|g_1|}{2\alpha|g_1|} < 2$, and we see that for each $m_c < m < \hat{m}$, and each $\alpha_{11} < \alpha < 1$, there is an $x = x(\alpha;m)$ such that

$$0 < x < 2$$

and

$$g_1(\alpha;m) - 2\alpha x g_2(\alpha;m) < 0. \tag{A-56}$$

Moreover, the values of $x = x(\alpha;m)$ defined by Eq. A-55 do range over the full interval $[0,2]$. To see this, we recall that $\alpha_{11}(m)$ is a root of $g_1(\alpha;m)$ and $g_2(\alpha;m) \neq 0$ for $\alpha_{11} < \alpha < 1$. Thus, if we set

$$(g_2)_{min} = \min\{|g_2(\alpha;m)| : \alpha_{11}(m) \leq \alpha \leq 1\}, \text{ then}$$

$$x(\alpha;m) = \frac{|g_1(\alpha;m)|}{2\alpha|g_2(\alpha;m)|} \leq \frac{|g_1(\alpha;m)|}{2\alpha_{11}(g_2)_{min}}$$

and the right side goes to zero as $\alpha \to \alpha_{11}$. Thus, when $\theta = \phi$, there are values $(\alpha,\beta) \in \hat{R}1$ when h as defined in Eq. A-37 is negative; hence, for these values $(\alpha,\beta) \in \hat{R}1$, the VWSUD scheme is unstable. It is worth noting that these points $(\alpha,\beta) \in \hat{R}1$ occur in a small region, as shown in Fig. A.3. Note that $\alpha_{11}(\hat{m}) = 0.97345$. The figure has exaggerated the values of $m_c, \hat{m}$ to illustrate the shaded region. Our conclusion is that the VWSUD scheme is essentially stable in $\hat{R}1$ when $\theta = \phi$.

Distribution for NUREG/CR-3505, EPRI NP-3547 (ANL-83-66)

Internal:

E.S. Beckjord
C.E. Till
R.S. Zeno
P.B. Abramson
M.L. Bottoni
A.R. Brunsvold
B.K. Cha
Y.S. Cha
B.C-J. Chen
F.F. Chen
W.L. Chen
H-N. Chi
T. Chiang
T.H. Chien
D.H. Cho
L.W. Deitrich
H.M. Domanus
D.R. Ferguson
P.L. Garner
J.R. Hull
M. Ishii
J.F. Kuzanek
G.K. Leaf
R.W. Lyczkowski
D. Malloy
C.C. Miao
R.C. Schmitt
W.T. Sha (45)
V.L. Shah (45)
Y.W. Shin
R.M. Singer
J.E. Sullivan
D.P. Weber
C.I. Yang
S.K. Zussman
ANL Patent Dept.
ANL Contract File
ANL Libraries (2)
TIS Files (3)

External:

USNRC, Washington, for distribution per R7 (250)
DOE-TIC (2)
Manager, Chicago Operations Office, DOE-CH
Components Technology Division Review Commmittee:
D.J. Anthony, General Electric Co., Schenectady, NY 12345
A.A. Bishop, U. Pittsburgh, Pittsburgh, PA 15261
B.A. Boley, Northwestern U., Evanson, IL 60201
F.W. Buckman, Wood-Leaver and Associates, Monroeville, PA 15146
R. Cohen, Purdue U., West Lafayette, IN 47907
J. Weisman, U. Cincinnati, Cincinnati, OH 35221
B.T. Chao, U. Illinois, Urbana, IL 61801
R.B. Duffey, Electric Power Research Institute, Palo Alto, CA 94303
E.L. Gluekler, General Electric Co., Sunnyvale, CA 94086
M.S. Kazimi, Massachusetts Institute of Technology, Cambridge, MA 01239
J.H. Kim, Electric Power Research Institute, Palo Alto, CA 94303 (3)
G.S. Lellouche, Electric Power Research Institute, Palo Alto, CA 94303
W.B. Loewenstein, Electric Power Research Institue, Palo Alto, CA 94303
R. Markley, Westinghouse Advanced Reactors Division, Madison, PA 15663
J.C. Mills, Atomics International, Canoga Park, CA 91306
A.L. Schor, Massachusetts Institute of Technology, Cambridge, MA 03129
B.R. Sehgal, Electric Power Research Institute, Palo Alto, CA 94303
A. Singh, Electric Power Research Institute, Palo Alto, CA 94303
J.C. Slattery, Northwestern U., Evanston, IL 61801
S.L. Soo, U. Illinois, Urbana, IL 61801
B.K.H. Sun, Electric Power Research Institute, Palo Alto, CA 94303
J.P. Sursock, Electric Power Research Institute, Palo Alto, CA 94303
J.R. Thompson, Mississippi State U., Mississippi State, MS 39762
N.E. Todreas, Massachusetts Institute of Technology, Cambridge, MA 02139

NRC FORM 335 (11-81)

U.S. NUCLEAR REGULATORY COMMISSION

**BIBLIOGRAPHIC DATA SHEET**

1. REPORT NUMBER (Assigned by DDC)
NUREG/CR-3505
ANL-83-66, EPRI NP-3547

4. TITLE AND SUBTITLE (Add Volume No., if appropriate)
A VOLUME-WEIGHTED SKEW-UPWIND DIFFERENCE SCHEME IN COMMIX

2. (Leave blank)

3. RECIPIENT'S ACCESSION NO.

7. AUTHOR(S) C. C. Miao, R. W. Lyczkowski, G. K. Leaf, F. F. Chen, B. K. Cha, B. C-J. Chen, H. M. Domanus, W. T. Sha, and V. L. Shah

5. DATE REPORT COMPLETED
MONTH: February YEAR: 1984

DATE REPORT ISSUED
MONTH: May YEAR: 1984

9. PERFORMING ORGANIZATION NAME AND MAILING ADDRESS (Include Zip Code)
Argonne National Laboratory
9700 South Cass Avenue
Argonne, Illinois 60439

6. (Leave blank)

8. (Leave blank)

12. SPONSORING ORGANIZATION NAME AND MAILING ADDRESS (Include Zip Code)
Containment Research Systems Branch
Division of Accident Evaluation
Office of Nuclear Regulatory Research
U. S. Nuclear Regulatory Commission
Washington, D.C. 20555

10. PROJECT/TASK/WORK UNIT NO.

11. FIN NO.
A2045

13. TYPE OF REPORT
Technical

PERIOD COVERED (Inclusive dates)
May 1982 - February 1984

15. SUPPLEMENTARY NOTES

14. (Leave blank)

16. ABSTRACT (200 words or less)

A numerical difference scheme, called volume-weighted skew-upwind difference (VWSUD), has been developed, and Raithby's two-dimensional skew-upwind difference (SUD) scheme has been extended to three dimensions. Both schemes have been implemented in the energy equation of the COMMIX-1B computer program. The VWSUD scheme has the following five major features: (1) it has the same order of accuracy as SUD, but eliminates all of the undershoots and overshoots observed in SUD; (2) it retains the simplicity of SUD, without resorting to the artificial cut-offs needed in SUD; (3) it significantly reduces numerical diffusion; (4) a linear stability analysis shows that VWSUD is numerically stable; and (5) a coarser mesh than for the pure-upwind difference scheme can be used while obtaining results that are of the same order of accuracy.

The assessments of SUD and VWSUD are accomplished by comparing several multidimensional thermal mixing benchmark computations with analytical solutions. In addition, the analysis of two thermal mixing experiments shows that use of the VWSUD scheme substantially improves agreement with thermocouple response data in regions with highly angled flows.

17. KEY WORDS AND DOCUMENT ANALYSIS

17a. DESCRIPTORS

Numerical diffusion
Thermal hydraulics
Numerical analysis
Finite difference solutions

17b. IDENTIFIERS/OPEN-ENDED TERMS

18. AVAILABILITY STATEMENT
Unlimited

19. SECURITY CLASS (This report)
Unclassified

21. NO. OF PAGES
91

20. SECURITY CLASS (This page)
Unclassified

22. PRICE
$

NRC FORM 335 (11-81)